Condensed Matter and Interphases. 2022;24(4): 407–458

ISSN 1606-867X (Print)
ISSN 2687-0711 (Online)
Condensed Matter and Interphases
Kondensirovannye Sredy i Mezhfaznye Granitsy
https://journals.vsu.ru/kcmf/

Review

Review article
https://doi.org/10.17308/kcmf.2022.24/10549

Thermodynamics, kinetics, and technology of synthesis of epitaxial layers of silicon carbide on silicon by coordinated substitution of atoms, and its unique properties. A review

S. A. Kukushkin✉, A. V. Osipov

Institute for Problems in Mechanical Engineering of the Russian Academy of Sciences, 61 Bolshoi Prospekt V.O., St. Petersburg 199178, Russian Federation

Abstract

The review analyses a new method for growing SiC epitaxial films on Si, which is based on the coordinated substitution of some silicon atoms in the Si crystal lattice with carbon atoms. The main idea and theory of the new method is presented. This method significantly differs from classical growth schemes of thin films. The developed method consists in replacing some Si atoms with C directly inside the silicon matrix and not in depositing atoms on the substrate surface. The method allows us to solve one of the main problems of heteroepitaxy, namely, to synthesise low-defect and unstrained epitaxial films with a large difference between the lattice parameters of the film and the substrate. For the first time in the world, a method of the coordinated substitution of atoms of one sort for atoms of another sort has been implemented right inside the original crystal without destruction of the crystal structure. The method resembles the "genetic synthesis" of protein structures in biology. The structural quality of layers obtained by this method significantly exceeds the quality of silicon carbide films grown on silicon substrates by the world's leading companies. The method is cheap and technologically advanced. The new growth method is compared with classical thin-film growth methods. The thermodynamic and kinetic analysis of the process of substitution of atoms in the solid phase is presented. Using the example of SiC formation, the mechanisms of a wide class of heterogeneous chemical reactions between the gas phase and a solid are described. The review describes a new method for the synthesis of epitaxial SiC layers on single-crystal sapphire substrates, which is based on the method of coordinated substitution of atoms. It is shown that an interface layer with non-standard optical and electrophysical properties appears at the SiC/Si interface formed by this growth method. The unusual properties are caused by a collapse (shrinkage) of the material at which silicon carbide, as a new phase, separates from the silicon matrix. The silicon is subjected to abnormally strong compression. As a result of such shrinkage, every fifth SiC chemical bond is fully consistent with every fourth Si bond, while the remaining bonds are deformed. The latter leads to a change in the structure of the SiC surface zones adjacent to Si and to a transformation of SiC into a "magnetic semimetal". The epitaxy of SiC films on Si due to the coordinated substitution of half of the Si atoms by C atoms results in absence of lattice misfit dislocations and thus ensures the high crystalline perfection of the SiC films. A description is given for two quantum effects observed in the SiC/Si structures at room temperature in weak magnetic fields: the Meissner–Ochsenfeld effect and the effect of the generation of the Aharonov-Bohm oscillations in the field dependences of the static magnetic susceptibility. A description is given for a discovered phenomenon of phase transition of charge carriers into a coherent state with the simultaneous appearance of a giant value of diamagnetism of the order of $1/4\pi$ in weak magnetic fields, which has been associated with the appearance of a superconducting state.

Keywords: Silicon carbide on silicon, Solid-state reactions, Heterostructures, Epitaxial films, GaN, AlN, ZnO, Spintronics, Wide-bandgap semiconductors, Heat-resistant coatings, Superconductivity, Meissner–Ochsenfeld effect, Aharonov–Bohm effect, LEDs

Funding: The study was supported by the Ministry of Science and Higher Education within the framework of the state task for the Institute for Problems in Mechanical Engineering of the Russian Academy of Sciences (FFNF-2021-0001).

✉ Sergey A. Kukushkin, e-mail: sergey.a.kukushkin@gmail.com
© Kukushkin S. A., Osipov A. V., 2022

The content is available under Creative Commons Attribution 4.0 License.

Acknowledgements: This work was carried out using the equipment of the unique scientific facility "Physics, Chemistry and Mechanics of Crystals and Thin Films" of the Institute for Problems in Mechanical Engineering of the Russian Academy of Sciences (St.-Petersburg). The authors would like to express their profound gratitude to T. V. Lavrova for her help with manuscript preparation. The authors express special gratitude to R. S. Telyatnik for the great work on editing the English text of this paper. The authors are especially grateful to the editorial board of the journal "Condensed Matter and Interphases" for the invitation to write and publish this review in this journal.

For citation: Kukushkin S. A., Osipov A. V. Thermodynamics, kinetics, and technology of synthesis of epitaxial layers of silicon carbide on silicon by coordinated substitution of atoms, and its unique properties. Review. *Condensed Matter and Interphases.* 2022;24(4): 407–458. https://doi.org/10.17308/kcmf.2022.24/10549

Для цитирования: Кукушкин С. А, Осипов А. В. Термодинамика, кинетика и технология синтеза эпитаксиальных слоев карбида кремния на кремнии методом согласованного замещения атомов и его уникальные свойства. Обзор. *Конденсированные среды и межфазные границы*. 2022;24(4): 407–458. https://doi.org/10.17308/kcmf.2022.24/10549

Table of contents

1. Introduction 409
2. The method of coordinated substitution of atoms: processes occurring in the solid Si phase during the growth of SiC epitaxial films on Si. A new mechanism of stress relaxation during the SiC nucleation on Si 412
2.1. The growth of an epitaxial SiC layer on a Si(111) surface....412
2.1.1. The stage of formation of dilatation dipoles as a necessary condition for the dislocation-free growth of SiC....412
2.1.2. The stage of transformation of dilatation dipoles into epitaxial SiC....414
2.2. The method of coordinated substitution of atoms as a first-order phase transition through an intermediate state 420
2.3. Growth of the epitaxial SiC layer on the Si(100) surface 421
3. Quantum-mechanical theory of epitaxial transformation of silicon into silicon carbide....424
3.1. Energy profile, intermediate and transition states of the reaction of heterogeneous synthesis of SiC 426
3.2. Transition of "pre-carbide" silicon into silicon carbide on the (100) surface 426
4. Diffusion mechanism of CO and SiO molecules into Si with the simultaneous chemical transformation reaction of Si into SiC....428
5. Vacancy growth of single-crystal silicon carbide — a new stage in the development of the method of coordinated substitution of atoms 430
6. Coating method for smooth and profiled Si surfaces by ultrathin silicon carbide layers....433
7. Formation of epitaxial SiC layers on the surface of other materials by the method of coordinated substitution of atoms 434
7.1. Synthesis of epitaxial silicon carbide films on sapphire substrates (α-Al_2O_3) 434
7.1.1. Current state and problems of growing of epitaxial SiC films on sapphire 434
7.1.2. Growth of epitaxial Si films on sapphire with the Si (100) and (111) layer orientations 435
7.1.3. Conversion of Si epitaxial films grown on sapphire into SiC epitaxial films by the method of coordinated substitution of atoms 437
7.1.4. Structural and morphological features of the formation of SiC films on sapphire 438
7.2. A new method of formation of protective SiC-C composite coatings on graphite....440
8. Crystal structure, polytypism, optical, electrophysical, mechanical, and other properties of SiC synthesised on Si by the method of coordinated substitution of atoms 443
9. Features and anomalies of optical, magnetic, and other properties of SiC films on Si grown by the method of coordinated substitution of atoms 445
9.1. The physical nature of the emergence of features and anomalies in the properties of SiC films on Si grown by the method of coordinated substitution of atoms....445
9.2. Structural features of the surface of SiC epitaxial films synthesised by theMCSA, determined using photoelectron spectroscopy 447
9.3. Anomalies of magnetic properties of epitaxial SiC films synthesised by the MCSA....451
9.4. Electronic phase transitions in SiC epitaxial layers synthesised by the MCSA....451
10. Conclusions....453

1. Introduction

The purpose of our study was to summarise the latest data on the growth mechanisms, properties, and applications of silicon carbide films on silicon that are synthesised by a new method of the topochemical coordinated substitution of atoms. The reader may rightly ask the following question. Why do we need another review dedicated to a description of this method? Only in the last year and a half have the authors of this article published two reviews [1, 2] and a chapter in the book [3] on this topic, and three more review articles [4–6] were published several years earlier. This topic, however, turned out to be so deep and multifaceted, while silicon carbide synthesised by the method of coordinated substitution of atoms has shown such unusual properties — and findings in this field are updated literally daily — that we hope that the question of readers about the need for another review article will vanish in the process.

Before proceeding to a description of the growth of silicon carbide on silicon, let us try to answer the following questions. Why is silicon carbide needed at all, and then why silicon carbide on a silicon substrate is required? How is it superior to other materials? What useful properties does it have? By what parameters does it exceed silicon?

Silicon is one of the key basic materials for most modern electronic devices, computers, communications equipment, sensors, transmission and playback equipment. This material has both a number of advantages and some significant disadvantages. One of the important advantages of silicon is its availability: producing silicon wafers for chips and microcircuits, polishing the wafers, cleaning and cutting them are well developed all over the world. Therefore, electronic devices based on silicon wafers are relatively cheap. Despite this, the parameters of silicon-based electronic devices have a number of limitations. For example, with an increase in the ambient temperature, the semiconductor properties of silicon deteriorate significantly, and instability in the operation of devices and failures appear. Silicon cannot operate stably under conditions of increased radiation, for example, in space and in nuclear reactors. It also has a number of other unavoidable limitations. In this regard, presently, it has become clear that, for some applications, other materials, which can at least partially, if not completely, replace silicon, should be used. Such semiconductor materials include wide-bandgap semiconductors [7]: silicon carbide (SiC), gallium nitride (GaN), aluminium nitride (AlN), gallium oxide (Ga_2O_3), their solid solutions, and a number of other materials. These semiconductors possess excellent electrical characteristics and can ensure the operation of electronic and optoelectronic devices at elevated temperatures and under conditions of increased radiation. These semiconductor materials have high hardness and high elastic moduli. Silicon carbide, for example, approaches diamond in terms of hardness. Semiconductor materials such as SiC, AlN, GaN, and Ga_2O_3 have a wide band gap. The width of the band gap of these materials varies from 2.4 eV for cubic SiC to 6.1 eV for AlN. Therefore, these materials are called wide-bandgap semiconductors. The main obstacle to realising the high potential of wide-bandgap semiconductors is a lack of technologies that allow producing epitaxial layers of these semiconductors to be affordable in terms of price and quality. It is also important to provide the possibility of integrating wide-bandgap semiconductors with traditional silicon electronics. This is necessary for the production of devices with wide-bandgap structures on silicon substrates, the production and the processing technologies of which have presently been brought to perfection. Currently, all industrialised countries and the largest electronic companies in the world are solving this problem.

Silicon carbide is the only binary compound of silicon and carbon that exists in the solid phase under normal conditions. Silicon carbide is a wide-bandgap semiconductor with a band gap between 2.32 eV and 3.24 eV, depending on the silicon carbide polytype. Single-crystal SiC has a high breakdown electric field strength, high drift velocity of electrons, and high thermal conductivity. Due to a dielectric strength of SiC that is an order of magnitude higher than that of silicon, the doping level of a SiC diode can be two orders of magnitude higher than that of silicon at the same breakdown voltage. Silicon carbide is a radiation-resistant material. The high thermal conductivity of SiC (at the level

of thermal conductivity of copper) significantly simplifies the problem of heat removal from devices. This property, combined with high allowable operating temperatures and high saturation velocities of charge carriers (high saturation currents of field-effect transistors), makes SiC devices very promising for use in power electronics. In addition, the high Debye temperature, which determines the temperature at which phonons arise, suggests a high thermal stability of SiC. Thus, in almost all important criteria, silicon carbide is superior to the classical semiconductor materials Si and GaAs. By the irony of history, the active use of silicon carbide in microelectronics began only recently, despite the fact that silicon carbide was one of the first materials used in solid-state electronics. Back in 1907, H. Round observed a luminescence when an electric current passed through a SiC crystal. Oleg Losev studied the electroluminescence of silicon carbide in more detail in 1923–1940. Losev also established the existence of a connection between rectification and electroluminescence in SiC. Thus, the two most important phenomena for semiconductor electronics — electroluminescence and rectification properties of *p*-*n* structures — were first discovered in SiC crystals.

The modern market requires the creation of a new type of light-emitting diodes, semiconductor lasers, high-electron-mobility transistors (HEMTs), sensors and gas transducers, microwave devices, and optical switches. Recently, there has been an urgent need for both LEDs emitting hard ultraviolet radiation and ultraviolet radiation sensors. It is possible to create such types of LEDs and sensors by using wide-bandgap semiconductors such as AlN and GaN. Currently, however, there are no cheap and high-quality native substrates of these materials. As a rule, these materials are grown on sapphire and silicon carbide substrates. Thus, silicon carbide is an indispensable material also as a substrate for creating heterostructures based on wide-bandgap semiconductors such as gallium and aluminium nitrides. It is heterostructures based on gallium nitride compounds grown on SiC substrates that make it possible to create transistors with high charge-carrier mobility, high-power LEDs, and blue lasers.

For many years, the use of single-crystal SiC in electronics has been constrained by the high cost of SiC and the difficulty of its production. Currently, this problem is gradually being solved. However, researchers are looking for other ways to produce SiC. One of these ways is the synthesis of SiC epitaxial layers on a silicon substrate. There is every reason to believe that in the future such structures will occupy their niche in micro- and optoelectronics, since they combine the properties of silicon as one of the main materials for electronics with the properties of such a wide-bandgap material as silicon carbide. These materials are much cheaper than SiC single crystals. Moreover, it is possible to grow SiC layers on Si substrates of a large diameter.

The complexity of obtaining SiC films of epitaxial quality is largely due to the fact that SiC crystallises in more than 250 different crystal structures (polytypes), and only one of these polytypes is cubic (3C-SiC). The remaining polytypes have hexagonal or rhombic symmetry. The cubic polytype has the narrowest band gap among all silicon carbide polytypes and slightly excels gallium phosphide (GaP) by maximum operating temperature. The width of the band gap of the 3C-SiC polytype is 2.32 eV. Although 3C-SiC has the width of the band gap and the dielectric strength lower than those of hexagonal polytypes of SiC, its electrical properties are much more isotropic than properties of the hexagonal and rhombic polytypes of SiC. In addition, the mobility of charge carriers in it is very high. Finally, and most important, the 3C-SiC polytype is the most suitable polytype for growth on cubic silicon, since the silicon crystal used as a substrate has cubic symmetry. At present, there are no commercial single crystals of the 3C-SiC polytype. Therefore, the only way to obtain the cubic SiC polytype is to grow 3C-SiC layers on a silicon substrate.

The first attempts to obtain SiC films on silicon substrates were made by S. Nishino [8]. He proposed to use the standard technique of chemical vapour deposition (CVD) for the formation of SiC films, which is widely used for the synthesis of semiconductor structures. Methyltrichlorosilane (CH_3SiCl_3) and mixtures of SiH_4 and C_3H_8 were used as sources of carbon

and silicon [8]. Based on the grown films, several types of field-effect transistors were created. However, the parameters of these devices, as well as the quality of the films, were low. This was due to the fact that the lattice parameters of Si and SiC differ by approximately 19%. This is the first (and main) problem preventing the production of SiC epitaxial films on Si. Due to the difference in the lattice parameters of Si and SiC, a large number of misfit dislocations and other growth defects are formed at the interface between the film and the substrate; thick SiC films on Si, with a thickness of more than 1 μm, contain cracks. The second but not less difficult problem is a large difference in thermal expansion coefficients between Si and 3C-SiC. According to the data provided in [9], the linear thermal expansion coefficient of 3C-SiC is $3.9 \cdot 10^{-6}$ K^{-1}, while the linear expansion coefficient of Si is $2.6 \cdot 10^{-6}$ K^{-1}. As a result, when a Si wafer with a SiC layer is cooled from the growth temperature to room temperature, a strong bending of the wafer and cracks occur. The review [10] presents a picture of the deflection of a Si wafer with an epitaxial SiC film. Finally, the third problem is associated with the low melting point of Si (Si melts at a temperature of 1412 °C). It is impossible to grow SiC films, synthesised on Si, at temperatures equal to or higher than 1500 °C. At temperatures above 1500 °C, the diffusion mobility of the components and the rate of the chemical reaction between the components from which SiC is grown are quite high. This allows implementing the oriented nucleation of two-dimensional SiC nuclei. Therefore, for the growth of SiC films at temperatures below 1412 °C, researchers have to apply various methods of preliminary modification of the Si surface. In the review [11], an analysis of a large set of experimental data on the growth of SiC films on Si was made. It turned out [10, 11] that, in order to obtain films of acceptable quality, the Si substrate must be carbonised before the growth. The SiC buffer layer grown as a result of carbonisation serves as a seed for further epitaxy of 3C-SiC layers and has a significant effect on their deformation. However, carbonisation failed to radically solve the problem of obtaining 3C-SiC layers with a low defect content suitable for creating commercial semiconductor devices.

The main reason that did not allow researchers to obtain low-defect 3C-SiC layers by the carbonization method and thereby to form a highly oriented seed layer for further SiC growth will be described below.

In 2008, in the work [12], a new method for synthesising epitaxial SiC films on Si was theoretically predicted, experimentally confirmed, and patented [13]. The method [12] is based on the chemical transformation (conversion) of silicon surface layers into silicon carbide epitaxial layers due to the chemical interaction of gaseous carbon monoxide (CO) with the silicon substrate surface in the reaction

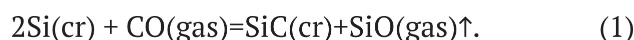

$$2Si(cr) + CO(gas)=SiC(cr)+SiO(gas)\uparrow. \qquad (1)$$

This method was called the method of coordinated substitution of atoms (MCSA) in later works [14]. The term "coordinated" means that new chemical bonds are formed simultaneously and in coordination with the destruction of old bonds, which leads to the preservation of the structure of chemical bonds. Later, in [4–12], a consistent theory that describes the entire spectrum of interconnected physicochemical processes occurring during the topochemical transformation of Si into SiC was developed.

A detailed description of processes of the SiC growth by the MCSA that were carried out from the beginning of the studies in 2004 and until 2014 can be found in the reviews [10–12]. These publications describe both theoretical and experimental studies and provide a detailed description of the installation for the growth of SiC. These studies also describe a number of technological methods necessary to obtain SiC layers of a high degree of crystalline perfection.

In this review, we will not discuss those. Here, we only briefly outline the basic technology of the SiC conversion from Si and then proceed to describe the new, obtained since 2014, theoretical and experimental data on the growth and structure of the SiC films.

2. The method of coordinated substitution of atoms: processes occurring in the solid Si phase during the growth of SiC epitaxial films on Si. A new mechanism of stress relaxation during the SiC nucleation on Si

2.1. The growth of an epitaxial SiC layer on a Si(111) surface

2.1.1. The stage of formation of dilatation dipoles as a necessary condition for the dislocation-free growth of SiC

In this section, we briefly outline the main theoretical provisions of the MCSA. Previously, they have already been repeatedly described in one or another form in a number of our reviews [1–6]. For the convenience of the reader, we briefly repeat these results and then proceed to describe the new data.

The MCSA is based on the "assembly" of a new silicon carbide matrix based on the old silicon matrix by partial substitution of silicon atoms in the substrate crystalline matrix with carbon atoms. The "assembly" of the SiC matrix is carried out due to the chemical reaction (1). Reaction (1) proceeds in two stages [4–6, 15–20]. During the first stage, an intermediate state in silicon is formed (an analogue of the activated complex): "silicon vacancy – carbon atom – silicon matrix" ($C{-}V_{Si}$). During this stage, carbon atoms are located in the interstitial positions of the silicon matrix. It can be said that a metastable superlattice is formed near the silicon surface. During the second stage of the reaction, it transforms into silicon carbide, and the released vacancies coalesce into pores that are being formed under the silicon carbide layer. In a crystal of cubic symmetry, these two dilatation centres (a carbon atom and a silicon vacancy) interact elastically with each other. If dilatation dipoles are located perpendicular to the plane (111) of silicon, then they are attracted to each other [15–20]. In this case, almost all of the dilatational elastic energy, arising due to the introduction of carbon atoms and the formation of vacancies, relaxes [15–20]. Since, during one of the stages of the transformation of Si into SiC, the formation of defects ($C{-}V_{Si}$) occurs, and a mechanical elastic interaction arises between them, we had to face the need to derive a formula for the energy of their interaction. As a result, the theory of elastic interaction of two point defects in crystals of cubic and hexagonal symmetry was developed [15, 16, 21], and the formula for the interaction energy of two point defects in these crystals was derived. For crystals of cubic symmetry, the interaction energy $E_{\text{int}}(\cos\varphi(x,y,z))$ of two point defects is [15,16,21]

$$E_{\text{int}}(\cos\varphi(x,y,z) = -\frac{E_0(\cos^4\varphi_x+\cos^4\varphi_y+\cos^4\varphi_z)}{r^3}, \tag{2}$$

where $E_0 = 15K(3c_{11}-4c_{44})\Omega^{\text{I}}\Omega^{\text{II}}\eta/8\pi(c_{12}+2c_{44})$; $K=(c_{11}+2c_{12})/3$ is the compression modulus (for Si $K^{\text{Si}}=0.98\cdot10^{-11}\,\text{N}\cdot\text{m}^{-2}$); c_{11}, c_{12}, and c_{44} are elastic moduli of a cubic crystal; for Si, $c_{11}=1.66\cdot10^{11}\ \text{N}\cdot\text{m}^{-2}$, $c_{12}=0.633\cdot10^{11}\ \text{N}\cdot\text{m}^{-2}$, $c_{44}=0.796\cdot10^{11}\ \text{N}\cdot\text{m}^{-2}$; $\eta=(c_{11}-c_{12}-2c_{44})/c_{44}$ is the crystal anisotropy parameter, $\eta=-0.689$ for Si; Ω^{I} and Ω^{II} are associated with the difference between the volumes of the inclusion and the vacancy cavity; r is the distance between defects; $\cos\varphi_i = x/r$ are the directional cosines between the x, y, z axes and the direction of the straight line connecting the centres of interacting defects. The value of $(\cos^4\varphi_x+\cos^4\varphi_y+\cos^4\varphi_z-3/5)$ has a maximum in the (100) direction equal to 0.4, a minimum in the <111> direction equal to –0.27, and a saddle point of –0.1 in the <110> direction. Therefore, the greatest attraction between point defects occurs if these defects are in interstices located along the <110> directions of silicon, i.e., if the carbon atom is located in the interstitial position under the (111) planes along the $(\bar{1}10)$ plane, and the vacancy should be located along the <111> direction with respect to this atom. In this case, the attraction between the silicon vacancy and the carbon atom will be at a maximum. The interaction energy is inversely proportional to the cube of the distance between defects. Such a system is a stable complex, which, by analogy with an electric dipole, was called a dilatation dipole [15, 16]. Formula (2) in this form was first obtained in [21]. It should be noted that the interaction of two point dipoles in crystals of cubic symmetry was first studied by Eshelby [22]. Subsequently, it turned out that the sign of the interaction energy obtained by him should be substituted by the opposite one. The sign of the interaction of point defects also turned out to be

incorrect when deriving the formula for the interaction energy from the anisotropic tensor Green's function obtained by Lifshits and Rozentsveig [23]. A detailed presentation of the interaction of point defects in anisotropic media can be found in [15, 16, 21–24].

The total elastic energy of a crystal during the formation of interacting defects in its volume has the form [16]:

$$W(\cos\varphi(x,y,z)) = E_C + E_V + E_{\text{int}}(\cos\varphi(x,y,z)) \quad (3)$$

Here, E_V is the elastic energy arising in the Si crystal due to the deformation caused by the removal of the Si atom and the formation of the silicon vacancy; E_C is the elastic energy arising in the Si crystal due to the deformation caused by the introduction of carbon into the interstitial space of the Si lattice; the magnitudes of these energies E_V and E_C are determined from the expression $E_{C,V} = \frac{2\mu^{\text{Si}} K^d}{2K^d + 4\mu^{\text{Si}}} \frac{(V^d + V^{\text{Si},m})^2}{3V^{\text{Si}}}$; V^d is the volume occupied by a defect (a Si or C vacancy in an interstitial) in silicon; $V^{\text{Si},m}$ is the volume of the interstitial position in silicon; μ^{Si} – shear modulus of Si, $\mu^{\text{Si}} = 5.2\cdot 10^{10}$ N/m^2; K^d is the bulk modulus of a point defect (Si or C vacancies in the interstitial). Since the carbon atom and the vacancy are modelled as point incompressible dilatation centres, their bulk moduli can be set equal to $K^d = \infty$; V^{Si} is volume per atom in silicon, $V^{\text{Si}} = 2.0\cdot 10^{-29}$ m^3. Calculations of the values of elastic energy according to formulas (2) and (3) can be found in [15, 16]. The calculations have shown that the dilatational elastic energy can completely relax only due to dipoles. The lifetime of dilatation dipoles at temperatures $1100-1250$ °C is approximately $\sim 10^{-1} \div 1$ sec, therefore, elastic dipoles also play the role of ordering centres of epitaxy. If point defects are located along the <100> direction, then, on the contrary, they will repel each other, dipoles will not be formed, and the resulting large elastic energy makes unfavourable the location of defects along the <100> direction, which leads to misorientation of the layers.

Thus, during the first stage of the reaction, the CO molecule interacts with the surface of the silicon substrate and decomposes into a carbon atom and an oxygen atom. Oxygen atoms enter into a chemical reaction with Si atoms, which results in the formation of SiO gas. The SiO gas is removed from the system, and a vacancy forms in the substrate in place of the silicon atom, converted into SiO gas. The excited carbon atom, which is released from the CO molecule by the chemical reaction, is shifted to an interstitial position in the silicon lattice [5, 14, 20]. This stage can be written as follows:

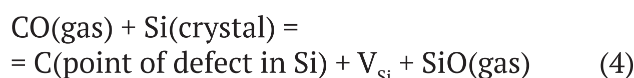

CO(gas) + Si(crystal) =
= C(point of defect in Si) + V_{Si} + SiO(gas) (4)

where V_{Si} is the silicon vacancy. It is at this stage the intermediate phase of the so-called "pre-carbide" silicon is formed. This phase is silicon saturated with defect pairs C + V_{Si}. As follows from (4), pairs of point dilatation defects C and V_{Si} always form and disappear in pairs. "Pre-carbide" silicon is actually silicon where every second Si atom is substituted with C atom via the reaction (4). Thus, one Si cell contains 4 pairs of dilatation defects C + V_{Si}, i.e., in "pre-carbide" silicon, everything is ready for the transformation of silicon into silicon carbide. This process occurs during the next stage of the reaction, which is described by the equation

Si(crystal) + C(point of defect in Si)+ V_{Si} =
= SiC(crystal) (5)

At this stage, the carbon atoms move in a coordinated manner towards the silicon vacancies, thus forming silicon carbide. The final topochemical reaction (1) is obtained by summing steps (4) and (5). It is the elastic interaction between pairs of point dilatation defects C and V_{Si} that determines the kinetics of reaction (1). It is important to emphasise that the first-order phase transition (5) proceeds in a coordinated manner, i.e., the breaking of old bonds between atoms and the formation of new bonds proceed simultaneously and in concert, which essentially ensures the high crystalline perfection of the silicon carbide film. Such a transformation is always accompanied by the formation of voids, since the volume of the Si cell is twice the volume of the SiC cell. The length of all bonds decreases by 20%, namely from 2.35 to 1.88 nm. The first-order phase transition (5) proceeds layer by layer, i.e., several layers of pre-carbide silicon are simultaneously converted into

SiC with the interface shifted perpendicularly to the substrate surface. The reaction rate constant of chemical reaction (5) is approximately two orders of magnitude higher than that of reaction (4), therefore step (5) proceeds noticeably later and much faster than step (4). This can explain the fact that the SiC film is formed with rather uniform thickness and without noticeable voids. All voids appear in silicon under the SiC film [1–6, 18–20].

A surprising feature of reaction (1) is the fact that reaction ends with the formation of silicon carbide, and the reaction does not proceed further to the formation of carbon or even diamond. This is related to both step (4) and step (5). For reaction (4), it is necessary to have “free space” in a silicon cell to accommodate a carbon atom in it. Only one carbon atom can be located inside this cell. This is the reason why only four atoms in the silicon lattice can be substituted, and not all of its eight atoms. Otherwise, we would obtain a very strongly elastically stretched diamond lattice. This would require overcoming a very high activation energy. Such a reaction cannot proceed under these conditions. Even a simpler reaction of placing a carbon atom in each crystal cell of silicon cannot proceed. Carbon atoms can be inside the cell only if one silicon atom is removed from the silicon cell, i.e., the cell contains a silicon vacancy. Moreover, the point defects (carbon and vacancy) must be located strictly along the [111] crystallographic direction in Si. Only in this case, due to the elastic mechanical attraction of the dilatation defects, their total elastic energy is equal to zero. Otherwise, along other crystallographic directions in Si, reaction (4) does not occur. Thus, reaction (4) not only “selects” the required four Si atoms but also “selects” one single direction in the crystal space, along which the future SiC crystal lattice is formed. However, reaction (4) is not sufficient for the transition of Si into SiC. Reaction (5) completes the process of SiC synthesis. When reaction (5) proceeds, it is important that five SiC crystal cells formed as a result of this reaction almost exactly coincide with four Si cells [4, 10]. As a result, the reaction of displacement of atoms (5) occurs with minimal energy consumption. It is reaction (5) that completes the process of the “final docking” of crystal lattices.

2.1.2. The stage of transformation of dilatation dipoles into epitaxial SiC

The destruction of the dipole leads to an increase in the elastic energy of the silicon crystal and, accordingly, to an increase in its total free energy. When the dipole is destroyed, the carbon atom must take the place of the vacancy. This leads, on the one hand, to an increase in elastic energy, and, on the other hand, to a decrease in the total internal energy of the system, since the chemical bonds become saturated. If a break occurs only in the mechanical attraction between defects, then the estimate of the lifetime of the activation complex at a temperature of 1250 °C provides approximately the following value $\tau_{lif} \sim 1$ sec. However, the transition of the intermediate substance into silicon carbide through breakage of the bond in a dipole and an increase in the elastic energy of the system are not acceptable for the growth of a single-crystal layer of silicon carbide. With such a transition, only a disordered defective carbide layer containing dislocations, cracks, etc. will grow, since the elastic energy at the beginning of such a transition will be high. There is another and the only possible way for the transition of the intermediate substance to silicon carbide without increasing the elastic energy in the system [5]. Let us turn our attention to Fig. 1. If carbon atoms move from interstitial positions to positions occupied by vacancies (numbers No. 1–No. 4), then a silicon carbide layer will be formed in the upper part of silicon. In silicon carbide, the lattice parameters are much smaller than in silicon. This means that part of the original volume occupied by the silicon lattice should be released. In this case, the relaxation of the elastic energy will occur. The placing sequence of the (111) planes of the silicon lattice in projection onto the $(11\bar{2})$ plane is shown in Fig. 2, as well as in Fig. 1. Let the upper layer of silicon, which has already passed into the intermediate state (Fig. 2a), be transformed into a layer of silicon carbide (Fig. 2b). The interatomic distance between Si atoms along the $(\bar{1}11)$ plane in the projection onto the plane $(11\bar{2})$ equals 3.84 Å. We assume that the interatomic distance in the intermediate substance has not changed and corresponds to the distance between silicon atoms. The distance between C atoms lying along the (111) plane in

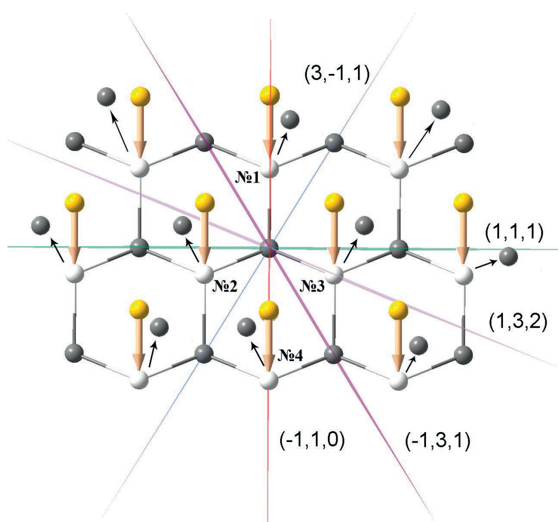

Fig. 1. Silicon lattice: the stacking sequence of (111) planes in the projection on $(11\bar{2})$ plane. ● – the silicon atoms, ● – the carbon atoms in interstitial positions, ○ – the silicon vacancies, ↓ – the directions of the interaction between defects in dilatation dipoles, № 1 – № 4 – the numbers of atoms to be removed for the formation of elastic dipoles

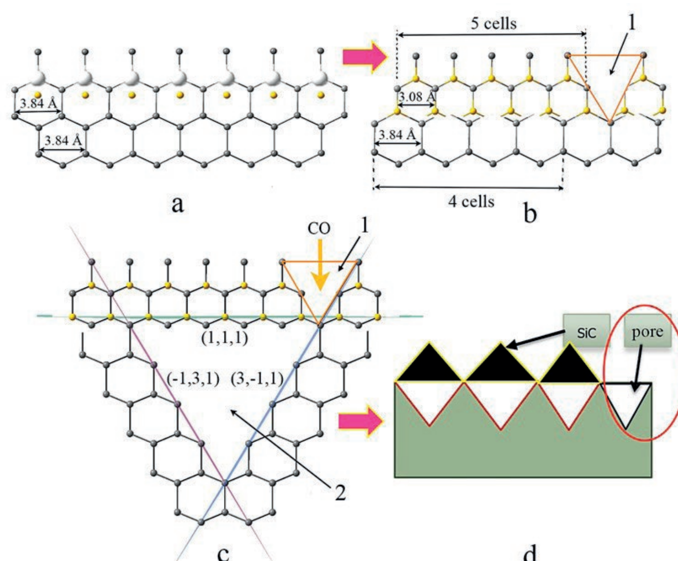

Fig. 2. Consecutive stages of transformation of the intermediate complex "carbon atom – silicon vacancy" into the silicon carbide (in the projection on $(11\bar{2})$ plane). (a) Intermediate stage. (b) Stage of the "displacement" type phase transformation with the formation of the silicon carbide and the contraction pores. (c) Silicon carbide, etch pit and contraction pore admitting carbon monoxide into silicon bulk. (b) Stage of the "displacement" type phase transformation with the formation of the silicon carbide and the contraction pores. (c) Silicon carbide, etch pit and contraction pore admitting carbon monoxide into silicon bulk [5, 6]

the projection on the $(11\bar{2})$ plane in SiC is 3.08 Å. The distance between the planes of five SiC cells ≈ 15.4 Å, which, up to the first decimal place, coincides with the distance between the planes of four Si cells ≈ 15.4 Å. This means that not all bonds are broken during the transformation of the intermediate substance into silicon carbide but only the bonds that do not coincide with the bonds in Si (Fig. 2b). In this case, under the place where the bonds have been broken, namely under the Si layer, an empty space is formed. If we consider a higher number of layers instead of two layers of cells as in Fig. 2a, than it follows from solely geometric considerations that the etch pits will have a pyramidal shape. In the section by the $(11\bar{2})$ plane, they will look like a triangle, bounded by the planes (111), $(\bar{1}31)$ and $(3\bar{1}1)$ (Fig. 2c). The shape of this figure will be similar to the shape of the etch pit formed during silicon etching [25]. Therefore, the voids under the silicon carbide layer will be called etch pits. Simultaneously with the etch pits, as can be seen from Fig. 2b, due to the decrease in the volume of the material, stresses are formed and lead to the initiation of shrinkage pores located along the surface of the substrate. Shrinkage pores are formed in places that are multiples of five cell sizes of silicon carbide. The minimum shrinkage pore has a size comparable to the size of a silicon cell (Fig. 2b).

Thus, the SiC layer formed according to this mechanism consists of a SiC film layer covering triangular pores located under its surface and shrinkage pores located along the substrate surface (Fig. 2d). For the growth of the epitaxial layer of silicon carbide, it is necessary for the releasing part of the volume occupied by the intermediate substance transforming into a SiC film to be redistributed only between the film and etch pits. The formation of shrinkage pores is an undesirable process, since in this case, part of the film is broken. The transition of the intermediate complex into silicon carbide occurs when carbon atoms are displaced from interstitial positions in silicon to positions occupied by vacancies

(numbers No. 1–No. 4 (Fig. 1)). In this transition, the C atom combines with the Si atom and, since the C atom is smaller than the Si vacancy, a vacancy in Si is formed at the same time. It follows from formula (2) that, in this case, the attraction of defects will be changed to repulsion, since the sign of the defects changes in this case. As a result of this process, the total elastic energy of the system increases. To avoid it, a phase transition occurs in the system with the formation of a SiC nucleus and a pore [5]. This process minimises the total free energy of the system. During the phase transition, the initial volume of the intermediate complex changes dramatically. From the volume initially occupied by it, a layer of silicon carbide and pores are formed. The volume of the formed silicon carbide is much lower than the volume occupied by silicon. This means that the transition of the intermediate substance into silicon carbide with the formation of etch pits is a typical first-order phase transition. In [5], the minimum work of formation (free energy) of a SiC nucleus and an etch pit was calculated. The transition of an intermediate substance into silicon carbide is a first-order structural phase transition of the displacement type (carbon atoms are displaced from their original positions into the region of silicon vacancies). As the carbon atom shifts to position No. 1, and if the top silicon atom has not evaporated, the silicon carbide nucleus will have a pyramid shape, and the etch pits take the shape of a triangular depression. In order to simplify the calculations in [5], we assumed that the silicon carbide nuclei and etch pits have the shape of a flat disk of a certain size with radius *r* and height H/2, which is not true in general. The scheme of the transformation of the intermediate complex into the SiC nucleus and the etch pit is shown in Fig. 3. As can be seen, the silicon carbide layer is formed near the surface of the silicon substrate and emerges on its surface. This layer is only partially coherently, without mechanical deformation, bonded to the underlying silicon atoms. The pore is located under the rest of the surface of the nucleus. If the SiC nucleus was completely coherently bonded to the substrate along the entire contact perimeter, then the expression for the minimum work of the nucleus formation would contain a term describing the elastic energy of interaction between the nucleus and the substrate. However, this is not the case, since simultaneously with the nucleus, an etch pit is also nucleated under its surface (Fig. 3c). This means that a part of the substrate material "turns into a void", turning the energy of the elastic interaction of the film with the substrate to zero. At the same time, in contrast to conventional film growth, a SiC nucleus formed in this way is already epitaxially oriented. Its orientation is determined not by the surface of the substrate but by its internal structure where the intermediate

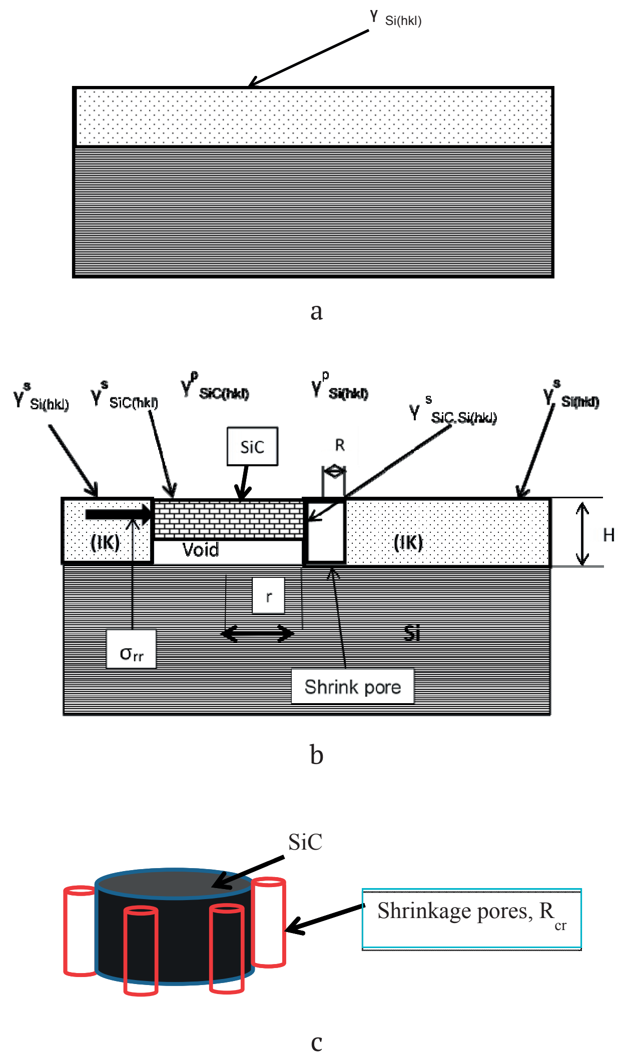

Fig. 3. Consecutive stages of transformation of the intermediate complex "carbon atom – silicon vacancy" into the silicon carbide (in the projection on $(11\bar{2})$ plane). (a) Intermediate stage. (b) Stage of the "displacement" type phase transformation with the formation of the silicon carbide and the contraction pores. (c) Silicon carbide, etch pit and shrinkage pore admitting carbon monoxide into silicon bulk [5]

substance — silicon with elastic dipoles — have existed. This process can take place only with the simultaneous nucleation of the nucleus and an etch pit, which is ensured by the shift of carbon atoms, which leads to the simultaneous creation of vacancies and SiC molecules. If the nucleus is formed before the etch pit, then the free energy of the system would increase by an amount equal to the elastic energy of the coherent interaction of the nucleus and the substrate. Thus, a joint nucleus containing the etch pit and the silicon carbide nucleus is formed.

The formula for the thermodynamic work of formation of the joint nucleus etch pit – SiC nucleus was derived in [5]. Note that the concept of thermodynamic work is wider than the concept of free energy or the isobaric-isothermal Gibbs potential of the formation of a new phase nucleus. If the volume of the system is preserved during the phase transition, then the work of formation of the new phase is equal to the change in free energy, and, as is known, in the case of the phase transition of the first kind, the volume of the new phase is different from the volume of the old phase. Therefore, it is necessary to use free energy in thermodynamic calculations of phase transitions with a certain degree of caution. If the pressure in the system is constantly maintained during the phase transition, then the work of nucleation coincides with the isobaric-isothermal Gibbs potential. Therefore, in [5], a general expression was obtained specifically for the work of formation of a new phase, and not for specific cases. This expression looks like:

$$R^{cr}_{\min}(\cos\varphi(x,y,z)) = \frac{\Gamma_1\Gamma_2(4\pi\Gamma_2 - \Gamma_3\varepsilon)}{\left[\xi - \Lambda(\cos\varphi(x,y,z))\right]^2} + \\ + \frac{\pi\Gamma_2\Gamma_3^2}{\mu^{Si}\varepsilon\left[\xi - \Lambda(\cos\varphi(x,y,z))\right]}. \qquad (6)$$

In this formula, $\Gamma_1 = \left(\gamma^S_{\mathrm{SiC}_{hkl}} + \gamma^p_{\mathrm{SiC}_{hkl}} - \gamma^S_{\mathrm{Si}_{hkl}} + \gamma^p_{\mathrm{Si}_{hkl}}\right)$ is the total surface energy of the formation of the SiC nucleus and etch pit; $\Gamma_2 \cong \left(\gamma_{\mathrm{SiC,Si}} + \gamma^p_{\mathrm{Si}_{hkl}}\right)$ is the total surface energy of the nucleus and etch pit bordering the shrinkage pore; $\Gamma_3 = (1/2)(\gamma^{\mathrm{p}}_{\mathrm{SiC}_{(hkl)p}} + \gamma^{\mathrm{p}}_{\mathrm{Si}_{(hkl)}} - 2\gamma_{\mathrm{SiC,Si}}/\pi)$ is the value describing the increase in surface energy in the system during the formation of the shrinkage pore; $\gamma^S_{\mathrm{SiC}_{hkl}}$ is the surface energy of the SiC nucleus for its facet with indices (hkl) appearing on the surface; $\gamma^s_{\mathrm{Si}_{(hkl)}}$ is the surface energy of the silicon substrate before substitution with the silicon carbide layer having the facet orientation (hkl); $\gamma^p_{\mathrm{SiC}_{hkl}}$ is the surface energy of the silicon carbide nucleus for the facet facing the etch pit; $\gamma^p_{\mathrm{Si}_{hkl}}$ is the surface energy of the (hkl) interface silicon–gaseous medium (vacuum) from the side of the pore; in the general case, $\gamma^p_{\mathrm{Si}_{hkl}}$ can be replaced by $\gamma^p_{\mathrm{SiC}_{hkl}}$ if the inner surface of the pore is covered with a layer of silicon carbide; $\gamma_{\mathrm{SiC,Si}}$, is the surface energy of the interface between the new SiC phase and the old Si phase (SiC–Si); $\cos\varphi_{x,y,z}$ are the direction cosines between the crystallographic coordinate system (the *x, y, z* axes in the crystal) and the direction of the straight line connecting the centres of the interacting defects; $\Lambda(\cos\varphi(x,y,z)) = W(\cos\varphi_{x,y,z})N_d + Y_{\mathrm{SiC}}$; $Y_{\mathrm{SiC}} \approx \mu^{\mathrm{Si}}\varepsilon^2/2$; N_d is the density of dilatation dipoles in the surface layer of the substrate; μ^{Si} is the shear modulus of Si; ε is the strain in the layer of the substrate surface, which occurs due to the difference in the distance between the atoms in Si and in SiC along the (111) planes, $\varepsilon \approx 0.2$; $\xi = \chi(1/V^{\mathrm{Si}} + 1/V^{\mathrm{SiC}})$; $\chi = k_B T \cdot \ln(P_{\mathrm{CO}}K^{eq}/P_{\mathrm{SiO}}$ is the chemical affinity; P_{CO} is the pressure of CO vapour; P_{SiO} is pressure of SiO vapour; $K^{eq} = P^{eq}_{\mathrm{CO}}/P^{eq}_{\mathrm{SiO}}$ is the equilibrium constant of reaction (1), P^{eq}_{CO} and P^{eq}_{SiO} are the equilibrium pressures of CO and SiO gases. The temperature dependence of the constant K^{eq} is provided in [12].

A distinctive feature of formula (6) is the following. In contrast to the standard expressions for the work of formation of a new phase [26], formula (6) consists of two terms. The first term at $\varepsilon = 0$ completely coincides with the standard expression for the formation of a cylindrical nucleus of a new phase [26], and the second term describes the effect of a shrinkage pore on the formation of a nucleus at $\varepsilon \neq 0$. Thus, the nucleation of silicon carbide stimulates the nucleation of a shrinkage pore, which, in turn, stimulates the formation of a SiC nucleus. In [5], we called the first, the main, phase transition the "master" one, and the transformation at which shrinkage pores are generated by the formation of the first phase was called the "slave" transition, since it is stimulated only by the formation of a new phase. In the process of nucleation of a new

phase, despite the existing connection, each of its components "fluctuates" independently. It is well known that at an increased concentration of one of the components of a chemical reaction, the precipitation of a pure phase of this component is possible [26, 27]. In our case, the situation is fundamentally different. Only one phase of SiC can be nucleated; shrinkage pores are nucleated only as a result of the formation of SiC nuclei. The SiC phase is the "master" phase, and the phase of the shrinkage pores is the "slave" phase. The formation of the SiC phase resembles a locomotive that pulls a train uphill. The composition itself can only reduce the speed of the transition over the hill, but it cannot speed up this process. The process of phase nucleation can be accelerated only by chemical affinity, which determines the rate of nucleation of SiC pulling the nucleation of shrinkage pores. In this case, the elastic field created by the SiC nuclei in the silicon substrate leads to a new phase transition, the formation of shrinkage pores. This process resembles the co-crystallization process that takes place in some solutions and melts. Thus, in some systems, one phase transition can cause another transformation, stimulated by excitation of some field. In our case, this field is an elastic field.

Nucleation rate of SiC with etch pits and shrinkage pores $I(\mathrm{n}_{cr},\beta_{cr})$, according to [5], has the form:

$$I(\mathrm{n}_{cr},\beta_{cr}) = \frac{2D_{cr}}{\sqrt{\pi}}(\mathrm{N}_d + \mathrm{N}^{Si})\exp\left(-\frac{R^{cr}_{\min}}{k_B T}\right) \quad (7)$$

where the dipole density $\mathrm{N}_d \approx 1.2\cdot 10^{28}$ m^{-3}, the density of silicon atoms $\mathrm{N}^{Si} \approx 5\cdot 10^{29}$ m^{-3}, D_{cr} is the diffusion coefficient in the "size space" — the kinetic coefficient that determines the rate of addition of atoms and vacancies to the SiC nucleus and pores. At a temperature of 1250 °C, $\Gamma_{(\overline{111})} = 0.86$ J·m^{-2} and $\ln K/K^{eq} \sim 0.2$, the diffusion coefficient in the size space is approximately equal to $D_{cr} \approx 10^{-7}$ sec^{-1} [5]. The density of dipoles and the density of atoms in silicon are approximately equal to the following values: $\mathrm{N}_d \approx 1.2\cdot 10^{28}$ m^{-3}and $\mathrm{N}^{Si} \approx 5\cdot 10^{29}$ m^{-3}. It follows that their ratio takes the following value: $\mathrm{N}^{\mathrm{Si}}/\mathrm{N}_d \approx 40$. In this case, it follows from formula (7) that their nucleation rates will differ from each other by approximately the same number, i.e., $I(\beta_{cr})/I(n_{cr}) \sim 40$. At a higher supersaturation, at which the critical radius of the SiC nucleus has a size of the order of several nanometres, the critical radius of the shrinkage pore will be of the order of atomic sizes. This means that the SiC nucleus will be surrounded by vacancy clusters, which can coalesce into thin cracks surrounding the nucleus grain (Fig. 3c). They will be located along the crystallographic directions. For the "healing" of shrinkage pores and cracks, we suggested to add silane (SiH_4) into the reaction zone [1, 2, 5, 6, 28]. SiH_4 increases the total volume of silicon entering the surface of the substrate, and, thereby, reduces mechanical stresses in it. This leads to a decrease in the nucleation rate of shrinkage pores. Additional introduction of SiH_4 into the system reduces the probability of formation of silicon vacancies in the near-surface layers of silicon, thereby reducing the driving force for the formation of shrinkage pores. Silane plays another important role, namely, it lowers the surface tension of the resulting silicon carbide and makes it possible to obtain not only C-terminated surfaces but also Si-terminated silicon carbide surfaces. This is due to the fact that the surface of silicon carbide, in this case, will interact not with vacuum (or CO gas) but with silicon carbide and adsorbed silicon and hydrogen atoms. The characteristic incubation time for the joint formation of SiC and shrinkage pores is of the order of $\tau_{inc} \sim 10^{-4}$ sec [5]. The critical thickness of the intermediate substance and, accordingly, the thickness of the film layer $H_{film} = H_{cr}/2$ depend on the quantity Γ_1. The thickness of the SiC film layer can be changed by changing Γ_1. The value of Γ_1 depends on the surface energies of silicon carbide and silicon. In [5], estimates of the surface energies and critical thicknesses of films formed at different temperatures of the synthesis and pressures of CO and SH_4 mixture are given.

Thus, during the first stage of a chemical reaction, a metastable compound with composition and structure different from both Si and SiC is formed (Fig. 4a). It consists of layers of silicon and, divalent in this compound, carbon, which are separated by a layer of vacancies. Dipoles stabilise this structure by replacing broken chemical bonds with elastic interaction (Fig. 4a). Partial substitution of chemical bonds with mechanical interaction occurs. This allows

the reactants to pass to the final state of the reaction products with the lowest energy cost. Such a transition is often a first-order phase transition, the height of the energy barrier of which is close to $k_B T$. In this case, elastic dipoles located along the <111> direction lead to the anisotropy of the chemical reaction, lengthen the chemical bonds in silicon, and promote the formation of silicon carbide with the lowest energy consumption (Fig. 5b). The destruction of dipoles due to thermal fluctuations leads to the formation of dislocation-free SiC, and the

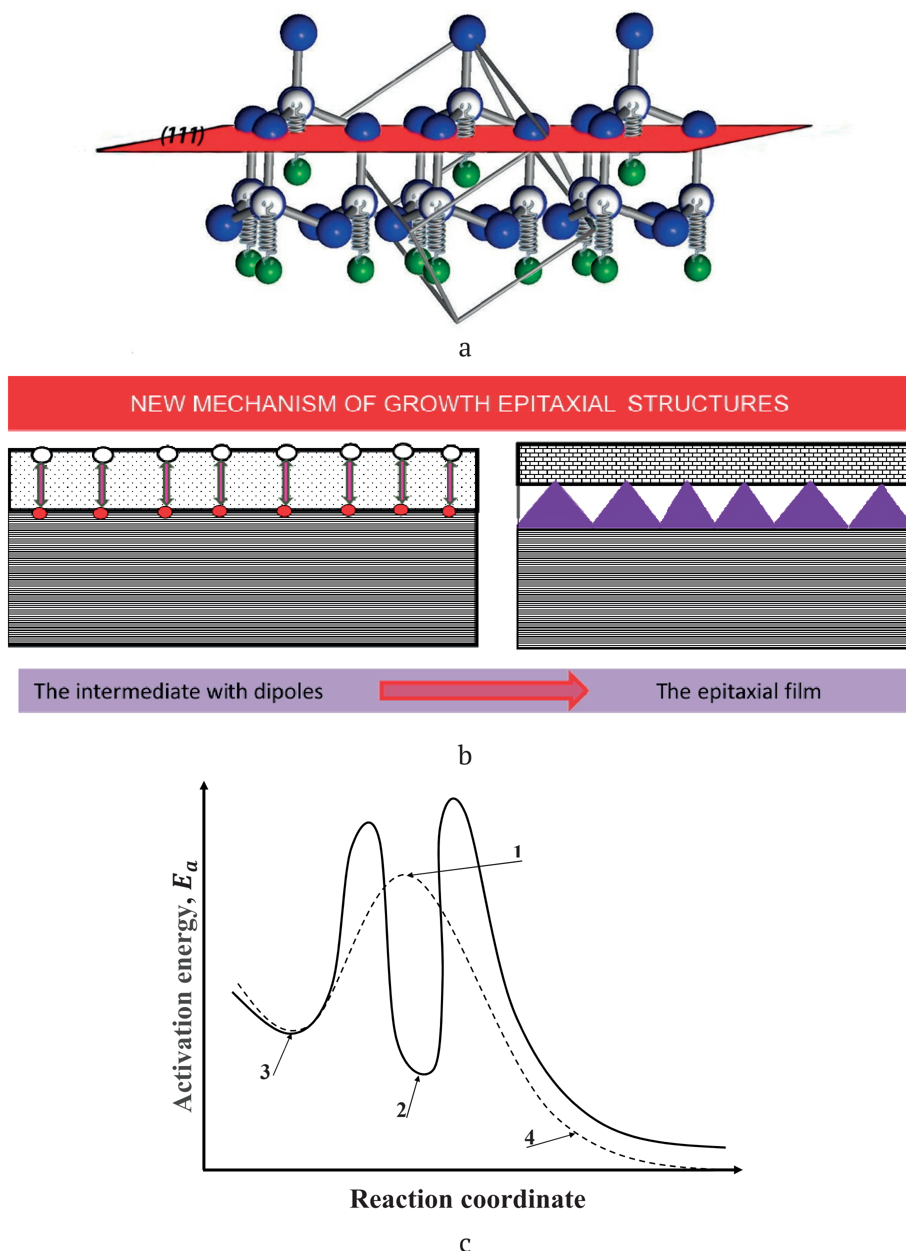

Fig. 4. Consecutive stages of the formation of the silicon carbide on the silicon substrate owing to reaction (1); (a) is the activated complex consisting of an ensemble of elastic dipoles in the silicon lattice; the plane (111) is perpendicular to dipole direction; springs indicate the elastic interaction between similar dilatation centers; (b) is the schematic representation of the new method of thin epitaxial film growth by the creation of dilatation dipoles ensemble; (c) is the path of the chemical transformation of Si into SiC by CO treatment (solid line) and a conventional path without dilatation dipoles formation (dashed line): *1* – activated complex of the standard chemical reactions, *2* – transition (intermediate) complex "silicon –dilatation dipoles", *3* – reactants $CO_{gas} + Si_{solid}$, *4* – reaction products $SiC_{solid} + SiO_{gas}$ [5, 6]

mobile silicon vacancies released in this case either move to the surface or gather together under the SiC film, thus forming pores in Si [13]. The majority of immobile carbon atoms that appear during the destruction of dipoles turn into SiC, but those that do not turn into SiC remain in SiC and may be present there as impurity. The phase transition from an intermediate complex to a final state is often accompanied by another first-order phase transition in the original matrix. This second transition is impossible without the formation of the final phase, i.e., without the first transition, therefore we can distinguish the "master" and "slave" phase transitions. As a result, the coordinate of the chemical reaction (1) in crystalline silicon along the <111> direction looks like it is shown in Fig. 4c. If elastic dipoles were not formed, then the reaction would proceed along the curve depicted by the dashed line. Since dipoles are formed, the reaction proceeds along the curve depicted by the solid line. This line has a minimum associated with the formation of dipoles. This minimum distinguishes the intermediate substance formed in this case from the concept of activated or transition complex widely used in chemistry [43]. The activated complex is formed at point 1 in Fig. 4c where the dashed line reaches its maximum, while the intermediate substance is located at point 2 in Fig. 4c where the solid line passes through the minimum.

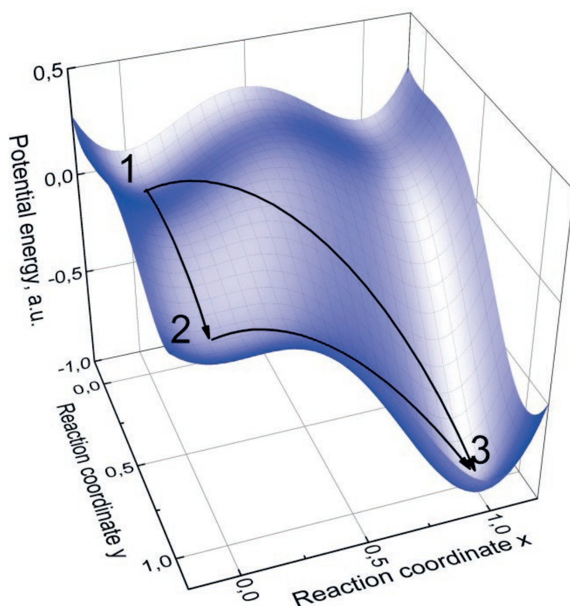

Fig. 5. Potential energy surface in the reaction coordinate space: (*1*) initial state, (*2*) intermediate state, and (*3*) final state. Arrows show the direct phase transition at $1 \to 3$ and the transition through the intermediate state $1 \to 2 \to 3$ [29].

For the transition to the equilibrium state, the system overcomes one more maximum. The nature of this maximum is related to the need for the system to overcome the energy of formation of new surfaces (of silicon carbide and pores) and the elastic energy at the moment of carbon atom bonding with silicon vacancies. For example, during phase transitions in solids, the "master" transition can lead to the appearance of elastic stresses between the original and new phases. The elastic stresses arising in this case will lead to another, "slave", phase transition in the initial phase. In this case, the master phase transition from Si to SiC leads to the formation of shrinkage pores in Si at the interface between SiC and Si. The slave phase transition is the nucleation of shrinkage pores.

It should be noted that it is also possible to obtain SiC as a result of the interaction of Si with CO_2. This will also lead to the formation of SiC. However, as a result of this reaction, solid amorphous SiO_2 will be formed instead of the SiO gas. In this case, a SiC film containing a large number of SiC twins and other growth defects will grow.

2.2. The method of coordinated substitution of atoms as a first-order phase transition through an intermediate state

We showed above that, before conversion into SiC, silicon interacting with CO first passes an intermediate state. This intermediate state is taken into account in formula (6) by the quantity included in its denominator: $\Lambda(\cos\varphi(x,y,z)) = [W(\cos\varphi_{x,y,z})\mathrm{N}_d + Y_{\mathrm{SiC}}]$. If dipoles were not formed in silicon, i.e., if the intermediate substance were not formed, then the value of $W(\cos\varphi_{x,y,z})\mathrm{N}_d$ would be equal to zero. In this case, $\Lambda(\cos\varphi(x,y,z))$ would contain only the term $Y_{\mathrm{SiC}} \approx \mu^{\mathrm{Si}}\varepsilon^2/2$. This term takes into account the appearance of elastic energy in the substrate when a SiC nucleus appears. The term Y_{SiC} with a minus sign in the denominator of the work of formation of a new phase (6) could reduce the driving force of the phase transition to such an

extent that a new phase could not be formed. This is due to the fact that it is subtracted from the value ζ proportional to the chemical affinity χ. However, nature behaves differently. The system minimises the free energy of the transition from solid Si and gas CO to solid SiC and gas SiO, thus forming the intermediate metastable state "elastic dipoles–silicon". The formation of this transitional complex allows the system to bypass the high barrier of new phase nucleation along the "pass". It should be noted that the work of formation of critical nuclei from the final phase from the transition state is much less than from the initial phase.

In [29], this approach was substantially developed. It was shown that the work of formation of a new phase in the presence of a transition state can even approach zero, providing a barrier-free transition through a single nucleus. In particular, during martensitic transformations, the transition through a pre-martensitic intermediate state occurs, and the melting of crystals proceeds through a pre-melting state. In the studied case, the transition from Si to SiC occurs through an intermediate "pre-carbide" state, which includes Si saturated with dilatation dipoles oriented along the [111] direction of silicon. It was proved in [29] that from the intermediate state the system enters the final state through the highest point of the lowest energy barrier in the coordinate space of the reaction or phase transition [29], i.e., the saddle point. Saddle points can only exist in systems with several independent reaction coordinates. It was established in [29] that the role of the order parameters in such systems belongs to the coordinates of chemical reactions. In the case of SiC growing from Si, two reaction coordinates, one responsible for the formation of SiC, and the other responsible for the formation of SiO, are the reaction coordinates. The reaction with the formation of gas is faster and ends earlier, since the reaction with the formation of the SiC crystal requires the restructuring of the entire crystal structure and the formation of shrinkage pores due to the fact that the volume of one cell decreases twice. The transition scheme is shown in Fig. 5. In [29], analytical formulas describing the phase transition through an intermediate state were obtained, and the instant formation of the new phase upon transition from an intermediate state from one island was shown, i.e., the intermediate state transforms into a new phase simultaneously throughout the entire volume. In this case, the entire matrix of the initial phase determines the crystalline orientation of the new phase, which is a great advantage of this thin film growth mechanism. This approach opens up completely new prospects for the synthesis of high-quality epitaxial films and other materials. It becomes possible to grow film structures entirely from one nucleus. There is no need to deal with grain boundary defects that arise when nuclei merge with each other.

2.3. Growth of the epitaxial SiC layer on the Si(100) surface

Thus, a distinctive feature of the MCSA is the formation of the (111) plane regardless of the initial Si crystallographic plane, on which SiC was synthesised. This effect is due to the fact that carbon-vacancy structures (these are dilatation dipoles at the initial stage) are always located along the <111> direction and located in the (–110) plane perpendicular to the (111) plane. Further, after the formation of elastic dipoles, SiC is formed according to reaction (5). In this case, shrinkage with the separation of the SiC nucleus from the Si matrix occurs with the simultaneous formation of shrinkage pores. In [5, 30], a theory of the formation of shrinkage pores was developed based on the model of the nucleation of cavities from an ensemble of vacancies that appear under the action of a tensile load [31]. Delamination of one material from another is also possible as a result of the formation of partial dislocations in slip planes and the initiation of vacancy dislocation loops [32]. It is known [33], that the slip planes in crystals with a diamond lattice at temperatures exceeding 0.5 of the melting point of the crystal (in our case, for the synthesis of SiC, this condition is certainly met for Si) are the family of (111) planes, while the slip itself occurs along the < 110> directions. Therefore, on a smooth (100) silicon surface, SiC with the (100) orientation cannot be nucleated. However, nature does otherwise. The (100) Si facet upon conversion transforms into a SiC facet consisting of many facets resembling sawtooth

structures, the side facets of which are covered with the (111), (110), and (210) planes, as shown in Fig. 6 [30]. The angle between the direction of the (100) facet and the (111) facets is 54°44’. Any arbitrarily small deviation of the (100) facet from this direction makes it vicinal, which leads to the instantaneous formation of a very thin (several atomic layers) film.

A different picture will be observed if SiC is grown by the MCSA on the (100) surface misoriented by 2–7° in the <011> direction. If this surface is heated to a temperature exceeding 600 °C, then the (100) plane of silicon will be covered with steps. The terraces of this structure will be the (100) planes, and the steps will be limited by the (011) planes. There are “channels” along the <011> directions in the silicon lattice, which is associated with the features of the crystallographic structure of the Si lattice. Therefore, along this direction, CO molecules move perpendicular to the steps deep into Si. The Si surface is saturated with CO, and, as described above, the interaction of Si with CO occurs, resulting in the formation of an intermediate state, which is further converted into SiC. During this transformation, part of the Si from the (011) step evaporates, and the (111) SiC step is formed [30]. This process is schematically shown in Fig. 7. This transformation removes the “degeneracy” inherent to the non-deflected (100) facet and leads to the formation of facets consisting of the (111) SiC facets, but located already on the former (011) steps, and not randomly located as on the (100) facet. Naturally, these facets also make an angle of ~55° with the (100) facet and ~35° with the (011) facet. Since the attraction between a silicon vacancy and a carbon atom in the silicon matrix is maximal along the <111> direction, a

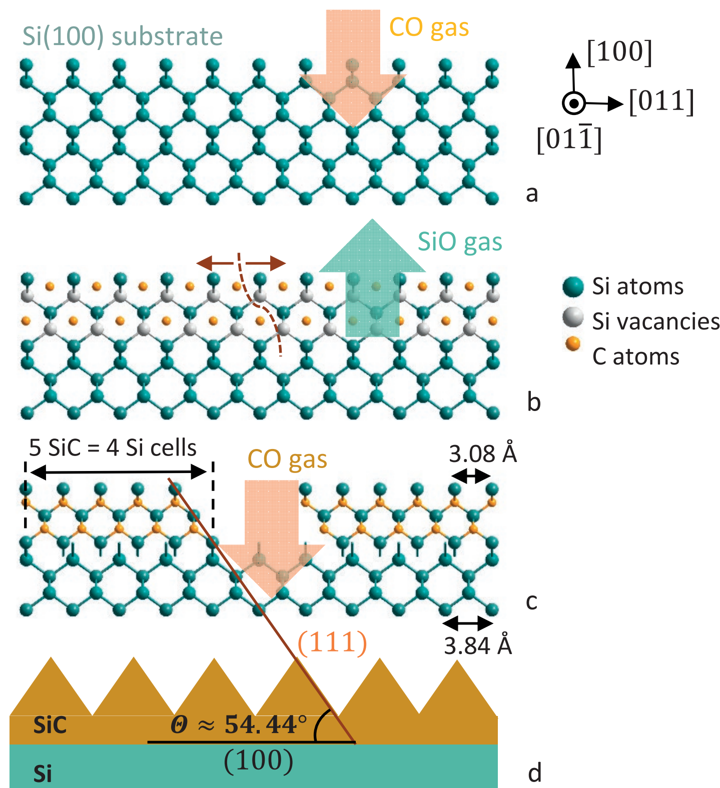

Fig. 6. Schematic representation of the successive stages of transformation of the singular Si(100) surface into SiC covered with facets during the exposure of the Si surface to the CO gas in accordance with reaction (1): (a) bringing the Si(100) surface in contact with the CO gas; (b) the first stage of the reaction, namely, the removal of Si using the SiO gas and the formation of dilatation dipoles ($C–V_{Si}$); (c) the phase transition from the intermediate state of silicon into a SiC layer; and (d) the formation of a sawtooth surface of the SiC film covered with (111) facets; $\theta = 54°44'$ is the angle between the SiC(111) facet and the Si(100) surface [30]

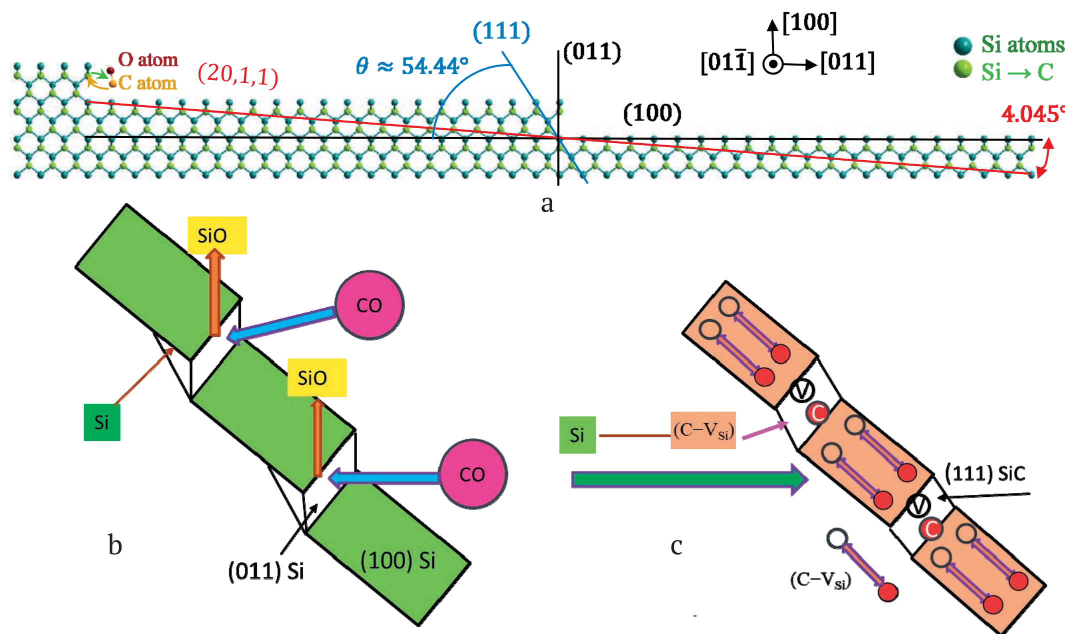

Fig. 7. Schematic representation of the mechanism of successive stages of the occurrence of reaction (1) on the vicinal Si(100) surface covered with (011) steps: (a) the vicinal Si(100) surface deviated by 4° in the [011] direction with (011) steps toward the plane; (b) the initial Si(100) surface covered with (011) steps; and (c) the intermediate state formed during the transformation of the intermediate state into the SiC(111) plane, which lies at an angle of $\theta = 54^{\circ}44'$ to the (100) face [30]

part of the (011) Si step can turn into the (112) SiC kink. It is known, that the angle between the (112) and (100) planes in a cubic crystal with the diamond lattice is ~35°. As a result, a longitudinal wedge-shaped protrusion of silicon carbide is formed with the top protruding above the step platform and an inclined edge reaching the platform of the underlying step, with the formation of a slope. These SiC facets resemble “fish scales” or “knight’s chainmail,” the wafers of which closely fit with each other [30]. The experimental AFM image of a SiC layer coated with the (111) facets grown on a (100) Si vicinal surface deviated from the <100> direction by 4° towards <011> is shown in Fig. 8. Thus, the Si(100) surface is covered with an array of wedge-shaped parallel steps, which are triangular prisms (side facets of pyramids).

Since the symmetry of such prisms is characteristic of both cubic and hexagonal crystals, the symmetry is not degenerate. This means that both crystals with cubic and hexagonal symmetry can grow on these

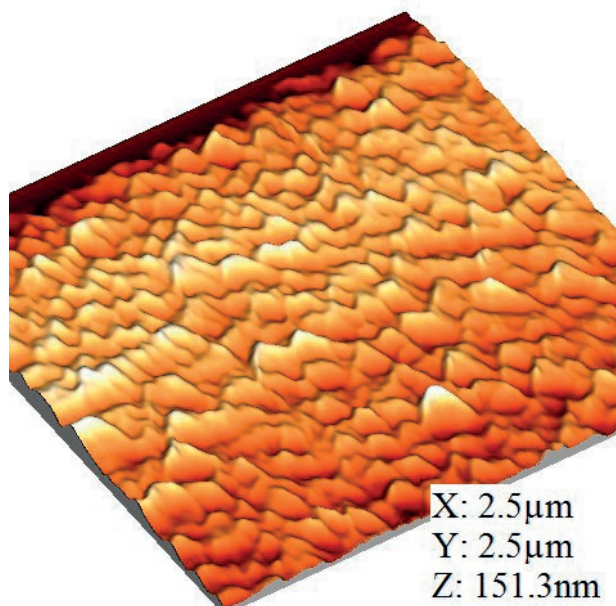

Fig. 8. AFM image of the SiC layer covered with the (111) facets grown on the vicinal (100) Si surface p-type conductivity deviated from the <100> direction by 4° toward <011> [30]

surfaces. Most importantly, this will depend not on the orientation of the substrate but only on the thermodynamic conditions, i.e., on the temperature and densities of the incident fluxes of the components from which the layer grows. If the hexagonal modification is stable under the given conditions, then the hexagonal modification will grow; if the cubic structure is stable, then the cubic modification will grow. This opens up completely new perspectives for growing hexagonal semi-polar crystals.

In [30], a fundamentally new mechanism was also discovered for the process of substitution of atoms on the vicinal Si facets of *n*- and *p*-type of conductivity that are deviated from the singular facet (100). The following findings were revealed. 1) On the vicinal Si surface of *p*-type of conductivity, deviated by 4° or more from the singular facet (100), an ordered SiC phase is formed in the process of SiC synthesis. The surface morphology of this phase has the form of facets (flakes) consisting of layers of both cubic and hexagonal phases. 2) On the vicinal Si surface of *n*-type of conductivity, deviated by 4° or more from the singular facet (100), only the ordered 3C-SiC cubic phase is formed in the process of SiC synthesis. The reasons for this difference are due to the different mechanism and different rates of formation of dilatation dipoles and carbon-vacancy structures on the (100) facet in Si doped with donor and acceptor impurities [30].

3. Quantum-mechanical theory of epitaxial transformation of silicon into silicon carbide

Thus, we found out that during the first stage (4) of SiC synthesis, pairs of defects of C and V_{Si} are formed and saturate the silicon crystal. The C atom is attracted to the silicon vacancy; therefore, the C atom actually replaces the Si atom in the Si crystal. When every second atom in the Si crystal is substituted by a C atom, the crystal will be saturated with pairs of C+ V_{Si} defects, and the stage (4) is completed. Such a Si crystal can be called "pre-carbide" silicon, since everything in it is ready for the transition into SiC. In the second stage (5), large areas of pre-carbide silicon "collapse" with the formation of SiC. Since the volume at stage (5) decreases (the volume of one SiC cell is two times smaller than the volume of one Si cell), this is a first-order phase transition. In [14, 34], the study of the main elementary processes that occur during the transformation of a silicon crystal into a silicon carbide crystal due to a chemical substitution reaction with CO gas was continued. As a result, a quantum-mechanical theory of the coordinated transformation of Si into SiC was proposed. In this case, the density-functional theory (DFT) in the generalised gradient approximation (GGA) was used. The energy profile of this reaction for the Si(100) surface was calculated using the nudged elastic band method (NEB) in the PBE functional approximation using pseudopotentials

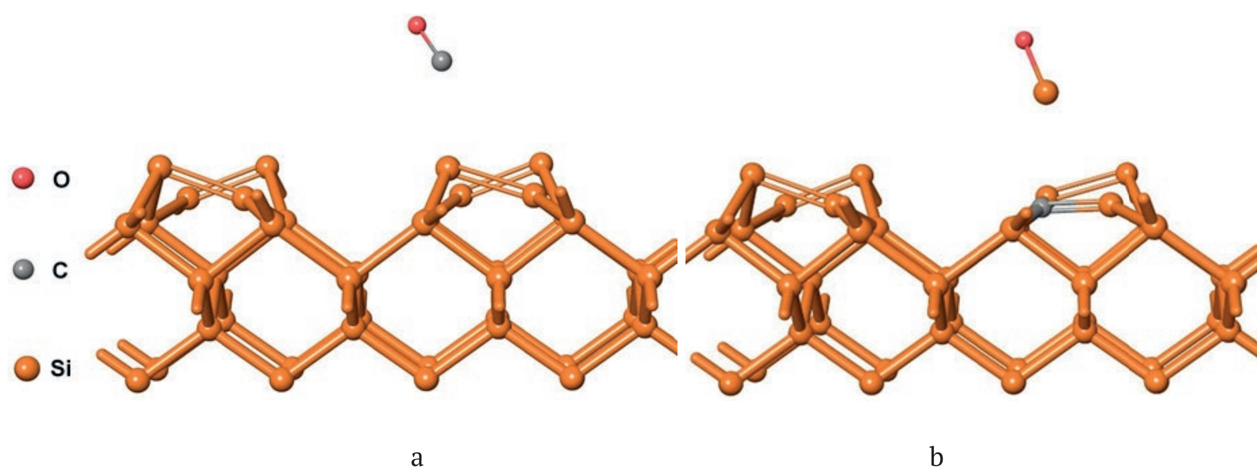

Fig. 9. Initial reactants (a) and final reaction products (b) of stage (4) with the reconstruction p(2 × 2) of the Si(100) surface. At the bottom the broken silicon bonds are saturated with hydrogen, which is not shown for simplicity. On all three axes, there are periodic boundary conditions. [14, 34]

and the plane-wave basis with the reconstruction of $p(2\times2)$ (Fig. 9). It has been established that this reaction (4) is feasible only since it proceeds through the intermediate state IS (Fig. 10b), in which all atoms are chemically bonded to each other. In fact, this intermediate state breaks the reaction into two independent steps. During the first stage, the entire CO molecule is absorbed by the Si surface, and then, after a slight rearrangement (Fig. 10e), the SiO molecule is pushed out by the surface. Due to this, the system reduces the activation barrier of this reaction to 2.6 eV. In [14, 34], the geometry of all intermediate and transition states was calculated (Fig. 10 a-e), and the frequency spectrum of the transition states TS1 and TS2 was found. The only imaginary frequencies of these states are $|\omega_{TS1}| = 160$ sm^{-1} and $|\omega_{TS2}| = 430$ sm^{-1}. The eigenvectors corresponding to the given eigenvalues show the minimum energy path (MEP) at these points (Figs. 10d and 10e). It was shown that the main transition state TS1 is reactant-like, and the auxiliary intermediate state TS2 is product-like. On the (100) surface, the geometry of pre-carbide silicon corresponding to the local energy minimum and the geometry of silicon carbide corresponding to the global minimum were calculated. It was shown that the C-Si bonds in pre-carbide silicon on (100) are stretched on average by 11%. The energy of the first-order phase transition from pre-carbide silicon into silicon carbide was calculated for a region of size $L\times L(4)$. It was shown that such a transition is possible only if the size of the transition region L is higher than a certain minimum size $L_{\min} = 30$ nm. Such an unusual character of the simultaneous transformation of silicon into silicon carbide with the preservation of the entire structure of chemical bonds explains the absence of lattice misfit dislocations in these SiC/Si films. This fundamentally distinguishes this method of SiC/Si growth from the standard one (for example, CVD), where islands grow atom by atom, which inevitably leads to the appearance of misfit dislocations. The estimates made in [16, 21] using the methods of classical mechanics are in qualitative agreement with the results of this study.

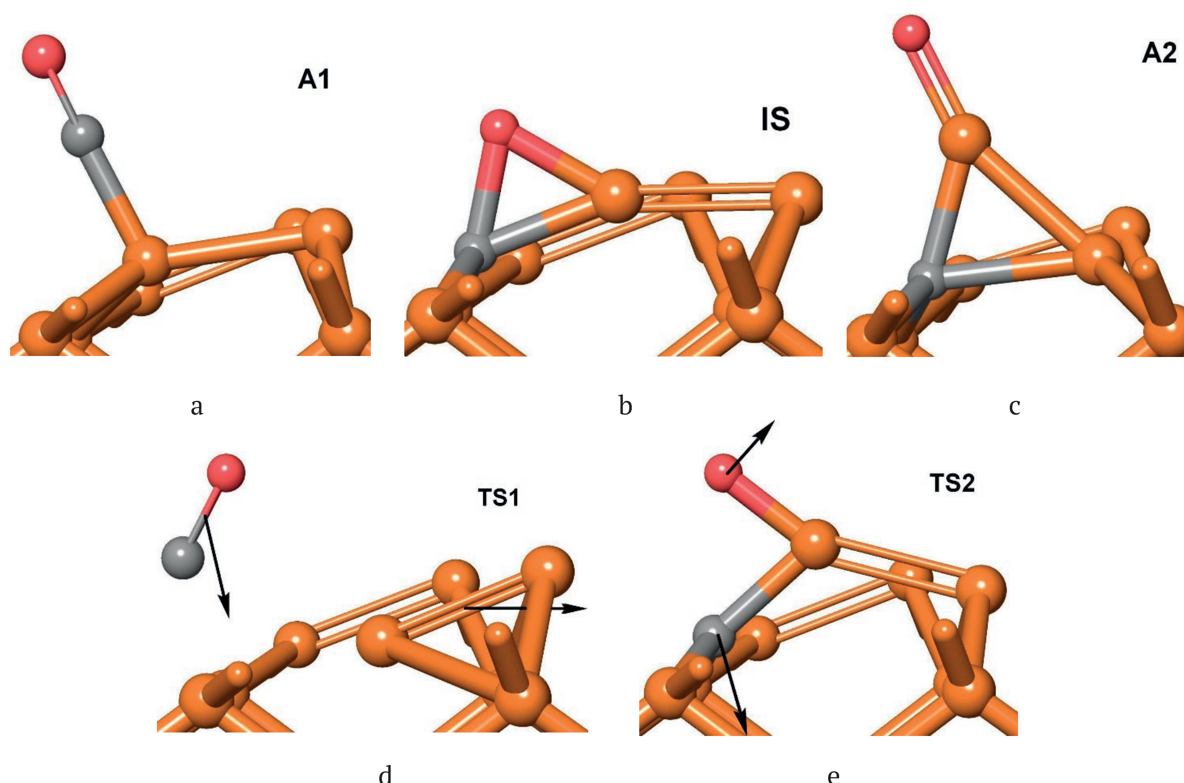

Fig. 10. Geometry of three intermediate states (a),(b), (c) and two transition states (d) and (e) of the reaction (4) [14, 34]

3.1. Energy profile, intermediate and transition states of the reaction of heterogeneous synthesis of SiC

It should be noted that, in addition to the predictable intermediate states A1 and A2 corresponding to CO and SiO molecules adsorbed on the crystal surface (such states always occur in the presence of a surface), the system has a key intermediate state IS (Fig. 10b), in which all atoms are in a chemically bound state. The decisive role of this intermediate state in the course of reaction (4) is that it changes the reaction path by lowering the height of the activation barrier. If it were not for the IS state, then the intermediate state would be different, and the height of the activation barrier would be approximately 4.0 eV. This means that at temperatures of 1200 – 1300 °C the rate of reactions (1) and (4) would be almost equal to zero. The intermediate IS state (Fig. 10b) splits the reaction from state A1 to state A2 into two elementary reactions and lowers the height of the activation barrier to 2.6 eV (Fig. 11). This means that the A1 state with an adsorbed CO molecule exists approximately 10^{-5} sec at T = 1250 °C. The found barrier provides the experimentally observed rate of reactions (1) and (4) [35].

The CO molecule moves vertically as a whole, ensuring that the C atom enters the right place

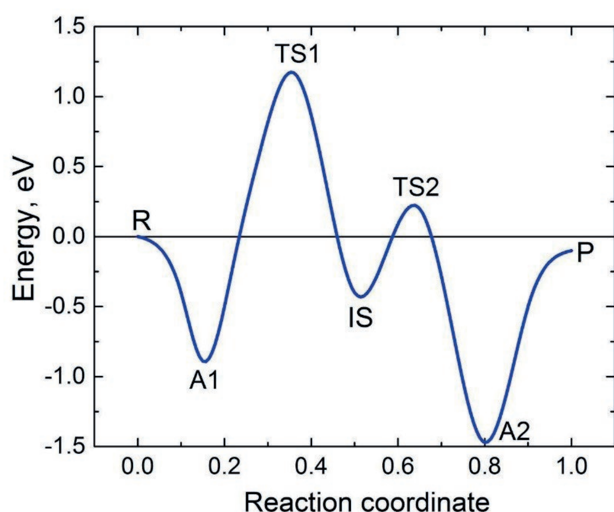

Fig. 11. Cross section of the surface of the potential energy of the reaction (2) along the reaction pathway. The geometry of the system of atoms corresponding to three intermediate states A1, IS, A2 and 2 transition states TS1, TS2 is shown in Fig.10; R is the reactants; P is the final products [14, 34]

(Fig. 10b). At the same time, the Si-Si dimer makes room for this (Fig. 11b), also moving as a whole in the horizontal direction. At the saddle point, the C atom is located at approximately the same distance ~2.65 Å from the three nearest Si atoms without forming a chemical bond with them. This explains such a low value of the frequency modulus ω_{TS1}. The positive frequencies of the TS1 spectrum are closer to the frequencies of the A1 spectrum than to the frequencies of the IS spectrum, therefore the TS1 transition state can be characterised as reactant-like.

In the TS2 transition state (Fig. 10e), atoms, not molecules, are moving. The carbon atom moves almost vertically down and reaches its final position (Fig. 11c). The oxygen atom moves almost parallel to the Si-C bond. Since both the O atom and the C atom are chemically bonded to Si atoms, the frequency $|\omega_{TS2}|$ is noticeably higher than the frequency $|\omega_{TS1}|$. The positive frequencies of the TS2 spectrum are closer to the frequencies of the A2 spectrum than to the frequencies of the IS spectrum, therefore the TS2 transition state can be characterised as a product-like one.

3.2. Transition of "pre-carbide" silicon into silicon carbide on the (100) surface

Thus, stage (4) ensures the substitution of every second Si atom by a C atom according to the mechanism described above. In this case, it is very important to emphasise that the breaking of Si-Si bonds in silicon and the formation of new C-Si bonds occur in a coordinated manner through the intermediate IS state and almost simultaneously (the IS state lives approximately $10–10^{-10}$ sec). If the Si→C substitution occurs in the volume of the Si crystal, then the C atom takes the place of the Si atom. This fact is related to the fact that the C atom and the silicon vacancy V_{Si} are attracted to each other, forming a bound state called a dilatation dipole by analogy with an electric dipole, as mentioned above. In the framework of classical solid body mechanics, for the calculation of the elastic energy of the dilatation dipole [16, 21, 36, 37], a number of strong assumptions had to be made, in particular, point defects were considered as having no dimensions. Using the apparatus of quantum mechanics, not only an estimation but a very accurate calculation of the interaction energy of C and V_{Si} is possible, which

was done by the methods of quantum mechanics in [14, 34].

Let us now consider the (100) surface of a silicon substrate where every second Si atom of the upper atomic monolayer with a thickness of 3.84 Å was substituted by a C atom according to the mechanism described above, after which the geometry of the system was optimised from this initial position (Fig. 12, left side). In order not to involve surface reconstruction in the considered processes, all broken bonds are saturated with hydrogen (for simplicity, hydrogen atoms are not shown in Fig. 12). The optimization of the geometry leads to the fact that the atoms of the film are slightly pressed against the substrate, reducing the bond length. The average C-Si bond length after optimization on the (100) surface is 2.09 Å. After substitution of every second Si atom with a C atom and optimising the geometry according to the terminology of [1, 2, 4–6], this silicon is "pre-carbide" silicon where everything is ready for transformation into silicon carbide. This silicon is obtained after the completion of the stage (2). Since the optimal C-Si bond length in silicon carbide is 1.88 Å, the bonds in pre-carbide silicon on the (100) surface are stretched by an average of 11%, which leads to additional elastic energy. This is the driving force of the transformation of pre-carbide silicon into silicon carbide (5).

Too many atoms are involved in the transition from pre-carbide silicon into silicon carbide (3) (the minimum required number of atoms is $\sim 10^5$), therefore it is not possible to construct an exact quantum-mechanical theory for this transition. Nevertheless, using relatively simple quantum-mechanical calculations, it is possible to determine all the main characteristics of the phase transition (5) and provide a qualitative description for it. In [14], this was done for the (100) surface.

The state of pre-carbide silicon, which corresponds to a local energy minimum in a simple two-dimensional model on the Si(100) surface, is shown in Fig. 12 (see the left side of Fig. 12). The two-dimensionality of the model means that the thickness of the considered layer perpendicular to the plane of the figure is equal to the size of the primitive Si cell, i.e., 3.84 Å. In this dimension (i.e., perpendicular to the plane of the figure), atoms cannot move, and periodic boundary conditions apply. The relaxation of atoms can occur only in two other dimensions, i.e., in the plane of the figure. The stretching of bonds by 11% leads to the fact that the energy of the system has a global minimum, located below the local minimum. The calculations by the density-functional theory method showed that, within the framework of the above-mentioned DFT approximations and two-dimensional model, the global minimum corresponds to the "collapse" of pre-carbide silicon into silicon carbide with the optimal C-Si bond length. In this case, 5 primitive SiC cells fit 4 primitive Si cells (their total length is equal to 15.36 Å) (see the right side of Fig. 12). It turned out that one of the upper Si atoms (i.e., every fourth one) actually enters the material of the SiC film and play an important ordering role, since it forms a bond with two Si atoms from the SiC film. The length of this bond is 2.59 Å, i.e., it is stretched by 10%.

Quantum-mechanical calculations within the above approximations show that the SiC state is more favourable than the state of pre-carbide silicon by the value $\Delta E_1 = 0.25$ eV per primitive SiC cell. However, for the formation of such state from pre-carbide silicon (Fig. 12), it is necessary to break two C–Si bonds in pre-carbide

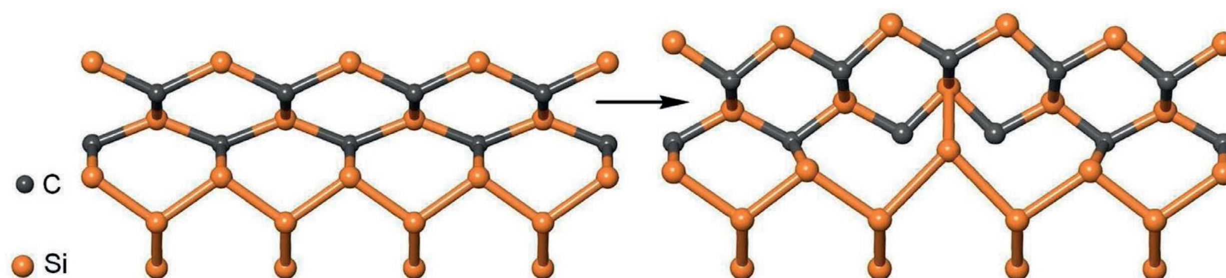

Fig. 12. Transition from precarbide silicon to silicon carbide on Si(10) (reaction (3)). Hydrogen saturating dangling bonds is not shown for simplicity [14]

silicon with the total energy $\Delta E_2 = 10.0$ eV. These bonds are stretched by 11%, therefore they are weakened, therefore the energy ΔE_2 is so low.

So, a square of the pre-carbide silicon monolayer located on the (100) surface and having the size $(L \times L)$ enclosing (L/a^2) primitive cells (a = 3.84 Å is the size of the primitive cell of silicon) requires the following energy to collapse into SiC:

$$\Delta E = -\Delta E_1 \left(\frac{L}{a}\right)^2 + 2\frac{L}{a}\Delta E_2 \tag{8}$$

since the bonds break up along half the perimeter. From the condition $\Delta E = 0$, it is possible to determine the minimum size of a cluster of pre-carbide silicon, for which the transformation into silicon carbide is beneficial:

$$L_{\min} = 2\frac{\Delta E_2}{\Delta E_1}a \tag{9}$$

As it follows from (8), the larger the cluster size, the more favourable the phase transition. However, the larger L, the larger activation barrier proportional to L must be overcome. The size of the barrier is influenced by many factors. First, during the collapse, the outermost atoms make a path equal to $0.2\sqrt{2}L$. In an ideal situation, when the substrate potential is exactly equal to the sine, the energy of cluster movement along the substrate is 0, since such movement is described by the soliton solution of the sine-Gordon equation. However, in practice, the potential of the silicon substrate differs from the sine, so energy has to be spent on moving. In addition, when the cluster moves, the length of the C-Si bonds changes, i.e., the cluster does not move as a whole, which also requires energy. Second, the "collapse" opens up part of the Si substrate surface, and some Si atoms can move upward, lowering the total energy. In addition, these atoms can react with CO and provide the appearance of SiC in the gap between SiC clusters. In practice, a certain amount of silane SiH_4 is added to CO gas exactly to "heal" the voids between SiC clusters [5]. This process facilitates the collapse of pre-carbide silicon clusters and reduces the corresponding activation barrier.

An estimate of the SiC cluster size made in [14] showed that the average size of a pre-carbide silicon cluster undergoing the first-order phase transition is of the following order of magnitude:

$$L \sim 2L_{\min} = 4\frac{\Delta E_2}{\Delta E_1}a = 160a \approx 60 \text{ nm}. \tag{10}$$

4. Diffusion mechanism of CO and SiO molecules into Si with the simultaneous chemical transformation reaction of Si into SiC

In [38], a new mechanism of film growth during the topochemical transformation reaction of Si into SiC under the action of CO was theoretically proposed and experimentally confirmed. The main idea of [38] is as follows. The drift of CO molecules during a chemical reaction with Si occurs first through the channels of the Si crystal saturated with dilatation dipoles C+ V_{Si} and then through the SiC channels due to the difference in CO pressures outside and inside the crystal. Film growth in this model stops when the reaction product SiO "block up" the crystal channels, reducing their hydraulic diameter. This is the fundamental difference between this model and the diffusion model, where the increase in film thickness continues indefinitely as $\sqrt{t}$. In this study, for the first time, experiments were performed to measure the dependence of the maximum film thickness on pressure for films on Si(111) and Si(100), and it was shown that there is a pressure corresponding to the maximum film thickness. With a further increase in pressure, the film thickness decreases, whereasit should be vice versa for ordinary diffusion growth, since diffusion only increases. In [38], a general formula describing the dependence of the thickness of a SiC film formed during the topochemical growth was derived. For small time values *t*, this dependence is diffusional:

$$L(t) = \sqrt{Dt} \tag{11}$$

and for bigger time values it is presented as:

$$L(t) = L_m\left[1 - \exp\left(-\frac{Dt}{2L_m^2}\right)\right] \tag{12}$$

$$L_m(P_{CO}) = L_* \frac{4P_{CO}/p_*}{\left[1 + \left(P_{CO}/p_*\right)^n\right]^2} \tag{13}$$

where p_* and L_* are parameters which have the dimensions of pressure and lengths, respectively;

n is the inverse polytropic index, $n = \frac{C - C_V}{C - C_p} = \frac{C - 2.5R}{C - 3.5R}$; $p_* = \left(\frac{p_0}{va}\right)^{\frac{1}{n}}$; $L_* = \frac{\pi (d_0/2)^2 p_*}{8\eta j_e}$; j_e is the volumetric equilibrium flow rate of CO gas per unit area of the channel; d_0 is the hydraulic diameter of the channel; η is the dynamic viscosity. The dependence of the thickness of the SiC layer growing on the Si (111) facet on the CO pressure is shown in Fig. 13a; the time dependence of the thickness of the SiC layer growing on the Si(111) facet is shown in Fig. 13b. Similar curves for the growth of SiC on the Si (100) facet can be found in [38]. It can be seen from these data that, starting from a certain value of the CO pressure, the growth of the layer thickness slows down, in contrast to the thickness of the layer growing due to diffusion. The growth of the layer thickness also stops with time (at a fixed pressure). After the layer reaches a certain thickness, it no longer grows [38, 39].

The study of the processes of diffusion of CO and SiO gases was started in [38] and continued in [40, 41]. The key role of vacancies V_{Si} and V_C in the kinetics of reaction (1) was shown in [40, 41] using quantum chemistry methods. The transport of the reagent CO gas into the reaction zone and of the reaction product SiO gas from the reaction zone occurs only in the <110> direction and equivalent directions, i.e., in the direction of the SiC channels. The migration of CO and SiO molecules is equivalent to the migration of the O atom and vacancies V_{Si} and V_C, since it is not necessary for the Si and C atoms to migrate, because the O atom easily forms a chemical bond with any atom of the SiC crystal. The energy barrier to migration of vacancies is more than 2 times lower than the barrier to the migration of atoms and, in an ideal crystal, is equal to 3.6 eV for V_{Si} and 3.9 eV for V_C. Therefore, at low temperatures, the synthesis of SiC is limited by migration of V_C. In a 3C-SiC crystal containing twin boundaries, the migration barriers can be 10–20% lower. Starting from a temperature of 1100–1200°C, a significant part of silicon vacancies will transform into carbon vacancies plus immobile carbon structures (the activation energy of this process is 3.1 eV). Therefore, due to the lack of silicon vacancies, they can limit the synthesis of SiC. In this case, SiC synthesised by the MCSA will contain both carbon clusters and traces of microexplosions caused by the accumulation of a large amount of SiO inside the SiC layer.

The processes of diffusion and evolution of a porous layer were also studied in [42]. In that study, the temporal evolution of the average thickness of the porous layer when the sample was kept in a CO atmosphere was studied experimentally and theoretically. The result of the study showed that the thickness at the initial stages is proportional to the cube root of time. A model that describes the process of formation of the porous layer both at the initial stages, when the layer represents isolated pores, and at the

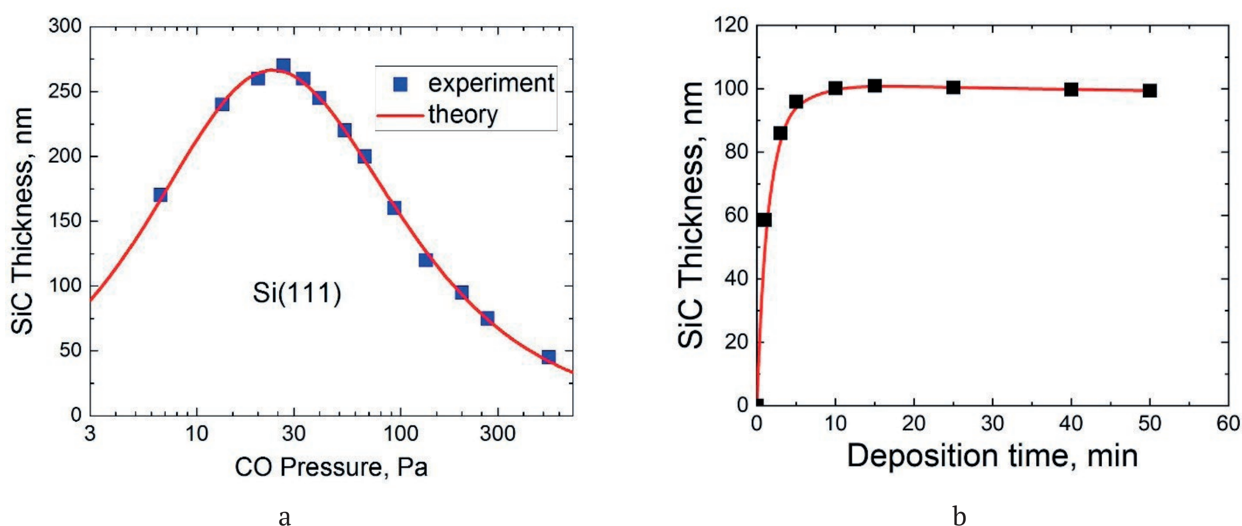

Fig. 13. Dependences of the final thickness of a SiC film on Si(111) on (a) the CO pressure (squares) and (b) growth time (squares). The solid lines stand for theoretical dependences calculated by formulas (11) and (12) [38]

later stages, when the pores coalesce and move deep inside as a single flat front, was proposed. It was theoretically shown that in the latter case the thickness of the porous layer is proportional to the square root of time.

5. Vacancy growth of single-crystal silicon carbide — a new stage in the development of the method of coordinated substitution of atoms

A surprising feature of the method of substitution of atoms is that the dependence of the thickness of the grown SiC layer on the pressure of carbon monoxide CO has a dome-like shape [38], i.e., at first it increases to a certain maximum value, then decreases almost to zero (Fig. 13).

The drift model of epitaxy, developed in [38], allowed to explain the similar behaviour of the layer thickness on the CO pressure. It turned out that the gaseous reaction product SiO interferes with the flow of the gaseous reagent CO through the channels of the crystal lattice, thus reducing their hydraulic diameter. Naturally, the thickness of the SiC films in this case is not high. In particular, at a growth temperature of 1300 °C, the highest-quality films on Si(111) have a thickness of $20-100\,\text{nm}$ and are obtained at the CO pressures $P_{\text{CO}} \approx 200-500\text{ Pa}$. The process of forming the SiC coating proceeds through a number of intermediate stages. During the first stage of the reaction, the CO molecule interacts with Si and decomposes into a carbon atom and an oxygen atom. The oxygen atom enters into a chemical reaction with the Si atom, which results in the formation of SiO gas. The SiO gas diffuses through the crystal lattice to the surface and is removed from the system by a vacuum pump. A vacancy is formed in place of the removed silicon atom. Vacancies of this type, formed as a result of the interaction of CO with Si, will be referred to below as vacancies of a chemical nature or just "chemical" vacancies. An excited carbon atom released from the CO molecule as a result of the chemical reaction does not immediately take the place vacated after the removal of the Si atom via SiO but occupies an intermediate interstitial position, thus forming the so-called dilatation dipole, i.e., the complex "interstitial C – 'chemical' Si vacancy". During the final stage, interstitial carbon atoms "collapse" into "chemical" silicon vacancies due to the relaxation of elastic energy, thus forming a SiC coating.

The main disadvantage of this method is the physically limited thickness of the resulting SiC coating. It is impossible to grow the SiC coating with a thickness of more than 200–250 nm by this method. This is due to the peculiarities of the course of the chemical reaction: CO gas – crystalline silicon. As the structure of the surface layers of silicon is transformed into silicon carbide, the access of the reactant gas to the reaction front in the volume of silicon becomes more difficult, and when the critical thickness is reached, the reaction stops. This is explained by the fact that during the transformation of Si into SiC, the distance between atoms in the crystal cell of the formed SiC is smaller than in the initial Si. Accordingly, the diameter of channels, through which CO gas penetrates and SiO gas is removed, is also smaller in SiC. Therefore, as SiC

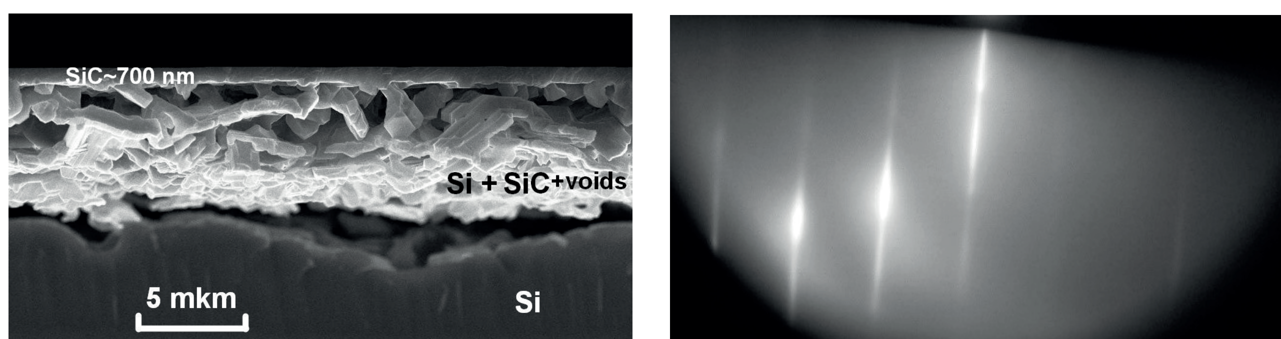

Fig. 14. Microscopic image of the cross-section of SiC-3C/Si(111) (a) and RHEED pattern obtained at an electron energy of 50 keV from its surface (b) samples grown by modified atomic substitution method at a temperature $T = 1350\,^0$C and CO pressure $p_{\text{CO}} = 80\text{ Pa}$ for 10 min with preliminary saturation of Si by vacancies. Under a high quality SiC-3C layer with thickness of $\sim 700\text{ nm}$ there is a layer of lower quality SiC with voids and unreacted silicon. The diffraction pattern corresponds to the epitaxial structure; polycrystalline phase is absent [43]

is formed, the rate of movement of gases slows down. As a result, CO gas cannot penetrate to a great depth, while SiO gas ceases to be removed from the system, so the chemical equilibrium is established – the reaction stops,. If the required thickness of the SiC layer exceeds 250 nm, it is necessary to repeat the procedure of depositing precursor layers (with the thickness up to 250 nm) on the already formed two-layer SiC coatings with their subsequent modification in a vacuum furnace in the presence of CO until the required thickness of the layered coating is reached. This significantly complicates the technology. In addition, repeated deposition of thin layers of silicon (the precursor layer) on an already formed SiC surface in order to increase the thickness leads to a deterioration in the crystalline perfection of the final layer, since during heterogeneous nucleation of Si on SiC, defects and dislocations are formed due to differences in the lattice parameters, and significant elastic stresses occur as well.

However, for some applications it is necessary to obtain high-quality single-crystal SiC films of noticeably higher thickness, for example, 200 – 1000 nm. In [43], a method that allows to increase the thickness of the silicon carbide layer by about an order of magnitude was proposed and implemented. The method is based on the theoretical conclusions of [5] and consists in the saturation of the surface of the silicon substrate with vacancies by pre-annealing in vacuum at T=1350 °C during ~1–30 min annealing time is determined by the need to obtain films of a given thickness). Thus, at the beginning of synthesis, silicon vacancies are specially created in the silicon substrate before the growth of SiC. This allows to create new pathways for CO diffusion and SiO removal in the substrate. Silicon vacancies penetrate from silicon into silicon carbide and provide a high rate of removal of the reaction product SiO outside of the reaction zone. Therefore, SiO much less hinders the growth of SiC, moreover, using vacancies, CO also penetrates deep into SiC more efficiently, which ultimately leads to much thicker SiC layers. This leads to the fact that when silicon atoms are substituted by carbon atoms, the interstitial-driven mass transfer mechanism switches to the vacancy-driven one. As a result, the SiC layer thickness not only increases, but, when it becomes higher than 400 nm, the layer delaminates from the Si substrate. The SEM micrograph of a thick SiC layer grown by the method [43] is shown in Fig. 14a.

During vacancy-driven growth, a silicon substrate is placed in a vacuum furnace and subjected to preliminary annealing at a temperature of 1250–1400 °C for 1–60 min under vacuum conditions (at a pressure of about 20 Pa or less). Due to preliminary annealing under vacuum conditions, the near-surface region of silicon is saturated with point defects in the silicon lattice — “thermal” vacancies (in contrast to the “chemical” vacancies that arise during the reaction of CO and Si and are mentioned earlier in the description of the prototype method). It is known that two types of “thermal” vacancies are formed in silicon crystals. Some “thermal” vacancies are Schottky vacancies, and others are Frenkel “thermal” vacancies. Schottky vacancies are formed near the surface of a silicon crystal as a result of the emergence of a silicon atom on the Si surface. Frenkel vacancies are formed as a result of the efflux of an atom from a crystal lattice site into the interstitial space. The higher the temperature, the higher the concentration of both “thermal” Frenkel vacancies and “thermal” Schottky vacancies.

After annealing in vacuum, a silicon carbide two-layer structure is formed by supplying CO gas at a pressure of 20–600 Pa into a vacuum furnace, and the substrate is kept in a CO atmosphere at a temperature of 1250–1390 °C. During this stage, chemical reaction (1) proceeds in the near-surface region of the substrate. However, unlike the described above method, in which vacancies are formed simultaneously with the occurrence of chemical reaction (1), in this case, at the stage of formation of “chemical” vacancies during the interaction of CO and Si, the system already contains a large number of “thermal” (nonequilibrium) vacancies. This makes it an open, non-equilibrium system. In the diffusion zone region, i.e., in the zone where the concentration of “thermal” (nonequilibrium) vacancies is increased, the chemical bonds within silicon are significantly weakened. The silicon lattice is in an unstable state. Gases easily penetrate inside silicon. The process

resembles the absorption of moisture by originally compressed porous sponge. Due to the creation of a high vacuum at the beginning of the process, silicon evaporates all the time from the surface of the silicon substrate, it does not deposit on the substrate and does not "block up" the formed vacancy channels. Hollow vertically oriented chains consisting of vacancies are formed inside silicon. When silicon evaporates, especially in a vacuum state, the presence of a vacancy leads to elastic compression of the silicon surface layer, since some of the silicon atoms have evaporated. It should be noted that since vacancies change the volume of the crystal, it is "more advantageous" for them to form in a coordinated manner, by forming lines or chains consisting of vacancies along the crystal surface. Such a process is impossible without the constant pumping-out of silicon vapours.

In the second step, as soon as CO gas is introduced into the system, it quickly saturates the elastically stressed layer, like a compressed sponge absorbs moisture. The elastic stresses relax, but the silicon structure prepared by such annealing already contains the gas that has penetrated into it, and a chemical reaction starts. In contrast to the method described in paragraph 2, in this case, the chemical reaction starts at a great depth and it starts evenly over the entire initially compressed silicon layer. The Si layer of thickness (0.5–5 μm) is converted into a layer of silicon carbide with the formation of a decompressed contact at the interface due to the formation of flattened gaps, the size of which exceeds the size of the pores by 2–3 times. The thickness of the SiC layer will depend on the rate of evaporation of silicon, which is determined by the temperature, the degree of vacuum created by the pump, and the reaction time. At temperatures below 1250 °C, the flow of evaporating silicon will not be large; therefore, the thickness of the SiC layer also will not be large. If the evaporating silicon is not pumped out, then it will quickly diffuse back from the surface, and the vacancies will "heal". The system will then reach a state of equilibrium, i.e., the process will follow the path outlined in paragraph 2. In this case, reaction (1) occurs much easier and, accordingly, faster. The diffusion layer is transformed into a two-layer silicon carbide structure, the upper layer of which is formed from silicon carbide and has a single-crystal structure, and the underlying transition layer has a nanoporous structure and is formed by silicon carbide and unreacted silicon residues. In addition, an increased concentration of "thermal" (nonequilibrium) vacancies allows the process of withdrawal of reaction products (SiO) to be significantly accelerated, which accelerates the process of chemical transformation of Si into SiC.

Thus, a two-layer structure, the upper layer of which is a continuous layer of SiC, and the lower layer is decompressed, is formed due to the following processes. Schottky vacancies consistently form lines or chains near the surface of the substrate. If atoms evaporating from the surface of the crystal are pumped out, then "thermal" Schottky vacancies will all the time diffuse deep into the crystal from the surface. They will diffuse in a consistent manner. The chains of vacancies formed on the surface will "move" deep into the substrate. This will lead to the formation of hollow vertically oriented channels (chains of vacancies). CO gas penetrates into the substrate through these channels. The higher the silicon pre-annealing temperature and the longer the annealing time, the thicker the silicon layer saturated with vacancies becomes and the higher the vacancy density in this silicon layer becomes. The presence of vacancies leads to a decrease in the volume of the upper Si diffusion layer. As a result, this layer becomes compressed. It should be noted, that if atoms are not removed from the surface by a pump, then, on the contrary, the crystal will swell, and its volume will increase. This is the fundamental difference between the nonequilibrium and equilibrium processes of the formation of Schottky vacancies. Diffusion of Schottky vacancies will occur up to the depth of the silicon layer at which the formation of Frenkel defects begins to predominate. Frenkel vacancies are formed as a result of the exit of an atom from the lattice into the interstitial space; therefore, they practically do not lead to a change in the volume of the crystal. The following processes will occur on the interface of these regions. Since any system tends to equilibrium, the interstitial atom of the Frenkel defect will move to the upper zone into a vacancy formed by the Schottky mechanism and will move to the surface under the action of an elastic stress gradient until it evaporates under

the action of the pump. The compressed layer of silicon will push it out, and the vacancy will again move in the opposite direction and again capture the next lower atom. This process will continue until the rate of evaporation of atoms, which is determined by the degree of pumping-out of gases, is equal to the rate of migration of atoms in the field of the elastic stress gradient. At a certain thickness of the elastic layer, they are balanced, and the process stops. As we noted above, this process depends on the degree and speed of pumping of gases and on the annealing temperature. When the diffusion zone, i.e., the ensemble of chains, in the process of diffusion, reaches the zone in which Frenkel defects are formed, the interstitial atoms will start to "jump" into these vacancy formations. It is obvious that the jumps of these atoms will also be performed in a coordinated manner, since in this case the total elastic energy decreases more than in the case when atoms move one by one. As soon as they enter vacancies, they start to move towards the surface. This movement resembles the movement of an elevator. When CO gas is supplied, it penetrates deep into the upper layer along "thermal" vacancies, thus converting the surrounding silicon into SiC. However, in this case, according to reaction (1), one Si atom is removed together with the SiO gas. In place of this atom, a "chemical" vacancy is formed. These vacancies will no longer form along the chains of "thermal" vacancies in the compressed layer (there are no silicon atoms in these directions, they have already evaporated), but in the directions specified by the emerging SiC crystalline layer. However, as soon as the gas reaches the layer in which "thermal" Frenkel vacancies are formed, the gas begins to "pull out" interstitial silicon atoms. In this case, additional randomly arranged vacancy "channels" are formed. The elastic deformation in this part of the crystal completely relaxes, and in the upper ordered part a strong compression (shrinkage) of the entire upper layer occurs, and it separates from the layer where vacancies are generated according to the Frenkel mechanism. The upper crystalline layer is formed as the result of compression. Most of the vacancies located in this layer disappear, some of them are displaced deep into the silicon, additionally forming a system of randomly oriented vacancy channels, which are transformed under the action of CO gas into a nanoporous layer containing lacunae. The degree of single-crystallinity of the layer depends on the initial concentration of vacancies in the upper layer of silicon and the degree of its "loosening". At temperatures below 1250°C, there are not enough vacancies for its formation, and at a temperature slightly below 1400°C (at a higher temperature silicon melts), the density of vacancies is very high, and the formed Si is "loose", consisting of many exfoliating crystalline patches (flakes). A typical electron diffraction pattern of the surface of a SiC/Si sample grown using the method of coordinated vacancy-driven substitution of atoms is shown in Fig.14b and unambiguously indicates the high crystalline perfection of the surface of this layer.

6. Coating method for smooth and profiled Si surfaces by ultrathin silicon carbide layers

In [44], a method was developed for coating Si surfaces with ultrathin layers of SiC, completely preserving their original morphology and structure. For the solution of a number of problems in electronics, it is often necessary to artificially create a certain type of profile of the nanometre scale on the surface. For example, the method that allows to artificially create the required nanoscale profile on the Si(100) surface was developed in [45]. The profile created in [45] was a nanoscale ridge-like structure, called by the authors of [45] nano-patterned silicon (NPSi(100), triangular in shape, oriented along the <011> direction with an average period $\lambda \approx 70$ nm and a height $h \approx 70\div90$ nm). A raster image of

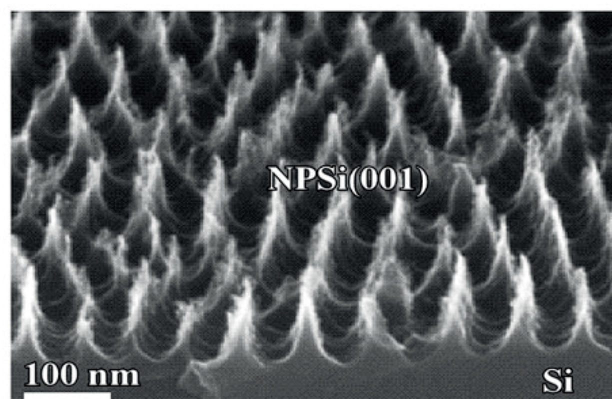

Fig. 15. SEM image of the end section and surface of the NPSi(100) structure [44]

the cleavage cross-section of this structure is shown in Fig. 15. Such structures are created for the formation of electron emitters. It seems important and natural to cover the surface of such silicon "pointed needle-shaped figures" with mechanically stronger chemically resistant material less prone to evaporation during field emission than silicon. Such a material, in particular, is silicon carbide. The MCSA described above in paragraphs 1–4 was used for covering of NPSi(100) structure. The main goal of the study was to determine the parameters of SiC synthesis, namely, the synthesis temperature, the pressure of synthesis gases (a mixture of carbon monoxide (CO) and monosilane (SiH_4) is used in the substitution method [8]), at which the profiled Si surface is transformed into a profiled SiC surface without changing its geometry and morphology. As a result of studies carried out in [44], it was found that the optimal synthesis temperature for creating such coatings is a temperature equal to 1050 °C. During the synthesis of a SiC film at this temperature, a continuous single-crystal coating of SiC with a thickness of about 3–5 nm is formed without nanopores and nanocracks. This film did not dissolve and remained unchanged when it was in the etching solution for more than 120 s. The SEM images of the cleavage cross-section of a SiC film synthesised at a temperature of 1050°C (Fig. 16a) and then kept in a selective etchant for 120 sec is shown in Fig. 16 (Fig. 16b). As can be seen from Fig. 16, the original NPSi(100) profile remained unchanged during etching. Only the silicon layer of the Si substrate was etched. The SiC layer covers the Si like a "lid". This layer is a replica of the original NPSi(100) structure completely converted into SiC.

At lower temperatures, the layer corresponding to the chemical composition of SiC is not formed. It can be said that at a temperature of 1000 °C and lower temperatures, "carbonization" of silicon rather than the formation of such a chemical compound as SiC occurs. At temperatures exceeding 1050 °C, the initial profile formed on silicon is not preserved.

Thus, the method of substitution of atoms can be used to transform (convert) pre-profiled Si surfaces with the desired geometric pattern or smooth Si surfaces into chemically stable SiC surfaces of the same geometry without any noticeable distortions.

7. Formation of epitaxial SiC layers on the surface of other materials by the method of coordinated substitution of atoms

7.1. Synthesis of epitaxial silicon carbide films on sapphire substrates (α-Al_2O_3)

7.1.1. Current state and problems of growing of epitaxial SiC films on sapphire

Researchers have been engaged in the growth of epitaxial SiC on sapphire for a long time. For example, in [46], β-SiC films were mechanically transferred to sapphire substrates for the creation of an optical waveguide. For the better conjugation of the sapphire and silicon carbide lattices, usually an AlN layer is applied as a buffer layer between sapphire and silicon carbide. The authors of [47]

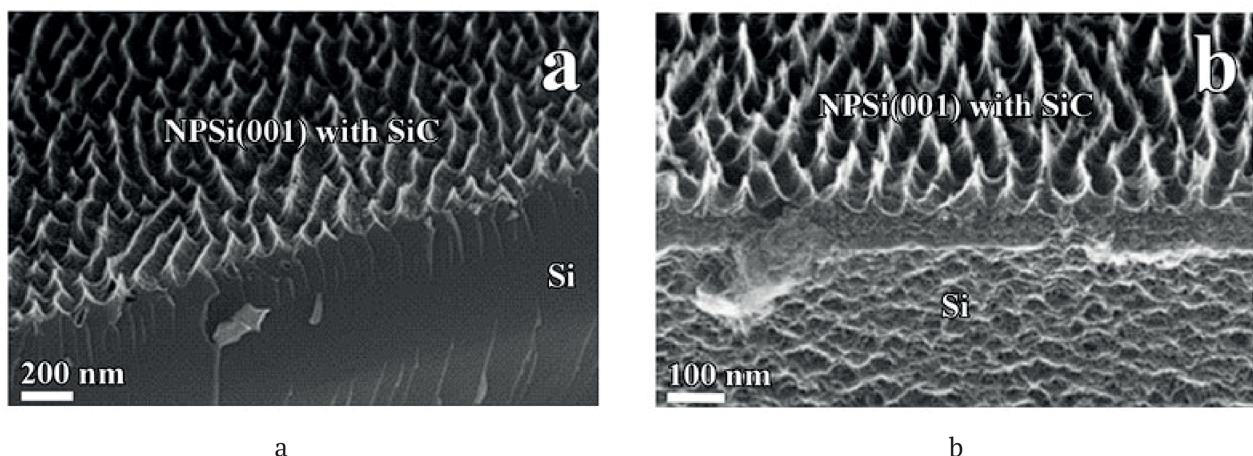

a b

Fig. 16. SEM images of end sections of SiC/Si nanostructure synthesized at 1050 °C. (a) Surface of the NPSi(100) structure with SiC layer after synthesis at 1050 °C. (b) The surface of the SiC/Si nanostructure after etching in a mixture of acids HF and HNO3 for 120 s [44]

showed that preliminary deposition of an AlN buffer layer on a sapphire substrate significantly improves the quality of the SiC layer and leads to the formation of an epitaxial 6H-SiC layer on sapphire. In [48], polycrystalline SiC layers were deposited on the "c" plane of sapphire by CVD in ultra-high vacuum in order to further obtain graphene layers on their basis on an insulating substrate, such as a sapphire substrate. In [49], polycrystalline SiC films were grown on sapphire by low-pressure CVD (LPCVD) for the obtaining optical temperature sensors based on the Fabry–Perot interferometric method. The authors of [50] used the MBE method to grow epitaxial films of the 4H-SiC polytype on a sapphire substrate with a preliminarily deposited AlN layer using fullerenes C_{60}. Rocking curves had the full width at half maximum FWHM $\omega_\theta \approx 0.24°$, which is a very good result. However, this method uses a complex MBE technology and also requires an additional layer of AlN to be applied to the sapphire. Later in [51], the authors, using an AlN layer as a buffer layer and pretreatment of the sapphire substrate or that with the AlN layer in a hydrogen flow and then in a propane flow (C_3H_8), were able to grow the 2H-SiC polytype by MCVD. According to the TEM images presented in this article, the quality of the 2H-SiC layer is very high in some places of the film, and the conjugation between the 2H-SiC and AlN layers is good. However, based on the data obtained from the rocking curves (Fig. 1 from [51]), the best samples had the value $FWHM_{\omega_\theta} = 40$ arcmin. On average, the best films had $FWHM_{\omega_\theta} \approx 80$ arcmin, i.e., they were closer to texture than to epitaxy. Therefore, in our opinion, the data presented in [51] are very contradictory. The authors of the study [52] grew 3C-SiC layers on the (0001) plane of sapphire using the MOCVD method. The grown 3C-SiC films had thicknesses of 5–7 µm. Unfortunately, nothing definite can be concluded about the quality of the grown layers, since the authors did not present the results of studies on the widths of the rocking curves, i.e., the values of $FWHM_{\omega_\theta}$. Based on the shown XRD plots, the XRD peaks corresponding to the 3C-SiC layer were quite broad, which indicates that the films were probably polycrystalline. Moreover, SEM images of cleavage cross-sections of the 3C-SiC films clearly show multiple dislocations (or twin grains). This is natural, since there is a large difference of about 12% between the lattice parameter of 3C-SiC and the lattice parameters on the (0001) plane of sapphire. Note that there is a patent dated May 12, 2012 [53], that describes a method for growing an epitaxial SiC layer on sapphire by the MCVD method in ultra-high vacuum (about 10^{-6} Torr.). The SiC films had thicknesses of about 90 nm. The study describes studies on the growth of 3C-SiC on sapphire from a melt [54].

Thus, at present, interest in the growth of SiC epitaxial films on sapphire is constantly increasing. Indeed, high hardness, inertness to chemically active media, and excellent insulating properties can ensure good use of sapphire substrates with a layer of such a wide-bandgap semiconductor as SiC in microelectronics, as well as in the manufacture of various types of sensors. In addition, based on SiC, it is possible to obtain graphene layers on an insulating sapphire substrate.

For growing a SiC layer on sapphire by the atom substitution method, it was proposed [55, 56] to first deposit a layer of epitaxial Si on the surface of a sapphire substrate and then convert it into SiC by reaction (1). It should be noted that the proposed approach of applying silicon carbide coatings to high-temperature materials can be used not only in semiconductor technology but also for creating a new class of composite, heat-resistant, and other hard coatings.

The growth of an epitaxial layer of silicon carbide on sapphire (Al_2O_3) by substitution of atoms is carried out in two stages. During the first stage, it is necessary to grow an epitaxial silicon layer, and during the second stage, it is necessary to convert the epitaxial Si into an epitaxial SiC layer by the MCSA method. This scheme was implemented in [55, 56].

7.1.2. Growth of epitaxial Si films on sapphire with the Si (100) and (111) layer orientations

The silicon on sapphire (SOS) structure is a thin layer of single-crystal silicon formed by heteroepitaxy on a dielectric substrate of synthetic sapphire (leucosapphire, α-Al_2O_3). The physicochemical interaction between silicon and sapphire at the stage of formation of the transition layer creates a strong bond at the interface between the layer and the

substrate, which ensures sufficient mechanical strength of the heteroepitaxial structure. High hardness, inertness to chemically active media, excellent insulating properties, sufficient thermal conductivity and transparency in the ultraviolet range of the sapphire substrate make it promising to use SOS structures in microelectronics (radiation-resistant integrated circuits (IC), combinational logic circuits, high-voltage fast recovery rectifiers), in the manufacture of transducers and sensors (photodetectors and resistive integrated circuits), as well as in the manufacture of microelectromechanical systems (MEMS) and nanoelectromechanical systems (NEMS) [57-61].

Barriers to the widespread use of SOS structures are the high density of structural defects in the SOS layer and the complexity of optimising the process of epitaxial growth. For SOS heteroepitaxial structures, the mismatch between the lattice parameters of silicon and sapphire in the lateral direction can reach 12.5% in case of formation of an epitaxial Si(111) layer on the c-plane (0001) of a sapphire substrate and about 6% when a Si(100) layer grows on the r-plane $(1\bar{1}20)$ of sapphire. The lattice mismatch and the difference in the values of the thermal expansion coefficients of silicon and sapphire lead to the formation of mechanical stresses in the epitaxial silicon layers and, as a consequence, to the formation of misfit dislocations. The vicinal surface of sapphire may contain a large number of centres for the formation of structural disturbances (disorientation centres), from which packing defects and twin lamellae (microtwins) occur during the initial stages of growth [57, 60, 61]. The growth of Si on sapphire occurs according to the Stranski–Krastanov mechanism, i.e., three-dimensional islands are formed at the initial stage of film growth. The deposited silicon can chemically interact with the sapphire surface, thereby contaminating the growth islands and thusincreasing their mutual misorientation and the defectiveness of the forming layer. The optimal conditions for the epitaxial growth process determine the structural characteristics of the SOS, which, in turn, are the key parameter for most applications.

In [56], epitaxial silicon layers with the thickness of 300–600 nm were grown on sapphire substrates with c-plane and r-plane orientations. The structures were obtained using an industrial vertical epitaxial reactor PE2061S (LPE, Italy). The operating pressure of about 1 atm was maintained in the reactor chamber, dried H_2 with a water vapour content < 5 ppb was used as the carrier gas. During growth, silicon layers were deposited on sapphire from a vapour–gas SiH_4 and H_2 mixture at a volume ratio of SiH_4:H_2 about 0.01:1. Si layers of the (100) orientation grew on the r-plane $\left(1\bar{1}20\right)$ of sapphire. The grown Si(100)/Al_2O_3 $\left(1\bar{1}20\right)$ layers had a high structural quality of epitaxial Si with the full width of the rocking curve at half maximum FWHM ⩽ 0.3°. The mean square roughness of the working surface did not exceed 1±0.5 nm.

For the growth of Si on the c-plane (0001) of Al_2O_3 sapphire from the same manufacturer was used [56]. Si of the (111) orientation grew on this substrate. The crystal structure of the Si(111)/Al_2O_3(0001) layers was a textured crystal with an ordered distribution of Si crystallites of the (111) orientation. The mean square roughness of these structures did not exceed 5 ± 0.5 nm.

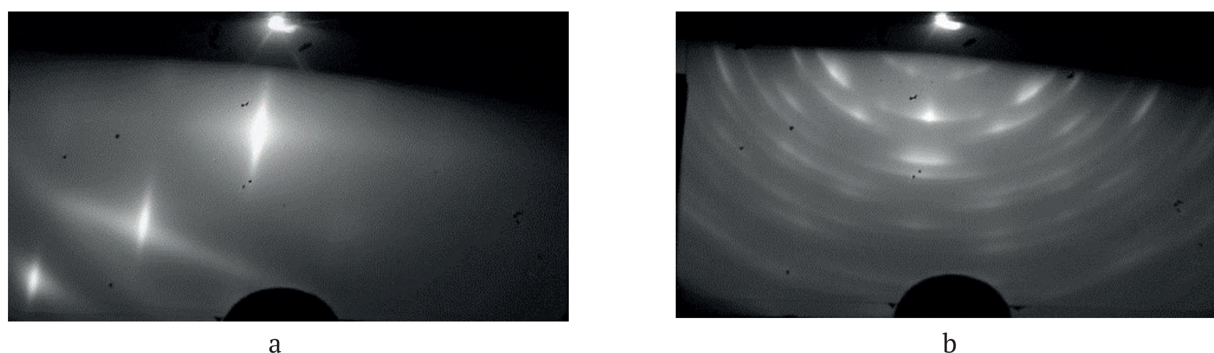

Fig. 17. RHEED pattern of fast electron diffraction from Si samples grown on Al_2O_3; (a) – Si(100)/ Al_2O_3 layer on r-plane $(1\bar{1}20)$; (b) – Si(111)/Al_2O_3 layer on c-plane (0001) Al_2O_3 [56]

Fig. 17 shows reflection high-energy electron diffraction (RHEED) images of a Si sample grown on the r-plane $(1\bar{1}20)$ of sapphire (Fig. 17(a)) and a Si sample grown on the c-plane (0001) of sapphire (Fig. 17(b)). It is clearly seen from these data that the Si(100) film grown on the r-plane of sapphire is epitaxial, well oriented, as evidenced from the nature of the reflections, and approaches the quality of a single crystal, since Kikuchi lines are present on its RHEED pattern indicating the high crystalline perfection of this layer (Fig. 17 (a)) .A Si(111) film grown on the c-plane sapphire is a texture (Fig. 17c).

Fig. 18 shows typical SEM micrographs of a cross section of a Si (100) sample grown on the r-plane $(1\bar{1}20)$ of sapphire (Fig. 18 (a)), and a cross section of a Si (111) sample grown on the c-plane (0001) of sapphire (Fig. 18 (b)). Fig. 18 clearly shows that the structure of the Si(111) film grown on the c-plane of Al_2O_3 is less dense and looser than the structure of the Si(100) film grown on the r-plane of Al_2O_3. The Si(111)/Al_2O_3(0001) interface contains dislocations and other defects.

In [56], there were obtained also X-ray diffraction patterns (XRD), which showed that the Si(100)/Al_2O_3 $(1\bar{1}20)$ structure is strained; therefore, for the Si(100) layer, the Si(200) forbidden reflection was observed. The XRD pattern of a sample of the Si(111)/Al_2O_3(0001) structure was measured in symmetrical geometry $\theta/2\theta$. The diffraction pattern showed that the silicon film is textured. The main orientations of silicon crystals present in the layers correspond to the [220] and [111] peaks.

Thus, Si films with the (100) orientation can be grown epitaxially, and for this, it is necessary to use the r-plane $(1\bar{1}20)$ of sapphire substrates, and Si(111) films cannot be obtained epitaxially on the c-plane of Al_2O_3 substrates. Supposedly, other sapphire facets should be used for epitaxial growth of Si.

7.1.3. Conversion of Si epitaxial films grown on sapphire into SiC epitaxial films by the method of coordinated substitution of atoms

After growing Si films on sapphire, in order to transform them into SiC layers, the resulting SOS structures must be chemically treated with CO gas according to reaction (1). Before this procedure, it is necessary to be clearly aware about the degree of the structural perfection of SiC layers which can be grown on Si(100)/Al_2O_3 and Si(111)/Al_2O_3 substrates. From the previous analysis it can be concluded that a SiC layer of the epitaxial quality but with a small admixture of SiC twins of the (110) orientation can be obtained on the Si(100)/Al_2O_3 substrates. On the Si(111)/Al_2O_3 substrates with a textured Si layer, it is only possible to obtain SiC as a textured layer. In the first case, this is due to the fact that, as shown in Section 2.3.1, SiC (111) facets will form on the Si (100) surface during the transformation of Si into SiC. Their

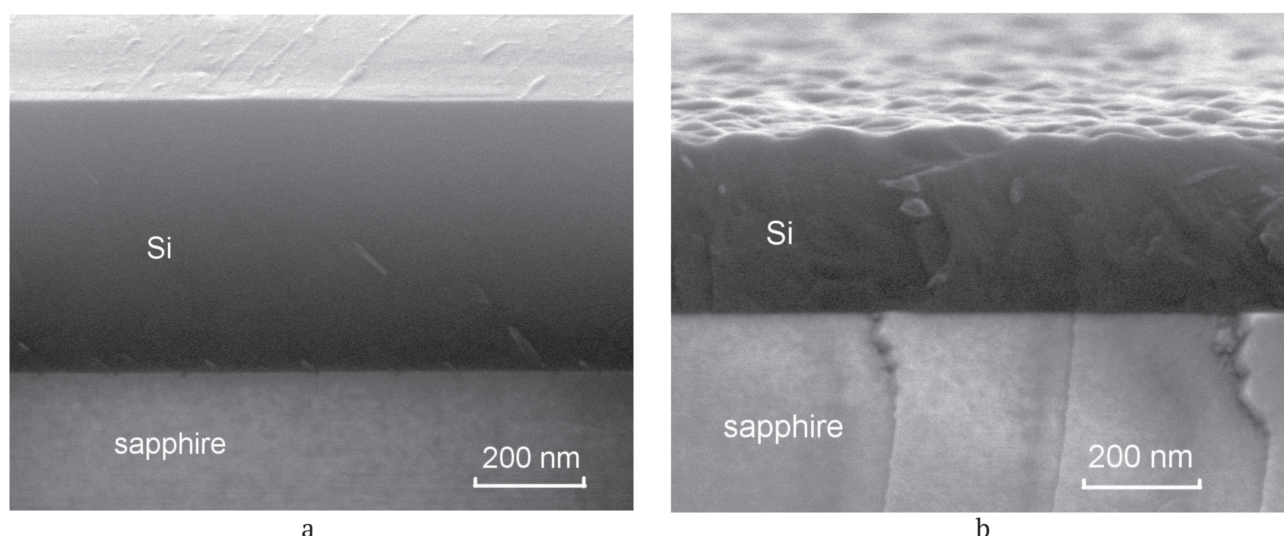

a b

Fig. 18. Typical SEM images of the cross-section and the surface of Si (100) and Si (111) films grown on Al_2O_3; (a) cross-section and surface of the Si (100)/r-plane Al_2O_3 structure; (b) cross-section and surface of the Si (111)/c-plane Al_2O_3 structure [56]

formation leads to the formation of epitaxial SiC with a small admixture of SiC facets of other orientations, in particular (110). In the second case, it is impossible to obtain a single-crystal SiC (111) layer until it will not be possible to grow a single-crystal (epitaxial) Si layer on sapphire. In principle, both of these tasks are solvable. In the first case, as was shown in paragraph 2.3.1, the growth of a vicinal Si surface, deviated by 4-6 degrees from the base plane (100), is required. Such a structure can be very attractive for the growth of semipolar AlN and GaN layers [62]. We expect to obtain it in the future. For SiC of epitaxial quality on Si(111)/Al_2O_3, it is necessary to obtain epitaxial Si(111) on Al_2O_3. As soon as such a silicon is obtained, epitaxial SiC will also be obtained.

Before the growth of SiC, as in the case of growth on silicon substrates, it is necessary to remove the silicon oxide layer, which can be formed during the interaction of Si with atmospheric oxygen from the surface. Otherwise, the chemical reaction between CO and Si, on the surface of which SiO_2 is located, will proceed differently compared to reaction (1). Dilatation dipoles will not form in this case, and the polycrystalline SiC film will grow. Thus, for obtaining an epitaxial SiC layer, before carrying out the reaction (1), it is necessary to prepare the Si surface for SiC growth, by obtaining a smooth (flat) surface at the atomic level and remove even silicon dioxide nanolayers from the surface of the silicon wafer. In addition, it is necessary to passivate the surface of the Si layer with hydrogen from its possible rapid oxidation during storage and transportation. The method of preparing and passivating the Si surface was developed for the growth of SiC in [63] and described in detail in [64].

In [56], the growth of SiC films was carried out according to the MCSA, which was described in detail above. To compare the growth of SiC films on Si/Al_2O_3 with the growth of SiC films on silicon single-crystal substrates under standard conditions selected by many years of research [1–6, 12], samples were synthesised under conditions when SiC films on single-crystal Si were obtained as highly oriented single-crystal structures. For example, Si(100) films on sapphire were converted into SiC layers at a temperature of T = 1290 °C. The total pressure of the gas mixture (CO+SiH_4) was 133 Pa. The CO gas flow was 12 sccm. The SiH_4 gas flow was 3.5 sccm. The synthesis was performed for 15 min. The growth of SiC films from Si(111) on sapphire was also carried out in a mixture of CO and SiH_4 gases. The growth temperature, growth time, and gas flow rate were the same as for the growth of SiC films from Si(100). Only the total pressure of the (CO+SiH_4) gas mixture was different. In this case, we grew films with a total gas mixture pressure of 67 Pa.

After the SiC formation process, the samples were examined by scanning electron microscopy, confocal Raman microscopy, ellipsometry, X-ray diffraction analysis, and reflection high-energy electron diffraction (REED).

7.1.4. Structural and morphological features of the formation of SiC films on sapphire

SEM images of cross sections from different parts of SiC/Si(100) and SiC/Si(111) samples on Al_2O_3 are shown in Fig. 19. Fig. 19a shows a cross section with a region almost free of pores in the SiC/Si(100)/r-plane $(1\bar{1}20)$ Al_2O_3 structure, Fig. 19b shows a cross section of the SiC/Si(111)/c-plane Al_2O_3 structure with an area practically free from pores.

The analysis of a large number of SEM micrographs taken in [56] from different parts of the surface of these samples showed that in the SiC/Si(100)/r-plane $(1\bar{1}20)$ Al_2O_3 there are places with a large number of pores. However, in general, the density of pores in the SiC/Si(100)/r-plane $(1\bar{1}20)$ Al_2O_3 sample was significantly lower than the density of pores in the SiC/Si(111)/c-plane Al_2O_3 sample. It is interesting to note that if structure of the initial silicon on sapphire more "loose", less crystalline, and closer to texture, then CO gas penetrate deeper into the Si layer. As it can be seen from Fig. 20, the c-plane, i.e., the (0001) sapphire plane, begins to be etched during the SiC synthesis (a pore in sapphire is clearly visible in Fig. 19b; other micrographs confirming this process are also presented in [56]. In our opinion, the etching can be associated with a chemical reaction of the type:

$$Al_2O_3(cr) + CO(gas) = Al_2O(gas) + CO_2(gas) \quad (14)$$

which, as shown in [56], can occur at temperatures of the order of $T \sim$ 1280 °C. CO_2 gas released during the reaction will react with Si at the Si/

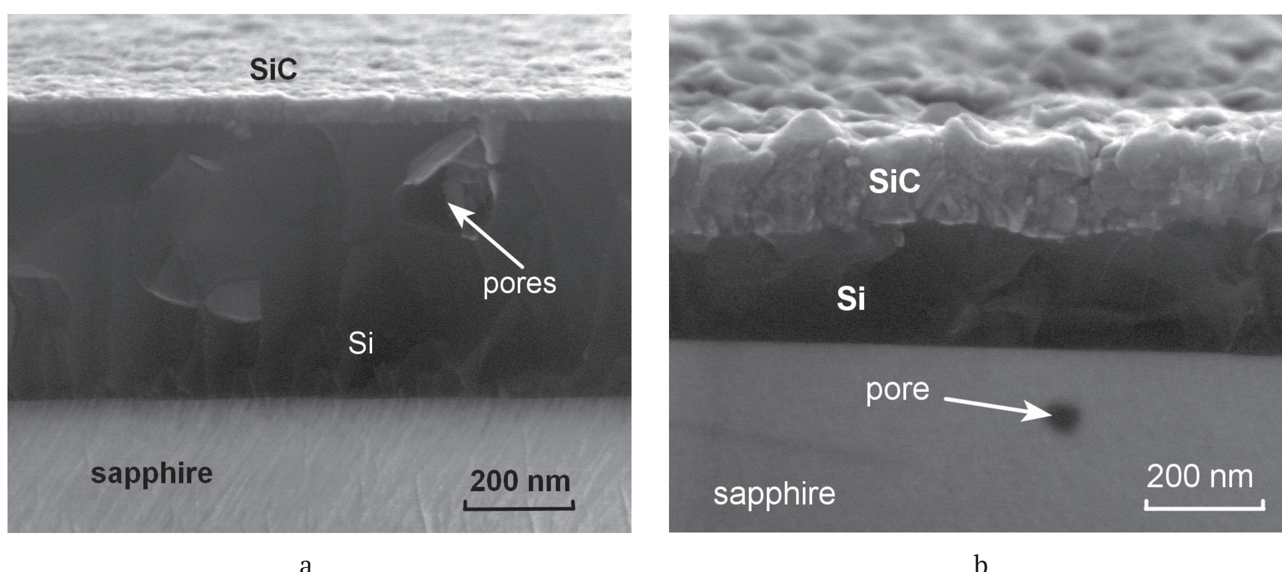

a b

Fig. 19. SEM images of the cross-sections of different areas of the SiC/Si (100) and SiC/Si (111) samples grown on Al_2O_3; (a) cross-section of a region containing pores, coated with a SiC layer in the SiC/Si (100)/r-plane $(1\bar{1}20)$ Al_2O_3 structure; (b) cross-section of an area practically free from pores on the SiC/Si(111)/c-plane Al_2O_3 structure [56]

Al_2O_3 interface and will again form SiC but with an admixture of quartz (crystalline SiO_2) in accordance with reaction (5):

$$CO_2\,(gas) + 2Si = SiC + SiO_2(cr). \quad (15)$$

Moreover, in the presence of CO and CO_2 a number of other reactions are also possible, which we do not consider here. Obviously, at the temperature at which SiC is synthesised, silicon oxide can be formed both in the form of quartz glass and in the form of crystalline quartz. It is quite possible that, during the formation inside the ordered phases (Si, SiC, Al_2O_3), more probably SiO_2 in the crystalline form will be formed, which we actually detected [56] in SiC/Al_2O_3 layers in the study of X-ray spectra of SiC samples grown on Si(100)/Al_2O_3 and Si(111)/Al_2O_3 and shown in Fig. 20. X-ray diffraction patterns (XRD) obtained from samples grown on Si(100)/Al_2O_3(r-plane) and Si(111)/Al_2O_3(c-plane) are shown in Fig. 20. On a SiC sample grown on Si(100)/r-plane Al_2O_3, XRD peaks were observed. The positions of these peaks corresponded to SiC of both the 2H-SiC and 3C-SiC modifications. There are peaks from the 2H-SiC and 3C-SiC phases on XRD taken from a SiC sample grown by the conversion of Si(111) on the c-plane of sapphire. A peak, the position of which corresponds to the α-quartz phase, can be distinguished for all samples. It should be noted that in this case, we cannot state with complete certainty that the 2H-SiC phase is formed on sapphire in the process of Si/Al_2O_3 conversion into SiC/Al_2O_3. This XRD peak is "blurred". It is known that XRD peaks of other hexagonal polytypes are also located in this region of the XRD scan (2θ). It was noted in reviews [1–6, 12] that SiC layers of various polytypes can form during the growth of SiC by the method of substitution of atoms. Therefore, the formation of 2H-SiC layers should not be surprising, since the physicochemical nature of the method of substitution does not prohibit the formation of this phase.

As it can be seen from the data in Fig. 20, along with SiC, α-quartz is also formed. We attribute its appearance to the occurrence of reactions (14) and (15), which take place during the growth of SiC on sapphire. During the growth of SiC by the method of substitution of atoms on pure Si, the formation of α-quartz under the given synthesis conditions was not observed.

In [56], RHEED, Raman, and ellipsometric spectra of SiC samples grown on a Si (100)/Al_2O_3 r-plane and on a Si(111)/Al_2O_3 c plane were shown. We do not present them in this review, but refer the reader to the original study [56]. Here it should be noted once again that the SiC layer grown on single-crystal Si is much more oriented than the layer grown on sapphire. However, as follows from our study of SiC growth on Si(100)/r-plane Al_2O_3 and Si(111)/Al_2O_3 c-plane, it is enough to deposit a

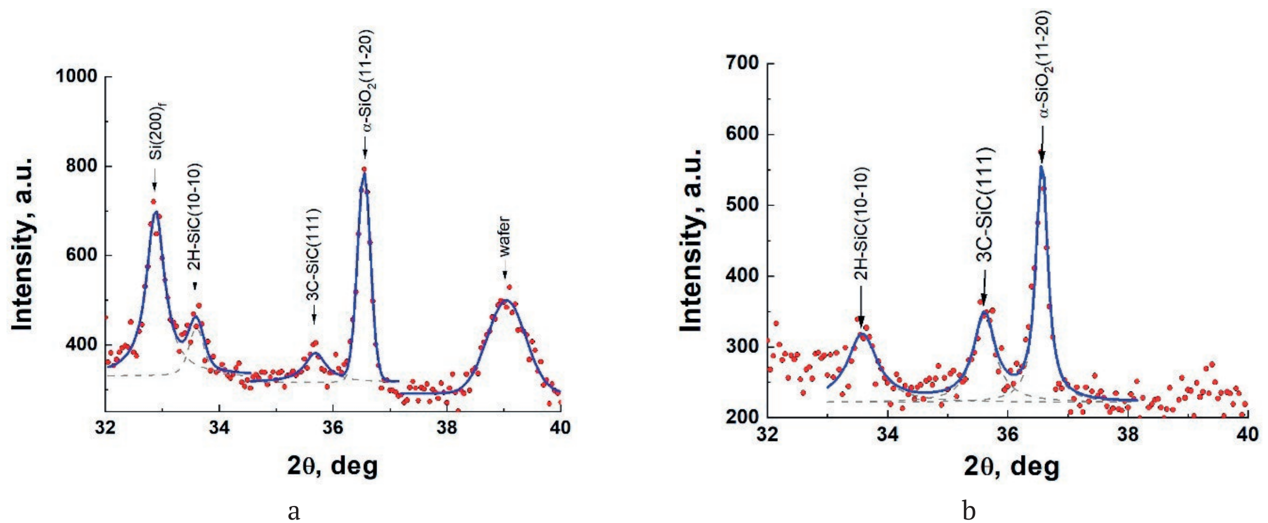

a b

Fig. 20. X-ray diffractograms from SiC samples grown Si(100)/Al_2O_3 r-plane and Si(111)/Al_2O_3 c-plane ; (a) SiC on Si(100) r-plane $(1\bar{1}20)$ Al_2O_3; (b) SiC на Si(111) на c-plane Al_2O_3 [56]

high-quality Si layer on sapphire, and as a result, the SiC layer will also be epitaxial. Moreover, the higher the degree of single-crystallinity of the Si layer, the higher the degree of single-crystallinity of the SiC layer.

7.2. A new method of formation of protective SiC-C composite coatings on graphite

Graphite products are widely used in various areas of technology and industry — from parts of high-temperature furnaces to nuclear reactors — and during use, these products are subjected to various loads: mechanical, chemical, and thermal. For the protection of graphite from such impacts, various protective coatings are often applied to it, ranging from niobium, oxides, nitrides, and ending with various composite layers. In particular, one of the promising coatings is silicon carbide, which has chemical resistance, high hardness and thermal conductivity. In [65, 66], a method for depositing silicon carbide coatings on graphite by annealing a graphite sample in contact with a Si melt in a carbon monoxide (CO) atmosphere was developed. The method is based on the interaction of CO and silicon with the formation of SiC and is similar in many respects to the MCSA but differs from it by relying not only on one reaction (1) but two chemical reactions occurring simultaneously inside the graphite. One of the reactions is the chemical interaction of Si melt, located on the surface of graphite, with CO at a temperature exceeding the melting point of silicon (1412 °C), which results in transformation of Si into SiC. This is the reaction (1). The second reaction, proceeding simultaneously with the first one, is the interaction of the product of the first reaction – gaseous silicon monoxide (SiO) – with graphite, which results in transformation of the latter into SiC. This reaction is as follows:

$$2C(cr) + SiO(gas) \rightarrow SiC\ (cr) + CO(gas) \qquad (16)$$

Thus, during the synthesis of a SiC coating on graphite, at the initial moment of time, as a result of reaction (1), SiC and gaseous SiO are formed. Then the gaseous SiO, which is removed from the system during the growth of SiC by the MCSA, reacts with graphite at the interface. In this case, SiC is formed, but already from the graphite side. At the same time, CO is released, it reacts from the interface side with Si and finally converts the residual silicon into silicon carbide. A schematic representation of the method of formation of this coating is shown in Fig. 21.

The coating formed as a result of these processes has high mechanical strength and hardness. In the process of composite synthesis by this method, a coating with a thickness exceeding 1 mm is formed. Samples of composite coatings were studied using scanning electron microscopy, energy-dispersive spectroscopy, Raman spectroscopy, and also by nanoindentation [65, 66].

Studies have shown that the composite material obtained by this method consists of a

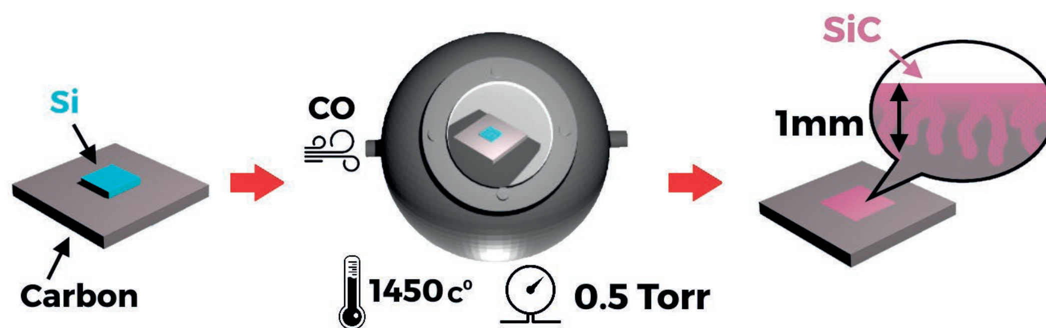

Fig. 21. Schematic representation of the method of forming the SiC-graphite composite on the surface of the graphite product [65]

continuous silicon carbide film on the surface and has a branched structure consisting of dendritic SiC crystals extending deep into the product, interspersed with large (up to 20 μm) single-crystal grains of predominantly cubic polytype with a small fraction of hexagonal polytypes. The deposition of the coating leads to a significant hardening of the material: the composite coating has a hardness of 28 GPa, which is ~254 times higher than the hardness of the original graphite surface.

For the experiments, MPG-7 graphite sample was used, on the top of which a silicon wafer with the thickness of 300 μm and an area of about 1 cm^2 was placed. The structure was annealed in a vacuum furnace in a CO atmosphere with the addition of silane at a temperature of 1450 °C and a total pressure of 0.5 Torr for 20 minutes. After the synthesis, the resulting samples of SiC coatings were studied by scanning electron microscopy using Tescan Mira 3 microscope. The mechanical properties of the surface were studied using a Nanotest 600 installation for nanoindentation.

SEM images of the sample surface and sample cleavage are shown in Figs. 22a and 22b, respectively. As can be seen from Fig. 22b, the coating is a continuous crystalline layer, on which there are areas with different contrasts. A detailed study of the surface after mechanical separation of the SiC film allowed to conclude that voids were observed under the dark regions

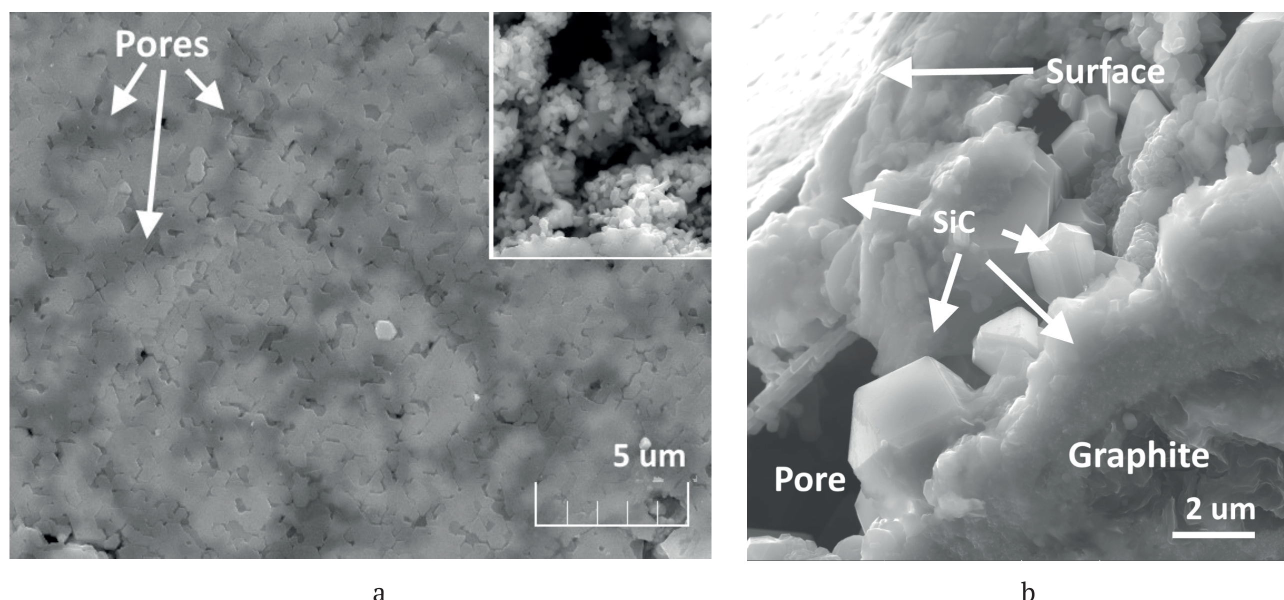

Fig. 22. SEM-image of the surface (a) and chip (b) of the sample of SiC composite coating on the graphite surface. The dark areas in figure (a) correspond to the pores under the SiC film surface. The inset to figure (a) shows the inner surface of the pore after removal of the SiC film [65]

(see the inset to Fig. 22b). The pores are also visible on the cleavage of the sample (Fig. 22b, right side). As can be seen on Fig. 22b, the immediate surface SiC layer is continuous and has a thickness of the order of several micrometres. At great depths from the surface, a mixed structure of pores, crystals, and druses of silicon carbide with graphite inclusions starts, and at depths of the order of several hundred micrometres, the volume fraction of SiC gradually approaches zero. The penetration of silicon carbide to such depths is due to the rather large porosity of the initial graphite matrix and the fact that the silicon melt that has flowed into the pores was converted into SiC as a result of the reaction with CO. SiC has a volume of the unit cell two times smaller than that of silicon [1–6,12]. As a result, during the formation of SiC, new voids appear, and the channels in the graphite are not "blocked", but remain open for further penetration of the silicon melt into the depths. As a result, "roots" of SiC, firmly binding the upper single-crystal SiC film with the graphite matrix are formed in the volume of graphite. Different shapes of the resulting SiC microcrystals, which correspond to the cubic polytype of silicon carbide can be seen on SEM images of regions of the crystal (see Fig. 23a) at a depth of about 150 μm. It should be noted that the Monte Carlo simulation of growth of SiC crystals of the cubic polytype using Crystal Grower package [67], performed in this study for various ratios of the Si and C components, provides a spectrum of crystal shapes actually observed in the experiment (Fig. 23b). Thus, regular octahedral crystals were observed during the formation of a crystal from a mixture of stoichiometric composition, while with an excess of carbon in the system, crystalline forms with "bevelled" facets were observed.

The microhardness of the coating was measured using a nanoindenter at a maximum indentation force of 1 mN. The indenter was loaded and unloaded at a rate of 0.5 and 1 mN/s, respectively. It should be noted that due to the presence of porous regions under the surface of a thin single-crystal SiC layer (see Fig. 22), in some cases, an increase in the indentation force led to the appearance of significant deformation jumps in the nanoindentation curves up to several hundreds of nanometres (see the dotted curve in Fig. 25a). Such jumps, caused by the presence of pores, significantly distort the result of the analysis of experimental data. It should be noted that deformation jumps were also recorded at nanoindentation up to 1 mN, but this happened much less frequently. For the determination of the hardness of the modified and original graphite, nanoindentation curves were selected exclusively

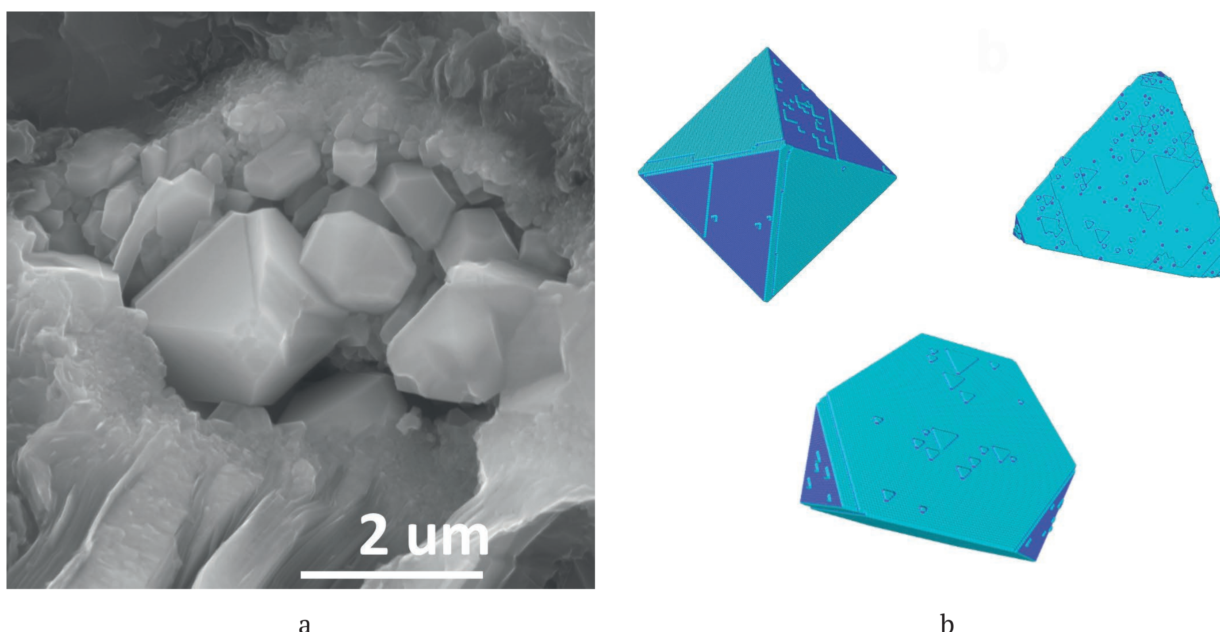

a b

Fig. 23. SEM - image of SiC crystals observed in the pores in the carbon matrix, and growth shapes of cubic SiC obtained by Monte Carlo simulation in the Crystal Grower package [67] at different ratios of Si and C components during growth [65, 66]

without strain jumps. Typical dependences of the indentation force on the depth of penetration of the indenter into the studied material for the modified and original graphite regions are shown by solid curves in Fig. 24a. The dependences of microhardness on depth, calculated using the standard method [68], are shown in Figs. 24b. It can be seen that the SiC coating significantly increased the surface hardness to 25–28 GPa, while the hardness of the original graphite was 100–130 MPa.

Thus, it was shown in [65, 66] that the annealing of graphite in contact with a silicon melt in a CO atmosphere allow to form a protective coating of silicon carbide, which is a continuous film on the surface and a branched system of crystals and crystalline druses extending to a large depth. The coating significantly increases the hardness and mechanical resistance of the material, and has antioxidant properties, thus protecting the surface of the graphite product from various influences.

8. Crystal structure, polytypism, optical, electrophysical, mechanical, and other properties of SiC synthesised on Si by the method of coordinated substitution of atoms

The semi-industrial technology [28, 69], which allows to grow epitaxial SiC layers with a diameter of 50.8 mm (2 inches); 76.2 mm (3 inches); 100 mm (4 inches) and 150 mm (6 inches) was developed based on the described above MCSA. Photographs of SiC/Si wafers of various diameters are shown in Fig. 25. The SiC layers were grown in a vacuum furnace VHT 8/18(22)-GR 1800 manufactured by Nabertherm GmbH. Heating of the graphite chamber with a volume of 8 litres was carried out using graphite heaters. Preliminary evacuation was carried out with a turbomolecular pump up to a pressure of 10^{-2} Pa. The heating and cooling rates in the temperature range 1000–1390 °C were 30 and 15 K/min, respectively. The chamber was supplied with carbon monoxide at a flow rate of 50–100 sccm (cm^3/min). For the stabilization of the partial pressure of silicon, silane (SiH4) with a flow rate of 10–20 sccm was supplied into the chamber. The temperature during the growth of SiC layers was 1000–1390 °C and the operating pressure was 70-700 Pa. The wafers were subjected to the maximum temperature for 5–30 min. The total time of the technological process (from loading to unloading) was 5-7 hours. Up to 20 SiC layers on silicon wafers with a diameter of 100 mm and 6 layers of SiC on silicon wafers with a diameter of 150 mm can be simultaneously grown in a single process. As substrates for silicon carbide epitaxy, we used silicon wafers of various grades, usually, (111), (110), (100) orientations; however, SiC growth was also carried out on Si wafers of other orientations. Before growing the SiC layer, the Si wafers were passivated with hydrogen according to the procedure [63, 64]. A detailed description

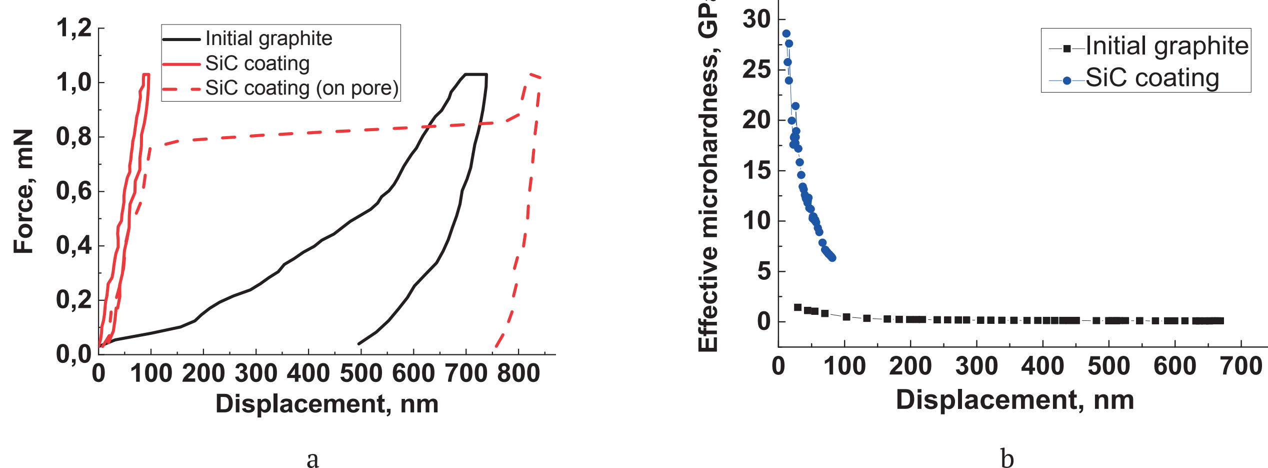

Fig. 24. Load-discharge curves of the original graphite (black solid line) as well as of the formed coating in two areas: lying directly on the graphite (blue solid line) and "hanging" over the pore (blue dashed line) (a). Dependence of the effective hardness of the materials on the depth (b) [65, 66]

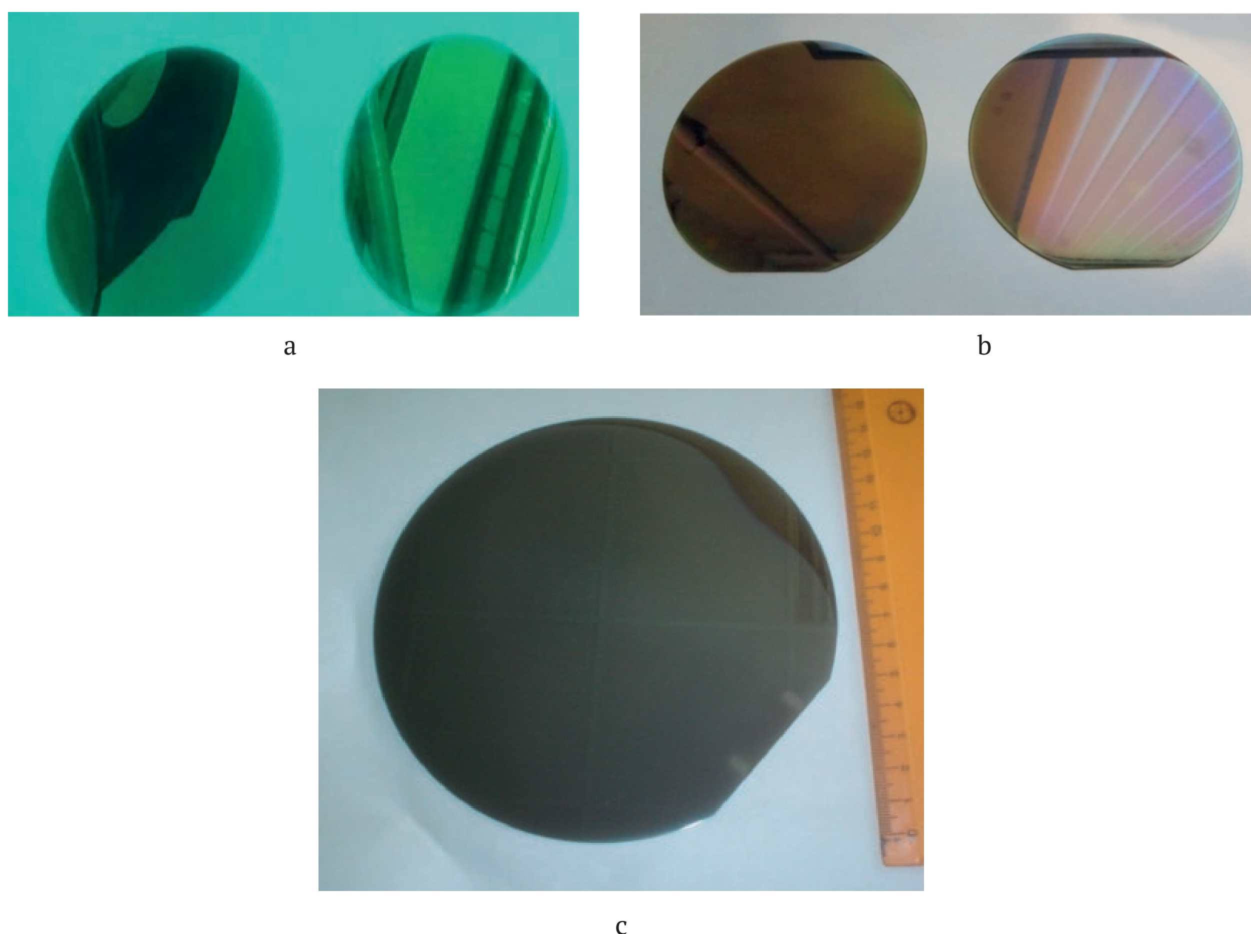

Fig. 25. Photographs of silicon carbide samples on silicon substrates 50.8 mm (2 in) in diameter (Fig. 25a); 76.2 mm (3 in) (Fig. 25b); and 150 mm (6 in) (Fig. 25c) grown by matched atom replacement on a small-scale industrial scale

of the procedure for synthesising SiC layers on wafers of a given diameter can be found in [69]. The SiC films grown on Si wafers were studied using spectral ellipsometry, SEM microscopy, X-ray diffraction, and Raman scattering. Studies have shown that the SiC layers were epitaxial over the entire surface of the 150 mm wafer. The plates were not stressed, even, without bends. The half-width of the x-ray rocking curve ($FWHM_{\omega_\theta}$) of the wafers varied from 0.35° to 0.55° at a layer thickness of 80–100 nm. Wafers are suitable for use as templates for growth of thick SiC, AlN, GaN, ZnO, films on their surface and other wide band semiconductors using standard CVD, HVPE, and MBE methods. The wafers were even and without bends, as can be seen from Fig. 25. RMS roughness, measured at scanning fields of 5×5 μm and 20×20 μm, was 1–5 nm and was constant over the entire diameter of the wafers. The crystal perfection of the SiC layer was determined using the widths of the X-ray rocking curves ($FWHM_{\omega_\theta}$) measured at various points of the wafer surface in the ω-θ mode, ellipsometry data, RHEED, Romanov spectroscopy, Rutherford backscattering, and a number of other methods. The films were studied using the following methods: spectral ellipsometry using a J. A. Woollam M2000-RCE ellipsometer in the range of 0.7–6.5 eV, Raman spectroscopy using a Witec Alpha 300R confocal Raman microscope, RHEED at an electron energy of 50 keV, X-ray diffraction (taken as diffraction patterns in the ω-2θ mode, and rocking curves in the ω-θ mode). The surface of the films was studied using atomic force microscopy (AFM method) and using a New View 6000 profilometer (Zygo). The surface of the SiC/Si layers and the surface of the end cleavages were studied by scanning electron microscopy (SEM) equipped with an X-ray spectrometer (EDS), which allowed determining the chemical composition of the

layers. The interface and defects in the layers were studied using high resolution tunnel electron microscopy (TEM). Many samples were studied using the Rutherford backscattering spectroscopy (RBS) method using helium and hydrogen ion beams [70], as well as by IR spectroscopy using a Brucker IFS-113v infrared Fourier spectrometer and an NicoletiS-50 IR spectrometer (Thermo Scientific, USA) [71-73]. SiC/Si samples were also studied by X-ray reflectometry [72, 73]. Photoemission studies of the samples were carried using the BESSY II synchrotron at Helmholtz Zentrum in Berlin (Germany) using synchrotron radiation with a photon energy in the range of 80–450 eV [74–78].

Thus, a comprehensive analysis of the structural, crystallographic, physicochemical, electrophysical, optical, and spectroscopic studies of SiC films on Si was carried out. These studies and results were described in a number of articles and summarised in reviews [1-6], therefore we do not provide a detailed description of them here. We only note the following. We have studied more than ten thousand film samples, as a result of which reliable information was obtained on the structure and properties of SiC films on Si. The result of the experimental studies was the following. 1) The main theoretical idea about the implementation of epitaxial growth of films via the formation of an ensemble of dilatation dipoles was proved. 2) It has been shown that as a result of the transformation of the intermediate into silicon carbide, a SiC film is formed, which is "hanging" over the cavities like a bridge over a river or a house built on piles. Further formation of SiC will occur inside the cavities. SiC crystals are deposited on the reverse, inner side of the film, i.e., on the side of the cavities. Such sediments resemble "stalactites" and "stalagmites" growing in a cave. The quality of the top layer of the film is high, since there are practically no elastic stresses and growth defects on the film surface. The reverse side of the film contains numerous disordered "stalactite-like" structures. The structure of the upper SiC layer obtained using the MCSA is epitaxial with a high degree of crystallinity.

The main polytype formed during the growth of SiC by the MCSA, is the cubic polytype 3C-SiC. During topochemical transformation, the 4H-SiC and 6H-SiC polytypes [1–6] and even rather rare 2H-SC and 8H-SiC polytypes can be formed. In [79], we determined the polytype composition of SiC films obtained on Si by the MCSA at T = 1250 °C, P = 2 Torr, and growth time of 15 min using a Woollam VUV-VASE JA ultraviolet ellipsometer with a rotating analyser in the range of 1.3–9.3 eV. It has been shown that, under these conditions, the cubic polytype 3C was mainly formed on Si(111), the hexagonal 4H polytype with a small admixture of 3C was mainly formed on (110), and a mixture of 3C, 6H, and 4H polytypes was formed on (100). It turned out that during the growth of SiC using the MCSA, under a number of synthesis conditions, the formation of new, previously unknown trigonal (rhombohedral) SiC phase is possible [81,82].

In the next section, we will describe only the most interesting and, from our point of view, unique properties of SiC/Si layers, which this heterostructure possesses due to the formation of silicon carbide by the coordinated substitution of atoms.

9. Features and anomalies of optical, magnetic, and other properties of SiC films on Si grown by the method of coordinated substitution of atoms

9.1. The physical nature of the emergence of features and anomalies in the properties of SiC films on Si grown by the method of coordinated substitution of atoms

The main feature of SiC grown on Si using the MCSA, is the presence of carbon-vacancy structures formed in the process of shrinkage or "collapse" of the material in it. It turned out, that the "collapse" leads not only to the formation of an ensemble of point defects. When separating from the silicon matrix, silicon is subjected to abnormally strong compression from silicon carbide. The "collapse" corresponds to a phase transition from a metastable state with stretched bonds, in which 4 SiC cells are consistent with 4 Si cells, into a stable SiC phase, in which already 5 SiC cells are consistent with 4 Si cells, and the Si-C bonds are much less distorted (about 0.2%). The pressure exerted by stretched Si-C bonds on the nearest silicon layer can reach 100 GPa. As a result of such shrinkage, every

fifth SiC chemical bond is fully consistent with every fourth Si bond, the remaining bonds either break (hence the appearance of vacancies and pores) or undergo compression. The latter obviously leads to a change in the structure of the surface zones of SiC adjacent to Si and its "metallization" or transformation into a "semimetal". When silicon carbide is doped with boron atoms, the latter enter the voids of carbon-vacancy structures (see Fig. 26) [1] and greatly change their properties. The "collapse" of one layer with the initial lattice into the SiC lattice and a model of the carbon-vacancy dipole formed in SiC [82, 83] schematically shown in Fig. 27. The investigation [82, 83] of SiC/Si samples grown on the (111), (110), and (100) Si facets by ellipsometry using a Woollam VUV-WASE JA ultraviolet ellipsometer with rotating analyser in the range 0.5–9.3 eV has revealed the following. At the 3C-SiC(111)/Si(111) interface, an interface layer with completely new optical and electrical properties was formed. The optical properties of this interface cannot be described in terms of the Effective Media Approximation (EMA) [82, 83]. For their theoretical description, a model with oscillators not related to either SiC or Si should be used. The best agreement with experiment was shown using the Tauc–Lorentz (TL) model, according to which the SiC/Si interface is a material with a zero band gap [82, 83]. Thus, in studies [82, 83] it was found that thin layers with semimetallic properties are formed at the 3C-SiC(111) and Si(111) interface. These layers are fundamentally different from the properties of both SiC and Si, and cannot be obtained using the EMA approach. This is due to the complex nature of the interaction of two surfaces when the SiC layer attracts individual Si atoms from the substrate, and the absence of misfit dislocations. As a result, an interface structure is formed (Fig. 27), where 88% of the Si atoms at the interface form a chemical bond with the substrate atoms, and 12% of the Si atoms at the SiC(111) interface do not form bonds, since they are located too far from the Si atoms of the substrate. Such a structure was described in detail within the framework of the density functional theory [82, 83] (Fig. 27) using quantum chemistry methods. It was shown, that *p*-electrons of 12% of Si atoms at the SiC(111) interface with dangling bonds provide a sharp peak in the density of electronic states just in the Fermi energy region (Fig. 28). In this case, the conduction band either touches or even goes deep into the valence band by a value on the order of several hundredths of eV, which approximately corresponds to the calculation error or is less than it. It was shown that this theoretical representation is in full

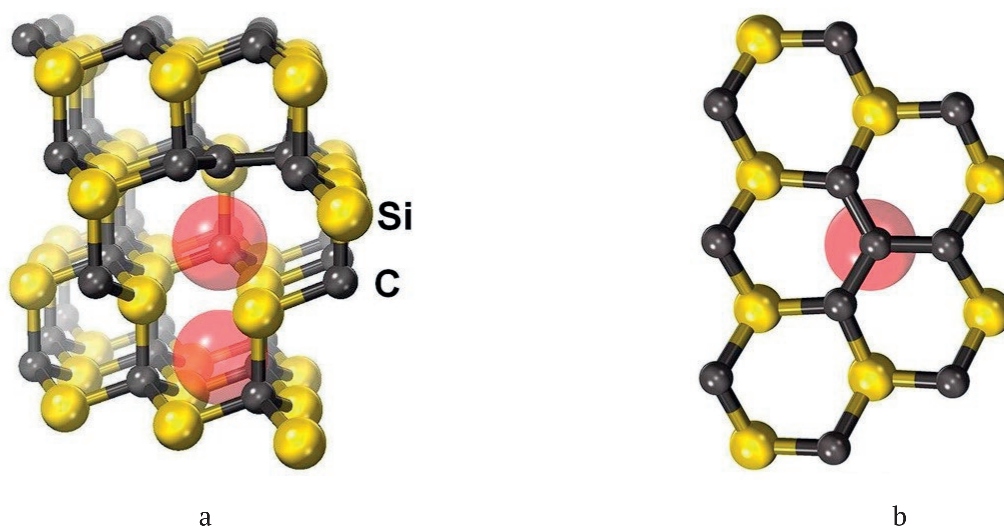

Fig. 26. Carbon–vacancy structure in SiC grown by the MCSA method: (a) a nearly planar cluster of four C atoms formed owing to the displacement of the C atom in the <111> direction (from bottom to top) to the site of the silicon vacancy and two voids (shown in red) above and below the initial position of the C atom (vertical axis corresponds to the <111> direction) and (b) the top view of the same structure [1]

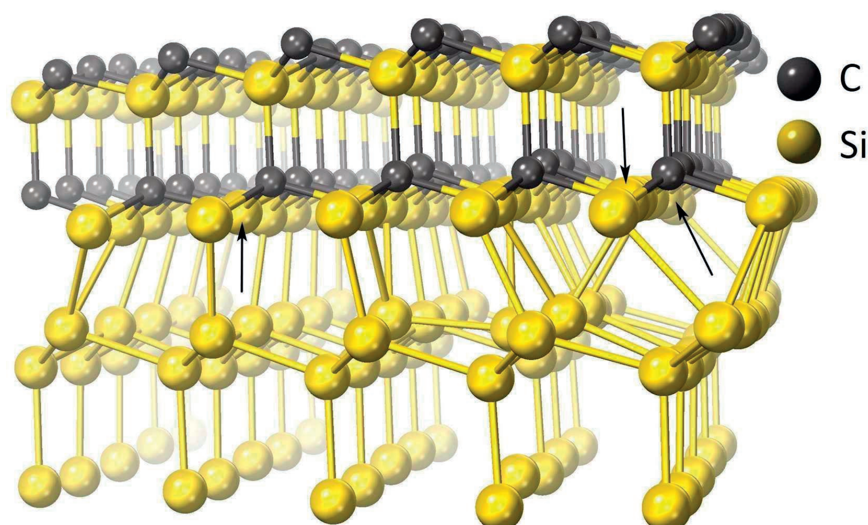

Fig. 27. Configuration of atoms at the dislocation-free 3C-SiC (111)/Si (111) interface corresponding to the minimum energy. The arrows indicate 3 out of 25 Si atoms that do not form bonds with atoms of the substrate. It is their p electrons that make the decisive contribution to the narrow peak of the density of electronic states in the vicinity of the Fermi energy (Fig. 28) [82, 83]

agreement with the experimental results on ellipsometry, according to which the optical properties of the layer at the 3C-SiC(111)/Si(111) interface correspond to the Tauc-Lorentz (TL) parameterization with a band width close to zero. The measured ellipsometric spectra show that the conductivity of the interface approximately corresponds to such a metal as lead at electric field frequencies of more than 700 THz. At lower frequencies, the conductivity deteriorated.

The experiment showed that in the samples of SiC films grown on the Si (100) surface, the formation of such a layer with the properties of a "semimetal" is not observed, and its optical properties are described with high accuracy by the simplest ellipsometric EMA model.

Samples of SiC films grown on the Si (110) surface had properties intermediate in the comparison with (111) and (110) interfaces. In this case, on this surface, we observed the formation of an interface with a very small (<0.5 eV) band gap, not equal to zero.

All SiC samples grown on Si by the standard CVD method (we studied samples produced by "Advanced EpiCo"), regardless of the orientation of the substrate (111), (110), and (100), are described with high accuracy by the simplest ellipsometric EMA model. There were no traces of the presence of "semimetal" in them.

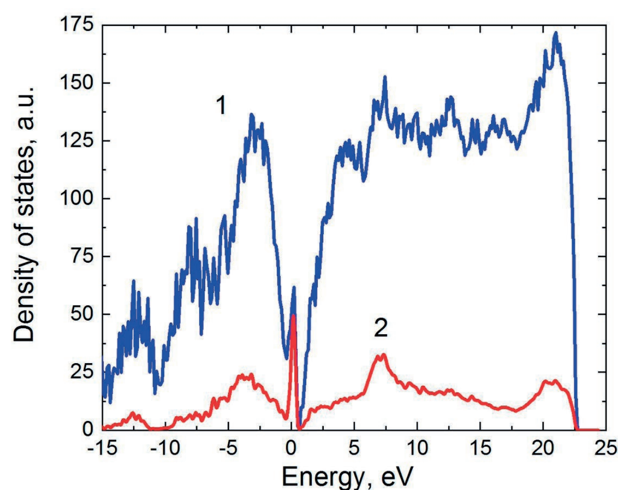

Fig. 28. Dependence of the density of electronic states of the studied system on energy (curve *1*). The Fermi energy corresponds to 0. Curve *2* is the contribution of the *p* electrons of the Si atoms at the SiC boundary that do not form bonds with the Si atoms of the substrate [82, 83]

9.2. Structural features of the surface of SiC epitaxial films synthesised by theMCSA, determined using photoelectron spectroscopy

Photoelectron spectroscopy (PES) is a powerful tool for studying the electronic properties of materials and the most important experimental method for obtaining the most complete information about the band structure of occupied electronic states, which are highly

sensitive to chemical interactions. Photoemission studies were carried out by us using a BESSY II synchrotron (Berlin, Germany) by the PES method at photon energies in the range of 130–450 eV. The experiments were carried out in ultra-high vacuum ~$5\cdot10^{-10}$ Torr at room temperature. Photoelectrons were recorded along the normal to the surface, and the excitation beam was incident on the sample surface at an angle of 45°. The total energy resolution was 50 meV.

It was found in [74, 75] that the adsorption of alkaline earth metals on the singular surface of SiC films synthesised by the MCSA results in a chemical shift of the electron density from silicon to carbon. This result fundamentally differs from similar data obtained both on hexagonal SiC crystals [84] grown by the standard method and on SiC crystals of the cubic polytype (Si_xC_{1x}) grown by CVD [85]. On the surface of these materials, the electron density shifts not only for Si, but also for carbon, towards higher energies. Moreover, these shifts are less distinct than the shifts in the SiC samples obtained by the MCSA. This means that in the electron density shift in SiC crystals and films grown by standard methods, as well as in hexagonal crystals, the reconstruction of their surface leads to the formation of chemical bonds between Si and C that are different from those in SiC synthesised by the MCSA. In the case of SiC grown by the MCSA, some of the bonds are simply broken on its surface. In this case, the carbon atom "pulls" the electron density from silicon. The adsorption of Ba atoms partially restores the equilibrium state of the electron density, returning the perturbed states to a state close to the state of Si and C atoms in the bulk of the SiC film. It is interesting to note that the (0001) surface of the 6H-SiC polytype has a more or less similar spectrum [86]. When this surface reconstructs to $\sqrt{3}\times\sqrt{3}$ the electron density shift of carbon coincides in direction with the electron density shift in the case of SiC grown by the MCSA. However, in this case, the electron density in silicon shifts in the opposite direction.

In [76–78], the electronic and photoemission properties of epitaxial SiC layers grown by the MCSA on vicinal silicon Si(111) surfaces deviated from the (111) plane by 4° and 8° were studied. The studies have shown that the electronic properties of SiC grown on vicinal Si facets are fundamentally different from the analogous properties of the same SiC grown on singular Si facets. The main differences were as follows. First, a feature of SiC grown by the MCSA is the excess content of carbon atoms compared to Si atoms and the presence of silicon vacancies, which, as we mentioned above, was also confirmed by other analytical methods. Second, the spectral lines of both carbon and silicon were shifted near the surface toward higher binding energies. This means that a chemical shift of the electron density occurs on the vicinal surface both at the Si atoms and at some of the C atoms. Thirdly, the adsorption of Ba atoms only enhances this process, leads to the formation of bonds between carbon atoms and the enhancement of the ionic component between C atoms and Ba atoms.

Fig. 29 shows the spectra of the core level C1*s* obtained for the pure SiC surface (curve *1* (Fig. 29a)) and for the Ba/SiC interface (Fig. 29b) with different Ba coatings (curves *2*, *3*). It was found that the C1*s* spectrum for the pure surface, SiC consists of two modes. The fundamental mode B corresponds to C atoms in the bulk of the sample. The S1 mode at a higher binding energy corresponds to carbon atoms that are located on terraces in the surface layer above Si atoms and, upon interaction, form a C–Si double layer. Sufficiently similar spectra can be observed for the 3C-SiC(111) surface [87]. The position of the S1 mode at high binding energies indicates that for a clean carbon-enriched surface in the C-Si layer, the degree of bond ionicity for C atoms increases. An extremely unusual C1*s* spectrum was observed for Ba/SiC(111)-8° interface formation (Fig. 29(a/b), curves *2*, *3*). It was found that two new modes S2 (energy shift by 3.8 eV) and SU (energy shift 7.0 eV). The S1 mode shifts towards higher binding energies by ~0.3 eV. Spectrum C 1*s* with such a rich set of intense modes in combination with the spectral width was observed for the first time during the adsorption of metal atoms on SiC. This points to the structural features of the vicinal surface of the SiC(111)-8 nanolayer° with terraces and steps, as well as unusual electronic and morphological features of surface C atoms forming C-Si bonds and hybridised sp^2 and sp^3 bonds in a carbon-rich C-C layer on the surface.

It should also be noted that the SU peak is a "shake-up" satellite. In this case, the binding

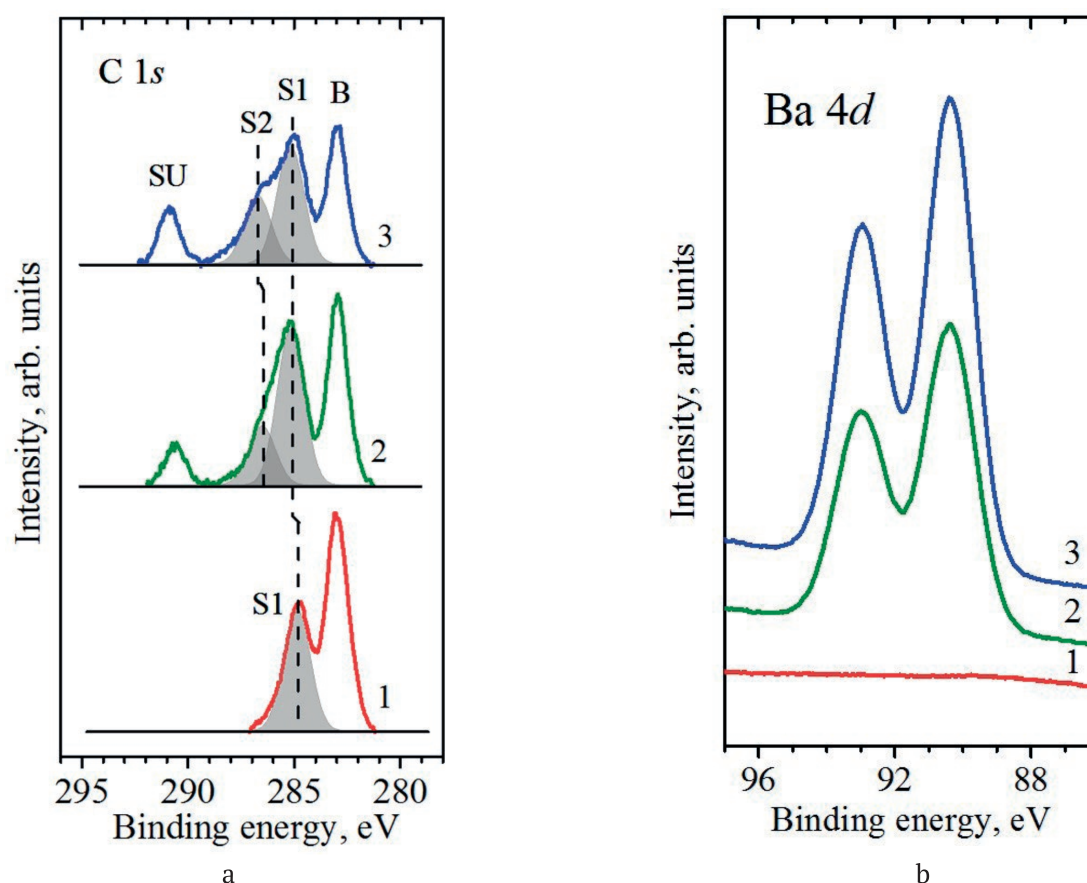

Fig. 29. Photoemission spectra of the core level C 1*s* (a) and the core level of Ba 4*d* (b) for the pure surface of SiC(111)-8° (1) and for the interface Ba/SiC(111)-8° when coated with Ba 0.5 (2) and 1.2 ML (3). Excitation energy *hv* = 450 eV (a) and *hv* = 130 eV (b) [76-78]

energy of the SU state coincides with the known value of the binding energy for the "shake-up" satellite in graphene on the 4*H*-SiC(0001) surface [88]. The SU shake-up satellite was also observed in the C 1*s* spectra in other organic compounds. The Raman spectrum of the SiC/Si(111)-8° sample in the initial state and the Raman spectrum of the Ba/SiC/Si(111)-8° interface with an adsorbed Ba monolayer were studied (see Fig. 30) for obtaining additional information about the state of the carbon layer on the vicinal surface after the adsorption of Ba and the nature of the unusual form of the C 1*s* spectrum. It was established that new features appeared for the interface in the spectral region 1200–1800 cm^{-1} that were not observed in this region for the same SiC layer, but without Ba. In the presence of Ba atoms, two D and G bands characteristic of aromatic compounds appeared. In the general case, the presence of G and D bands indicated the presence of sp^2 hexagonal carbon rings with a sp^2-type of hybridization. Thus, Raman spectroscopy also confirmed the conclusions about the formation of a new, previously unknown aromatic-like carbon compound during the adsorption of Ba on vicinal SiC samples grown by the atom substitution method.

Fig. 31 shows a diagram of a possible modification of the atomic structure of the SiC surface and the formation of new carbon bonds during the adsorption of Ba. The effect of the formation of aromatic-like rings on the surface of SiC samples is new and is stably observed only on the vicinal SiC-4° and SiC-8° surfaces during the adsorption of Ba and Cs metals. However, the presence of the shake-up satellite SU peak in Fig. 29 with a binding energy in the region of 292 eV, according to the data of [89–91], unambiguously indicates that the loss of energy by photoelectrons is used for the excitation of transitions between π bonding and π* antibonding (π → π*) molecular orbitals (MO) in aromatic rings of organic compounds. Shake-up satellites were formed due to the relaxation

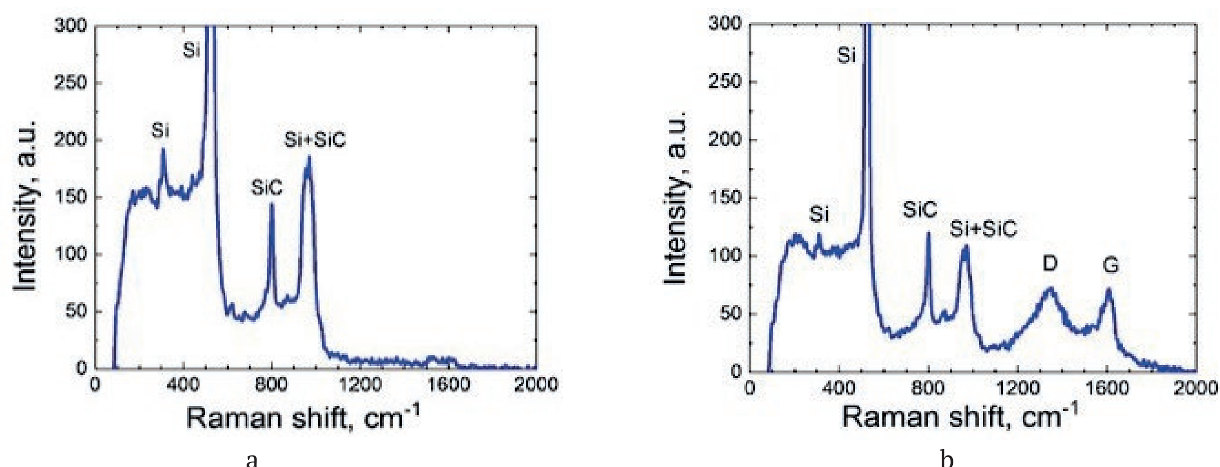

Fig. 30. Raman spectra of SiC/Si(111)-8° samples; (a) without a Ba monolayer; (b) of the same sample, but covered with an absorbed Ba monolayer [76-78]

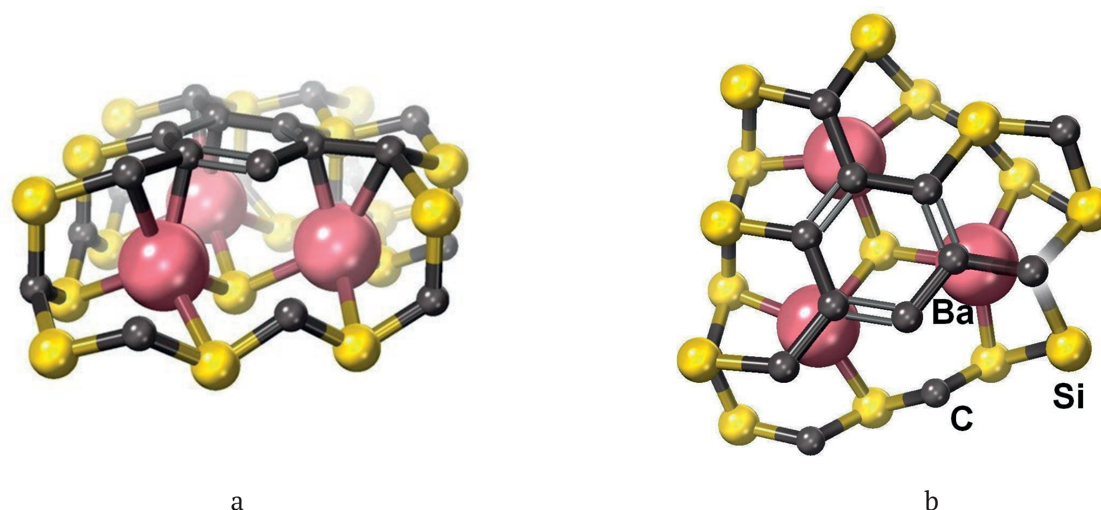

Fig. 31. Schematic representation of the carbon-based 2D structure stabilized by Ba atoms on the vicinal surface of the SiC nanolayer. The 2D cluster structure consists of carbon rings, in which the chemical bonding is close in character to the bonding in aromatic-like compounds. (a) is the Side view; (b) is the Top view [76-78]

of the electron subsystem of the core hole after its photoionization. After photoionization, the shielding of formed core hole occurs (relaxation of the electron system), as a result of which the relaxation energy is released. This energy is added to the energy of the electron leaving the atom. The appearance of the core hole potential can cause the rearrangement of the electron subsystem up to the excitation of valence electrons to higher free energy levels. In this case, the energy used for electronic excitations reduces the energy of the emitted photoelectron. As a result, the kinetic energy of the photoelectron recorded by the analyser decreases by the value of the excitation energy.

Thus, special 2D carbon structures were formed on the surface of inorganic SiC nanoscale samples grown on vicinal Si surfaces due to the special structure of SiC layers and in the presence of adsorbed Ba atoms. These 2D structures (see Fig. 31) consist of carbon rings, in which the chemical bond between carbon atoms, in our opinion, is close in nature to the bond realised in organic aromatic compounds. The formation of shake-up satellites is characteristic of many organic substances and, in particular, various kinds of organic alcohols, polymethyl methacrylate, as was recently shown in [91]. Similar spectra were also observed in complex, so-called organometallic complexes synthesised on

the basis of metals *d* elements such as Au, Cu, Ag [92]. The described effects were not observed both for the formation of graphene structures obtained on the surface of hexagonal 6H-SiC(0001) crystals [93] and on the surface of 4H-SiC crystals with facet orientation $(1\bar{1}02)$.

9.3. Anomalies of magnetic properties of epitaxial SiC films synthesised by the MCSA

In [94], a series of experimental studies of the magnetic properties, namely, the field and temperature dependences of the static magnetic susceptibility were performed for samples of thin films with a thickness of about 80–100 nm of single-crystal SiC grown on the (100), (110), and (111) surfaces of a single-crystal Si by the MCSA due to the chemical reaction of silicon with carbon monoxide gas CO. As a result of studies in SiC structures grown on Si (110) and Si (111), two quantum effects at room temperature were found to occur in weak magnetic fields. These effects were: firstly, the formation of a hysteresis of the static magnetic susceptibility [94], and secondly, the appearance of the Aharonov-Bohm oscillations in the field dependences of the static magnetic susceptibility [94]. The formation of the first effect we associated with the Meissner-Oxenfeld effect, and the second effect was due to the presence of microdefects in the form of nanotubes and micropores in these structures under the SiC layer. These microdefects were formed during the synthesis of these structures, and silicon in the state of "magnetic semimetal", as we mentioned above. In SiC structures grown on Si(100), these effects were not found [94], which was due to the different mechanism of SiC formation on the (100) Si surface, discussed above. Thus, as a result of experimental studies, the following nontrivial quantum effects at room temperature were discovered for the first time: the appearance of the magnetic moment quantization effect in SiC structures grown by the MCSA for Si (110) and Si (111); the formation of a hysteresis of the static magnetic susceptibility at room temperature in weak magnetic fields, which was interpreted by us as a manifestation of the Meissner – Ochsenfeld effect [94].

The simultaneous occurrence of the hysteresis of the static magnetic susceptibility and the Meissner – Ochsenfeld effect was explained in [94] by the suppression of the electron–electron interaction by electric fields. These electric fields arise due to the presence of microdefects in the SiC/Si structures, which consist of dipole centres with a negative correlation energy. In turn, dipole centres are formed from carbon-vacancy structures at the SiC(111)/Si(111) interface, where silicon is in a state close to that of a magnetic semimetal. In SiC structures grown on Si(100), in which carbon-vacancy structures are practically absent and silicon in the semimetallic state is not formed at the SiC-Si interface, these effects were not observed [94].

9.4. Electronic phase transitions in SiC epitaxial layers synthesised by the MCSA

In [95], at temperatures equal to 56, 76, 122, and 130°C, unusual features of the temperature dependences of the longitudinal resistance and heat capacity of epitaxial SiC films grown on Si by the MCSA were detected. The observed features of the heat capacity and longitudinal resistance, taking into account the previously discovered Meissner-Ochsenfeld effect [94] and the emergence of gigantic diamagnetism in weak magnetic fields of the order (1/4π) were interpreted in [95] as electronic phase transitions in ensembles of charge carriers into a coherent (possibly superconducting, if diamagnetism is taken into account) state. Fig. 32 shows the temperature dependences of longitudinal resistance R_{xx} and heat capacity C_p obtained by differential scanning calorimetry (DSC) for epitaxial SiC/Si structures grown by MCSA [95]. It follows from these data that the temperature dependences of the heat capacity are characterised by synchronously arising features at temperatures 56, 76, 122, and 130 °C (which were recorded as the temperature decreased from high to low values). It should be noted that a similar behaviour was also observed in the temperature dependences of the static magnetic susceptibility [94]. Sharp peaks are clearly visible on the graphs of dependencies and longitudinal resistance and heat capacity C_p. First of all, it is a sharply distinguished peak in the region of 56 °C. Next comes the system of peaks up to 130 °C. In this region, peaks are distinguished in the region of 76–130 °C and a peak in the region

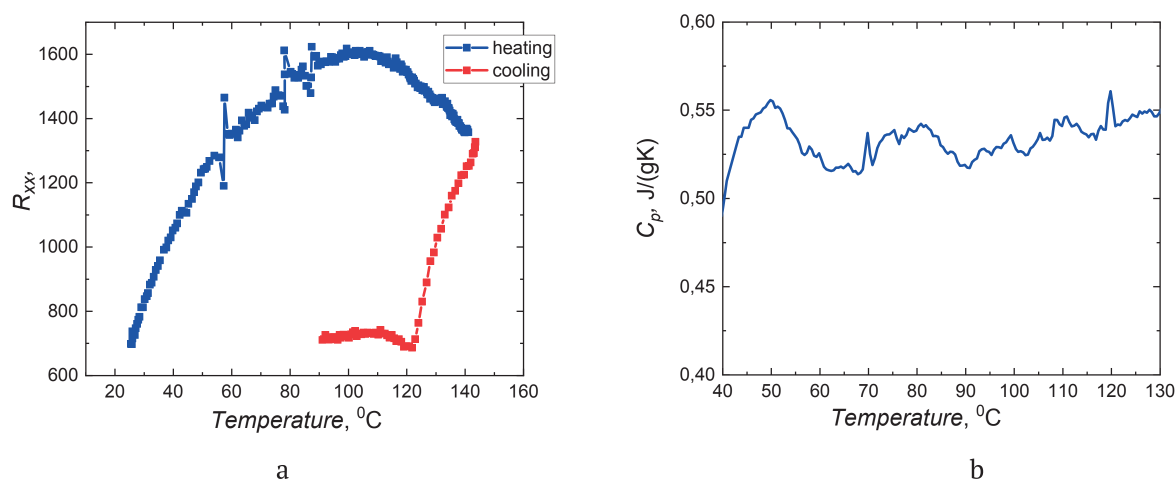

Fig. 32. Temperature dependences of the longitudinal resistance R_{xx} and the heat capacity C_p obtained by the differential scanning calorimetry (DSC) of epitaxial SiC/Si structures grown by the method of the coordinated substitution of atoms. Dependence of the (a) longitudinal resistance and (b) heat capacity C_p obtained by heating the SiC/Si sample in the range from 30 to 200 °C at a rate of 6 °C per minute in air after subtracting the heat capacity C_p of the initial silicon measured under the same conditions [95]

of 122 °C. Peculiarities above 130°C (Fig. 32b) were not considered in [94], since, as it is known, various transitions can be observed in this region, associated exclusively with silicon, which are not related to this problem. The observed features of peaks in heat capacity and longitudinal resistance can be interpreted as a consequence of phase transitions of charge carriers into a coherent (superconducting, if diamagnetism is taken into account) state. It should also be taken into account that the value of the critical temperature is interconnected with the size of the energy gap (in the framework of the BCS theory), and, accordingly, with the frequency (wavelength) of terahertz radiation, if the pixel length is represented as a characteristic of the Josephson transition. In [94], a pixel is understood as a microdefect limited by a different number of centres with a negative correlation energy and containing pairs of charge carriers. Pixels can form chains consisting of several pixels. Communication between pixels depends on temperature. If the temperature is higher than a certain critical temperature, then there is a destruction of coherence in a chain consisting of pixels containing pairs of charge carriers. In [94], a table containing data on the widths of the energy gaps, the sizes of microdefects, and the values of critical temperatures, i.e., temperatures at which features in the behaviour of the longitudinal resistance and heat capacity appear, is presented.

It should be noted that the data presented in a number of recently published papers [96–98] show that obtaining record high values of the critical temperatures of the transition to the superconducting state is associated with the use of high sample compression pressures. These pressures are of the order of 100-270 GPa when the samples are compressed. Thus, it was found in [96] that in lanthanum and yttrium hydrides compounds at temperatures of 245–260 K and pressures of the order of 1 million atmospheres; $LaH_{10\pm x}$ becomes a superconductor upon cooling to 250 K at a pressure of 188 GPa. In YH_6 compounds, a superconducting transition was observed at a temperature of 227 K and a pressure of 237 GPa. It was found in [96, 97] that upon compression of LaH_{10} compound up to 170 GPa, the critical transition temperature was T_c = −13 °C. In 2020, a new record for carbon-doped sulphur hydride was published in Nature [98]. At a pressure of 267 GPa, the critical transition temperature of this compound was raised to 15°C.

In this regard, we note once again that SiC films grown by the MCSA, by the nature of their formation [1, 2, 4–6], are substances in which phase transitions of charge carriers into a coherent state can be observed. With standard methods of growth of SiC films on Si, in which the SiC layer grows due to the supply of matter

to the Si surface, the SiC layer is not compressed. The SiC layer on the contrary is subjected to tensile strains from the side of silicon. In the synthesis of SiC on Si by the MCSA, in contrast to the classical growth of SiC, the SiC layer shrinks, during which great compression pressures appear for a short time at the SiC-Si interface. It should be noted that the SiC synthesis method based on the substitution of atoms and proposed in [12] opens up new possibilities for creating high pressures in materials using "chemical" transformations in the process of substitution of some of their atoms.

10. Conclusions

The review reflects the main results of the theory, mechanisms, and technology of growing SiC on Si by the method of coordinated substitution of atoms (MCSA). New unique physicochemical properties of the SiC/Si structures have been described in detail. The possibilities of the MCSA for growing epitaxial SiC films not only on Si single crystals but also on other materials, in particular, sapphire, have been described. A new method for creating heat-resistant and antioxidant carbide-carbon coatings, which is based on the new fundamental principles of the MCSA, is described. In this review, we have completely ignored our studies on the practical application of SiC/Si and our studies on the growth of a whole class of semiconductor compounds on the SiC/Si substrates, such as A^3B^5 compounds (AlN, GaN, AlGaN, and Ga_2O_3) and A^2B^6 semiconductor compounds, almost the entire series of which was grown by us on the SiC/Si substrates. An overview of these studies can be found in our previous review articles [1–6,62]. Also, for the first time, we have developed a semi-industrial technology for the production of chips for micro-LEDs on silicon, and a working prototype of a white LED on silicon was created, a photograph of which is shown in Fig. 33.

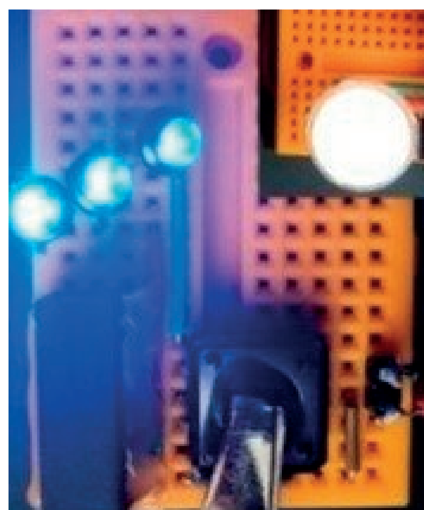

Fig. 33. Packaged Micro-LED: three Micro-LEDs without phosphor coating and an LED with a polymer lens containing a phosphor [99]

Author contributions

All authors made an equivalent contribution to the preparation of the publication.

Conflict of interests

The authors declare that they have no known competing financial interests or personal relationships that could have influenced the work reported in this paper.

References

1. Kukushkin S. A., and Osipov A. V. Nanoscale single-crystal silicon carbide on silicon and unique properties of this material. *Inorganic Materials*. 2021;57(13): 1319–1329. https://doi.org/10.1134/S0020168521130021

2. Kukushkin S. A., Osipov A. V. Epitaxial silicon carbide on silicon. Method of coordinated substitution of atoms (A Review). *Russian Journal of General Chemistry*. 2022;92: 584–610. https://doi.org/10.1134/S1070363222040028

3. Kukushkin S., Osipov A., Redkov A. SiC/Si as a new platform for growth of wide-bandgap semiconductors. In: *Mechanics and Control of Solids and Structures. Advanced Structured Materials*. V. A. Polyanskiy, A. K. Belyaev (eds.). Vol. 164. Springer; 2022. pp. 335–367. https://doi.org/10.1007/978-3-030-93076-9

4. Kukushkin S. A., Osipov A. V. Feoktistov N. A. Chemical self-assembly of a single-crystal SiC film on a silicon substrate: a new method of directed nucleation. *Rossiiskii khimicheskii zhurnal*. 2013;57(6): 36–47. (In Russ., abstract in Eng.). Available at: https://www.elibrary.ru/item.asp?id=24069701

5. Kukushkin S. A., Osipov A. V. Topical review. Theory and practice of SiC growth on Si and its applications to wide-gap semiconductor films. *Journal of Physics D: Applied Physics*. 2014;47: 313001-313001-41. https://doi.org/10.1088/0022-3727/47/31/313001

6. Kukushkin S. A., Osipov A. V., Feoktistov N. A. Synthesis of epitaxial silicon carbide films through the substitution of atoms in the silicon crystal lattice: A

review. *Physics of the Solid State*. 2014;56: 1507–1535. https://doi.org/10.1134/S1063783414080137

7. Takahashi K., Yoshikawa A., Sandhu A. (eds.). *Wide bandgap semiconductors*. Springer-Verlag Berlin and Heidelberg GmbH & Co. K; 2007. 470 p. https://doi.org/10.1007/978-3-540-47235-3

8. Nishino S., Powell J.A., Will H.A. Production of large-area single-crystal wafers of cubic SiC for semiconductor devices. *Applied Physics Letters*. 1983;42(5): 460–462. https://doi.org/10.1063/1.93970

9. Kukushkin S. A., Osipov A. V., Bessolov V. N., Medvedev B. K., Nevolin V. K., Tcarik K. A. Substrates for epitaxy of gallium nitride: new materials and techniques. *Reviews on Advanced Materials Science*. 2008;17: 1–32. Available at: https://www.ipme.ru/e-journals/RAMS/no_11708/kukushkin.pdf

10. Severino A., Locke C., Anzalone R., Camarda M., Piluso N., La Magna A., Saddow S., Abbondanza G., D'Arrigo G., La Via F. 3C-SiC film growth on Si substrates. *ECS Transactions*. 2011;35(6): 99–116. https://doi.org/10.1149/1.3570851

11. Ferro G. 3C-SiC heteroepitaxial growth on silicon: The quest for holy grail. *Critical Reviews in Solid State and Materials Sciences*. 2015;40(1): 56–76. https://doi.org/10.1080/10408436.2014.940440

12. Kukushkin S. A., Osipov A. V. New method for growing silicon carbide on silicon by solid-phase epitaxy: Model and experiment. *Physics of the Solid State*. 2008;50: 1238–1245. https://doi.org/10.1134/S1063783408070081

13. Kukushkin S. A., Osipov A. V., Feoktistov N. A. A method of manufacturing an article containing a silicon substrate with a silicon carbide film on its surface*. Patent RF, No. 2363067. Publ. 27.07.2009; bul. No. 21. (In Russ.)

14. Kukushkin S. A., Osipov A. V. Quantum mechanical theory of epitaxial transformation of silicon to silicon carbide. *Journal of Physics D: Applied Physics*. 2017;50 (46): 464006 (7pp). https://doi.org/10.1088/1361-6463/AA8F69

15. Kukushkin S. A., Osipov A. V. Thin-film heteroepitaxy by the formation of the dilatation dipole ensemble. *Doklady Physics*. 2012;57: 217–220. https://doi.org/10.1134/S1028335812050072

16. Kukushkin S. A., Osipov A. V. A new mechanism of elastic energy relaxation in heteroepitaxy of monocrystalline films: Interaction of point defects and dilatation dipoles. *Mechanics of Solids*. 2013;48: 216–227. https://doi.org/10.3103/S0025654413020143

17. Kukushkin S. A. and Osipov A. V. A new method for the synthesis of epitaxial layers of silicon carbide on silicon owing to formation of dilatation dipoles. *Journal of Applied Physics*. 2013;113(2): 4909-1-4909-7. https://doi.org/10.1063/1.4773343

18. Kukushkin S. A., Osipov A. V. Anisotropy of the solid-state epitaxy of silicon carbide in silicon. *Semiconductors*. 2013;47: 1551–1555. https://doi.org/10.1134/S1063782613120129

19. Kukushkin S. A., Osipov A. V. First-order phase transition through an intermediate state *Physics of the Solid State*. 2014;56: 792–800. https://doi.org/10.1134/S1063783414040143

20. Kukushkin S. A., Osipov A. V. Mechanism of formation of carbon-vacancy structures in silicon carbide during its growth by atomic substitution. *Physics of the Solid State*. 2018;60: 1891–1896. https://doi.org/10.1134/S1063783418090184

21. Kukushkin S. A., Osipov A. V., Telyatnik R. S. Elastic interaction of point defects in cubic and hexagonal crystals. *Physics of the Solid State*. 2016;58: 971–980. https://doi.org/10.1134/S1063783416050140

22. Eshelby J. D. *The continuum theory of dislocations in crystals*. New York: Academic Press; 1956. pp. 79–144.

23. Lifshits I. M., Rozentsveig L. N. On the construction of the Green tensor for the basic equation of the theory of elasticity in the case of an unbounded elastically anisotropic medium*. *Journal of Experimental and Theoretical Physics*. 1947;17(9): 783–791. (In Russ.)

24. Kuz'michev S. V., Kukushkin S. A., Osipov A. V. Elastic interaction of point defects in crystals with cubic symmetry. *Mechanics of Solids*. 2013;48: 431–438. https://doi.org/10.3103/S0025654413040110

25. Sangwal K. *Etching of crystals: Theory, experiment and application*. North-Holland: 1987. 497.

26. Kukushkin S. A., Osipov A. V. Thin-film condensation processes*. *Physics-Uspekhi* (1998),41(10): 983–1014. https://doi.org/10.1070/PU1998v041n10ABEH000461

27. Kukushkin S. A., Slezov V. V. Disperse systems on the surface of solids (evolutionary approach): mechanisms of thin film formation. St. Petersburg: Nauka Publ.; 1996. 304. (In Russ.)

28. Zhukov S. G., Kukushkin S. A., Lukyanov A. V., Osipov A. V., Feoktistov N. A. *Method of manufacturing products containing a silicon substrate with a silicon carbide film on its surface**. Patent RF: No. 2522812. Publ. 20.07.2014, bul. No. 20. (In Russ.)

29. Kukushkin S. A., Osipov A. V. First-order phase transition through an intermediate state. *Physics of the Solid State*. 2014;56: 792–800. https://doi.org/10.1134/S1063783414040143

30. Kukushkin S. A., Osipov A. V., Soshnikov I.P. Growth of Epitaxial SiC Layer on Si (100) Surface of n- and p-type of Conductivity by the Atoms Substitution Method. *Reviews on Advanced Materials Science*. 2017;52: 29-42. Available at: http://www.ipme.ru/e-journals/RAMS/no_15217/05_15217_kukushkin.pdf

31. Kukushkin S. A. Nucleation of pores in brittle solids under load. *Journal of Applied Physics*. 2005;98: 033503-1–033503-12. https://doi.org/10.1063/1.1957131

32. Geguzin Ya. E. *Diffusion zone*. Moscow: Science Publ.; 1979. 34 p. (In Russ.)

33. Kelly A., Groves G. W. *Crystallography and crystal defects*. London: Longman; 1970. 428 p.

34. Kukushkin S. A., Osipov A. V. A quantum-mechanical model of dilatation dipoles in topochemical synthesis of silicon carbide from silicon. *Physics of the Solid State*. 2017;59: 1238–1241. https://doi.org/10.1134/S1063783417060130

35. Kukushkin S. A., Osipov A. V. Phase equilibrium in the formation of silicon carbide by topochemical conversion of silicon. *Physics of the Solid State*. 2016;58: 747–751. https://doi.org/10.1134/S1063783416040120

36. Kukushkin S. A., Osipov A. V. The equilibrium state in the Si-O-C ternary system during SiC growth by chemical substitution of atoms. *Technical Physics Letters*. 2015;41: 259–262. https://doi.org/10.1134/S1063783416040120

37. Grudinkin S. A., Golubev V. G., Osipov A. V., Feoktistov N. A., Kukushkin S. A. Infrared spectroscopy of silicon carbide layers synthesized by the substitution of atoms on the surface of single-crystal silicon. *Physics of the Solid State*. 2015;57: 2543–2549. https://doi.org/10.1134/S1063783415120136

38. Kukushkin S. A., Osipov A. V. Drift mechanism of mass transfer on heterogeneous reaction in crystalline silicon substrate. *Physica B: Condensed Matter*. 2017;512(1): 26–31. https://doi.org/10.1016/j.physb.2017.02.018

39. Kidalov V. V., Kukushkin S. A., Osipov A. V., Redkov A. V., Grashchen-ko A. S., Soshnikov I. P., Boiko M. E., Sharkov M. D., Dyadenchuk A. F. Properties of SiC films obtained by the method of substitution of atoms on porous silicon. *ECS Journal of Solid State Science and Technology*. 2018. 7(4): P158–P160. https://doi.org/10.1149/2.0061804jss

40. Kukushkin S. A., Osipov A. V., Osipova E. V. Mechanism of molecule migration of carbon and silicon monoxides in silicon carbide crystal. *Materials Physics and Mechanics*. 2019;42: 178–182. https://doi.org/10.18720/MPM.4222019_3

41. Kukushkin S. A., Osipov A. V. Mechanism of diffusion of carbon and silicon monooxides in a cubic silicon carbide crystal. *Phys. Solid State*. 2019;61: 2338–2341. https://doi.org/10.1134/S1063783419120242

42. Редьков А. В., Гращенко А. С., Кукушкин С. А., Осипов А.В., Котляр К.П., Лихачев А. И., Нащекин А. В., Сошников И.П. Эволюция ансамбля микропор в структуре SiC/Si в процессе роста методом замещения атомов. *ФТТ*. 2019; 61(3): 2334–2337. DOI: 10.1134/S1063783419030272.

43. Grashchenko A. S., Kukushkin S. A., Osipov A. V., Redkov A. V. Vacancy growth of monocrystalline SiC from Si by the method of self-consistent substitution of atoms. *Catalysis Today*. 2022;397–399: 375–378. https://doi.org/10.1016/J.CATTOD.2021.08.012

44. Grashchenko A. S., Kukushkin S. A., Osipov A. V. Coating of a nanostructured profiled Si surface with a SiC layer. *Technical Physics Letters*. 2020;46: 1012–1015. https://doi.org/10.1134/S1063785020100235

45. Smirnov V. K., Kibalov D. S., Orlov O. M., Graboshnikov V. V. Technology for nanoperiodic doping of a metal-oxide-semiconductor field-effect transistor channel using a self-forming wave-ordered structure. *Nanotechnology*. 2003;14: 709–715. https://doi.org/10.1088/0957-4484/14/7/304

46. Tang X., Wongchotigul K., Spencer M. G. Optical waveguide formed by cubic silicon carbide on sapphire substrates. *Applied Physics Letters*. 1991;58: 917. https://doi.org/10.1063/1.104476

47. Sywe B. S., Yu Z. J., Burckhard S., Edgar J. H., Chaudhuri J. Epitaxial growth of SiC on sapphire substrates with an AlN buffer layer. *Journal of The Electrochemical Society*. 1994;141: 510. https://doi.org/10.1149/1.2054756

48. McArdle T. J., Chu J. O., Zhu Y., Liu Z., Krishnan M., Breslin C. M., Dimitrakopoulos C., Wisnieff R., Grill A. Multilayer epitaxial graphene formed by pyrolysis of polycrystalline silicon-carbide grown on c-plane sapphire substrates. *Applied Physics Letters*. 2011;98: 132108. https://doi.org/10.1063/1.3575202

49. Cheng L., Steckl A. J., Scofield J. SiC thin-film Fabry-Perot interferometer for fiber-optic temperature sensor. *IEEE Transactions on Electron Devices*. 2003;50: 2159. https://doi.org/10.1109/TED.2003.816106

50. Li J. C, Batoni P., Tsu R. Synthesis and characterization of 4H-SiC on C-plane sapphire by C_{60} and Si molecular beam epitaxy. *Thin Solid Films*. 2010;518(6): 1658. https://doi.org/10.1016/j.tsf.2009.11.088

51. Luong T. T., Tran B. T., Ho Y. T., Wei T. W., Wu Y. H., Yen T. Ch., Wei L. L., Maa J. Sh., Chang E. Yi. 2H-silicon carbide epitaxial growth on c-plane sapphire substrate using an AlN buffer layer and effects of surface pre-treatments. *Electronic Materials Letters*. 2015;11: 352–359. https://doi.org/10.1007/s13391-015-4208-9

52. Beisenov R., Ebrahim R., Mansurov Z. A., Tokmoldin S. Zh, Mansurov B. Z., Ignatiev A. Growth of 3C-SiC films on Si (111) and sapphire (0001) substrates by MOCVD. *Eurasian Chemico-Technological Journal*. 2013;15(1): 25. https://doi.org/10.18321/ectj136

53. Chu J. O., Dimitrakopoulos C. D., Grill A., McArdle T. J., Saenger K. L., Wisnieff R. L., Zhu. Yu. *Epitaxial growth of silicon carbide on sapphire*. Patent US: No. US 2012/0112198 A1. Pub. Date: May 10, 2012. Available at: URL:https://patentimages.storage.googleapis.com/91/9f/23/96f2953b645053/US20120112198A1.pdf

54. Shibata K., Harada Sh., Ujihara T. 3C-SiC crystal on sapphire by solution growth method. *Materials Science Forum*. 2015;821–823: 185. https://doi.org/10.4028/www.scientific.net/MSF.821-823.185

55. Kukushkin S. A., Osipov A. V. Mechanisms of epitaxial growth of SiC films by the method of atom substitution on the surfaces (100) and (111) of Si single crystals and on surfaces of Si films grown on single crystals Al_2O_3. *IOP Conference Series: Materials Science and Engineering*. 2018;387: 012044-1-5. https://doi.org/10.1088/1757-899X/387/1/012044

56. Kukushkin S. A., Osipov A. V., Redkov A. V., Grashchenko A. S., Feoktistov N. A., Fedotov S. D., Statsenko V. N., Sokolov E. M., Timoshenkov S. P. A new method for synthesis of epitaxial films of silicon carbide on sapphire substrates (α-Al_2O_3). *Reviews on Advanced Materials Science*. 2018;57(1): 82-96. https://doi.org/10.1515/rams-2018-0050

57. Cristoloveanu S., Li Sh. S. Electrical characterization of silicon-on-insulator materials and devices. In: *Springer Science and Business Media*. 1995;305: 381. https://doi.org/10.1007/978-1-4615-2245-4

58. Munteanu D., Cristoloveanu S., Rozeau O., Jomaah J., Boussey J., Wetzel M., Houssaye P. de la, Lagnado L. Characterization of silicon-on-sapphire material and devices for radio frequency applications. *Journal of The Electrochemical Society*. 2001;148(4): 218. https://doi.org/10.1149/1.1355693

59. Colinge J. P. SOI CMOS for high-temperature applications. In: *Perspectives, Science and Technologies for Novel Silicon on Insulator Devices*. Hemment P. L. F., Lysenko V. S., Nazarov A. N. (eds.). NATO Science Series. Vol. 73. Dordrecht: Springer; 2000. pp. 249–256. https://doi.org/10.1007/978-94-011-4261-8_24

60. Celler G. K., Cristoloveanu S. Frontiers of silicon-on-insulator. *Journal of Applied Physics*. 2003;93(9): 4955–4978. https://doi.org/10.1063/1.1558223

61. Sokolov E. M., Fedotov S. D., Statsenko V. N., Timoshenkov S. P., Emelyanov A. V. Study of the structural properties of silicon-on-sapphire layers in hydride-chloride vapor-phase epitaxy. *Semiconductors*. 2017;51(13): 1692–1697. https://doi.org/10.1134/S1063782617130127

62. Bessolov V. N., Konenkova E. V., Kukushkin S. A., Osipov A. V., Rodin S. N. Semipolar gallium nitride on silicon: technology and properties. *Reviews on Advanced Materials Science*. 2014;38(1): 75–93. https://www.ipme.ru/e-journals/RAMS/no_13814/08_13814_kukushkin.pdf

63. Kalinkin I. P., Kukushkin S. A., Osipov A. V. *Method for processing the surface of a single-crystal silicon wafer**. Patent RF: No. 2323503. Publ. 04/27/2008, bul. No. 12.

64. Kalinkin I. P., Kukushkin S. A., Osipov A. V. Effect of chemical treatment of a silicon surface on the quality and structure of silicon-carbide epitaxial films synthesized by atom substitution. *Semiconductors*. 2018;52: 802–808. https://doi.org/10.1134/S1063782618060118

65. Grashchenko A. S., Kukushkin S. A., Osipov A. V., Redkov A. V. Formation of composite SiC-C coatings on graphite via annealing Si-melt in CO. *Surface & Coatings Technology*.2021;423(15): 127610. https://doi.org/10.1016/j.surfcoat.2021.127610

66. Grashchenko A. S., Kukushkin S. A., Osipov A. V., Redkov A. V. The mechanical properties of a SiC composite coating on graphite produced by the atom-substitution method. *Technical Physics Letters*. 2022;48, 62–65. https://doi.org/10.1134/S1063785022030038

67. Perdew J. P., Burke K., Ernzerhof M. Generalized gradient approximation made simple. *Physical Review Letters*. 1996;77(18): 3865–3868. https://doi.org/10.1103/PhysRevLett.77.3865

68. Fischer-Cripps A. C. *Nanoindentation*. (Third Edition) Springer; 2004. 279 p. https://doi.org/10.1115/1.1704625

69. Kukushkin S. A., Lukyanov A. V., Osipov A. V., Feoktistov N. A. Epitaxial silicon carbide on a 6″ silicon wafer. *Technical Physics Letters*. 2014;40: 36–39. https://doi.org/10.1134/S1063785014010088

70. Egorov V. K., Egorov E. V., Kukushkin S. A., Osipov A. V. Structural heteroepitaxy during topochemical transformation of silicon to silicon carbide. *Physics of the Solid State*. 2017;59: 773–779. https://doi.org/10.1134/S1063783417040072

71. Grudinkin S. A., Kukushkin S. A., Osipov A. V., Feoktistov N. A. IR spectra of carbon-vacancy clusters in the topochemical transformation of silicon into silicon carbide. *Physics of the Solid State*. 2017;59: 2430–2435. https://doi.org/10.1134/S1063783417120186

72. Kukushkin S. A., Nussupov K. K., Osipov A. V., Beisenkhanov N. B., Bakranova D. I. X-ray reflectometry and simulation of the parameters of SiC epitaxial films on Si(111), grown by the atomic substitution method. *Physics of the Solid State*. 2017;59: 1014–1026. https://doi.org/10.1134/S1063783417050195

73. Kukushkin S. A., Nussupov K. Kh., Osipov A. V., Beisenkhanov N. B., Bakranova D. I. Structural properties and parameters of epitaxial silicon car-bide films, grown by atomic substitution on the highresistance (111) oriented silicon. *Superlattices and Microstructures*. 2017;111: 899–911. https://doi.org/10.1016/j.spmi.2017.07.050

74. Benemanskaya G. V., Dementev P. A., Kukushkin S. A., Lapushkin M. N., Osipov A. V., Senkovskiy B., Timoshnev S. N. Photoemission study of nano SiC epitaxial layers synthesized by a new method of the

atom substitution in Si crystal lattice. *Materials Physics and Mechanics*. 2015;22(2): 183–190. Available at: https://ipme.ru/e-journals/MPM/no_22215/MPM222_09_kukushkin.pdf

75. Kukushkin S. A., Benemanskaya G. V., Dementev P. A., Senkovskiy B., Timoshnev S. N. Synchrotron-radiation photoemission study of the ultrathin Ba/3C–SiC (111) interface. *Journal of Physics and Chemistry of Solids*. 2016;90: 40–44. https://doi.org/10.1016/j.jpcs.2015.10.018

76. Benemanskaya G. V., Dementev P. A., Kukushkin S. A., Osipov A. V., Timoshnev S. N. Carbon-based aromatic-like nanostructures on the vicinal SiC surfaces induced by Ba adsorption. *ECS Journal of Solid State Science and Technology*. 2019;8(6): M53–M59. https://doi.org/10.1149/2.0031906jss

77. Benemanskaya G. V., Dement'ev P. A., Kukushkin S. A., Osipov A. V., Timoshnev S. N. A new type of carbon nanostructure on a vicinal SiC(111)-8° surface. *Technical Physics Letters*. 2019;45: 201–204. https://doi.org/10.1134/S1063785019030039

78. Benemanskaya G. V., Kukushkin S. A., Dementev P. A. Aromatic-like carbon nanostructures created on the vicinal SiC surfaces. *Physics of the Solid State*. 2019;61(12): 2455–2458. https://doi.org/10.1134/S1063783419120059

79. Kukushkin S. A., Osipov A. V. Anisotropy of the solid-state epitaxy of silicon carbide in silicon. *Semiconductors*. 2013;47: 1551–1555. https://doi.org/10.1134/S1063782613120129

80. Kitaev Y. E., Kukushkin S. A., Osipov A. V. Evolution of the symmetry of intermediate phases and their phonon spectra during the topochemical conversion of silicon into silicon carbide. *Physics of the Solid State*. 2017;59: 28–33. https://doi.org/10.1134/S1063783417010164

81. Kitaev Y. E., Kukushkin S. A., Osipov A. V., Redkov A. V. A new trigonal (rhombohedral) SiC phase: ab initio calculations, a symmetry analysis and the Raman spectra. *Physics of the Solid State*. 2018;60: 2066–2071. https://doi.org/10.1134/S1063783418100116

82. Kukushkin S. A., Osipov A. V. The optical properties, energy band structure, and interfacial conductance of a 3C-SiC(111)/Si(111) heterostructure grown by the method of atomic substitution. *Technical Physics Letters*. 2020;46: 1103–1106. https://doi.org/10.1134/S1063785020110243

83. Kukushkin S. A., Osipov A. V. Anomalous properties of the dislocation-free interface between Si (111) substrate and 3C-SiC (111) epitaxial layer. *Materials*. 2021;14(78): 1–12. https://doi.org/10.3390/ma14010078

84. Virojanadara C., Hetzel M., Johansson L. I., Choyke W. J., Starke U. Electronic and atomic structure of the 4H-SiC $(1\bar{1}02)-c(2\times2)$ surface. *Surface Science*. 2008;602 (15): 525–533. https://doi.org/10.1016/j.susc.2007.11.012

85. Santoni A., lancok J., Dhanak V. R., loreti S., Miller G., Minarini C. A valence-band and core-level photoemission study of a-Si_xC_{1-x} thin films grown by low-temperature low-pressure chemical vapour deposition. *Applied Physics A*. 2005;81: 991–996. https://doi.org/10.1007/s00339-004-2976-4

86. Sieber N., Seyller Th., Ley L., James D., Riley J. D., Leckey R. C. G. Synchrotron x-ray photoelectron spectroscopy study of hydrogen-terminated 6H-SiC{0001} surfaces. *Physical Review B*. 2003;67(20): 205304-1-13. https://doi.org/10.1103/PhysRevB.67.205304

87. King S. W., Nemanich R. J., Davis R. F. Photoemission investigation of the Schottky barrier at the Sc/3C-SiC (111) interface. *Physica Status Solidi (b)*. 2015;252(2): 391–396. https://doi.org/10.1002/pssb.201451340

88. Watcharinyanon S., Johansson L. I., Xia C., Virojanadara C. Changes in structural and electronic properties of graphene grown on 6H-SiC(0001) induced by Na deposition. *Journal of Applied Physics*. 2012;111: 083711-1-6. https://doi.org/10.1063/1.4704396

89. Maiti J., Kakati N., Lee S. H., Yoon Y. S. Fluorination of multiwall carbon nano-tubes by a mild fluorinating reagent HPF6. *Journal of Fluorine Chemisty*. 2012;135: 362–366. https://doi.org/10.1016/j.jfluchem.2011.10.004

90. Flesch R., Serdaroglu E., Blobner F., Feulner P., Brykalova X. O., Pavlychev A. A., Kosugid N., Rühl E. Gas-to-solid shift of C 1s-excited benzene. *Physical Chemistry Chemical Physics*. 2012;14(26): 9397–9402. https://doi.org/10.1039/C2CP23451C

91. Kong M. J., Teplyakov A. V., Lyubovitsky J. G., Bent S. F. NEXAFS studies of adsorption of benzene on Si(100)-2×1. *Surface Science*. 1998;411(3): 286–293. https://doi.org/10.1016/S0039-6028(98)00336-7

92. Makarova A. A., Grachova E. V., Krupenya D. V., Vilkov O., Fedorov A., Usachov D., Generalov A., Koshevoy I. O., Tunik S. P., Rühl E., Laubschat C., Vyalikh D. V. Insight into the electronic structure of the supramolecular "rods-in-belt" Au^I-Cu^I and Au^I-Ag^I self-assembled complexes from X-ray photoelectron and absorption spectroscopy. *Journal of Electron Spectroscopy and Related Phenomena*. 2015;192: 26–34. https://doi.org/10.1016/j.elspec.2014.01.004

93. Kang C., Tang J., Li L., Pan H., Pengshou X., Wei S., Chen X., Xu X. In situ study on the electronic structure of graphene grown on 6H–SiC $(000\bar{1})$ with synchrotron radiation photoelectron spectroscopy. *Applied Surface Science*. 2012; 258(6): 2187–2191. https://doi.org/10.1016/j.apsusc.2011.02.068

94. Bagraev N. T., Kukushkin S. A., Osipov A. V., Romanov V. V., Klyachkin L. E., Malyarenko A. M.,

Khromov V. S. Magnetic properties of thin epitaxial SiC layers grown by the atom-substitution method on single-crystal silicon surfaces. *Semiconductors*. 2021;55: 137–145. https://doi.org/10.1134/S106378262102007X

95. Bagraev N. T., Kukushkin S. A., Osipov A. V. et al. Phase transitions in silicon-carbide epitaxial layers grown on a silicon substrate by the method of the coordinated substitution of atoms. *Semiconductors*. 2022;56: 321–324. https://doi.org/10.1134/S1063782622070016

96. Somayazulu M., Ahart M., Mishra A. K., Geballe Z. M., Baldini M., Meng Y., Struzhkin V. V., Hemley R. J. Evidence for superconductivity above 260 K in lanthanum superhydride at megabar pressures. *Physical Review Letters*. 2019;122(2): 027001. https://doi.org/10.1103/PhysRevLett.122.027001

97. Thapa D. K., Islam S., Saha S. K., Mahapatra P. S., Bhattacharyya B., Sai T. P., Mahadevu R., Patil S., Ghosh A., Pandey A. Coexistence of diamagnetism and vanishingly small electrical resistance at ambient temperature and pressure in nanostructures. *Superconductivity (cond-mat.supr-con.)*. 2019; arXiv:1807.08572. https://doi.org/10.48550/arXiv.1807.08572

98. Snider E., Dasenbrock-Gammon N., McBride R., Debessai M., Vindana H., Vencatasamy K., Lawler K. V., Salamat A., Dias R. P. Room-temperature superconductivity in a carbonaceous sulfur hydride. *Nature*. 2020;586: 373–377. https://doi.org/10.1038/s41586-020-2801-z

99. Markov L. K., Kukushkin S. A., Smirnova I. P., Pavlyuchenko A. S.,. Grashchenko A. S, Osipov A. V., Svyatets G. V., Nikolaev A. E., Sakharov A. V., Lundin V. V., Tsatsulnikov A. F. A light-emitting diode based on AlInGaN heterostructures grown on SiC/Si substrates and its fabrication technology. *Technical Physics Letters*. 2022;48: 31–34. https://doi.org/10.1134/S1063785022020043

*Translated by author of the article.

Information about the authors

Sergey A. Kukushkin, Dr. Sci. (Phys.–Math.), Professor, Head of the Laboratory of Structural and Phase Transitions in Condensed Matter, Chief Researcher, Institute for Problems in Mechanical Engineering of the Russian Academy of Sciences (IPME RAS) (Saint-Petersburg, Russian Federation).

https://orcid.org/0000-0002-2973-8645
sergey.a.kukushkin@gmail.com

Andrey V. Osipov, Dr. Sci. (Phys.–Math.), Chief Researcher of the Laboratory of Structural and Phase Transitions in Condensed Matter, Institute for Problems in Mechanical Engineering of the Russian Academy of Sciences (IPME RAS) (Saint-Petersburg, Russian Federation).

https://orcid.org/0000-0002-2911-7806
andrey.v.osipov@gmail.com

Received 07.10.2022; approved after reviewing 12.10.2022; accepted for publication 17.10.2022; published online 25.12.2022.

Translated by Valentina Mittova
Edited and proofread by Simon Cox